

Heat pump concepts for Nearly Zero Energy Buildings



Heat pump concepts for nZEB – Technology developments, design tools and testing of heat pump systems for nZEB in the USA

Country report IEA HPT Annex 40 Task 2, Task 3 and Task 4 of the USA

Authors

Van D. Baxter, PE
 Oak Ridge National Laboratory
 baxtervd@ornl.gov

W. Vance Payne, Ph.D.
 A. Hunter Fanney, William Healy, Joshua Kneifel, Farhad Omar, Steven Bushby, Lisa Ng
 Dustin Poppendieck, Tania Ullah, and Brian Dougherty
 National Institute of Standards and Technology
 vance.payne@nist.gov

Jiazhen Ling, Ph.D.
 Prof. Reinhard Radermacher, Ph.D.
 Center for Environmental Energy Engineering, University of Maryland
 raderm@umd.edu
 jiazhen@umd.edu

December 2015



International Energy Agency

Heat Pumping Technologies

Imprint



Van D. Baxter
Building Equipment Research Group
Building Technologies Research & Integration Center
Energy and Transportation Science Division
Oak Ridge National Laboratory
P.O. Box 2008, Building 3147
Oak Ridge, TN 37831-6070
Tel: 865-574-2104
Fax: 865-574-9338
E-mail: baxtervd@ornl.gov
Internet: <http://web.ornl.gov/sci/buildings/>



Jiazhen Ling, Ph.D.
Prof. Reinhard Radermacher, Ph.D.
University of Maryland
Department of Mechanical Engineering
Center for Environmental Energy Engineering (CEEE)
4164 Glenn L. Martin Hall
College Park, Maryland 20742
Tel: 301-405-5286
E-mail: raderm@umd.edu
jiazhen@umd.edu
Internet: <http://www.enme.umd.edu/>



W. Vance Payne, Ph.D.
National Institute of Standards and Technologies NIST
HVAC&R Equipment Performance Group
Energy and Environment Division
100 Bureau Drive Stop 8631
Bldg. 226, Rm. B118
Gaithersburg, MD 20899-8631
Tel: 301-975-6663
Fax: 301-975-8973
E-mail: vance.payne@nist.gov
Internet: http://nist.gov/el/building_environment/hvac

IEA HPT Annex 40

IEA HPP Annex
Heat pump concepts **40** Nearly Energy Buildings

IEA HPT Annex 40 is a corporate research project on heat pump application in Nearly Zero Energy Buildings. The project is accomplished in the Heat Pumping Technologies (HPT) Programme of the International Energy Agency (IEA).
Internet: <http://www.annex40.net>



Abstract

The IEA HPT Annex 40 "Heat pump concepts for Nearly Zero Energy Buildings" deals with the application of heat pumps as a core component of the HVAC system for Nearly or Net Zero energy buildings (nZEB). This report covers Task 2 on the system comparison and optimisation and Task 3 dedicated to the development of adapted technologies for nZEB and field monitoring results of heat pump systems in nZEB.

In the US team three institutions are involved and have worked on the following projects:

- The Oak Ridge National Laboratory (ORNL) will summarize development activities through the field demonstration stage for several integrated heat pump (IHP) systems – electric ground-source (GS-IHP) and air-source (AS-IHP) versions and an engine driven AS-IHP version. The first commercial GS-IHP product was just introduced to the market in December 2012. This work is a contribution to Task 3 of the Annex.
- The University of Maryland will contribute a software development project to Task 2 of the Annex. The software ThermCom evaluates occupied space thermal comfort conditions accounting for all radiative and convective heat transfer effects as well as local air properties.
- The National Institute of Standards and Technology (NIST) is working on a field study effort on the NIST Net-zero Energy Residential Test Facility (NZERTF). This building was constructed on the NIST campus and officially started operating in the summer 2013. During the first year, between July 2013 and June 2014, baseline performance of the NZERTF was monitored under a simulated occupancy protocol. The house was equipped with an air-to-air heat pump which included a dedicated dehumidification operating mode. Outdoor conditions, internal loads and modes of heat pump operation were monitored. Field study results with respect to heat pump operation are reported and recommendations on heat pump optimization for a net-zero energy building are provided. This work is a contribution to Task 3 of the Annex.

US technical contributions related to Task 4 of Annex 40 will mostly be related to the work under IEA HPT Annex 42 entitled heat pumps in smart grids.

Contents

- Imprint**..... 2
- Abstract**..... 3
- Contents**..... 4
- 1 Overview of US Contributions in Annex 40 5
 - 1.1 Background of nZEB and developments in the USA..... 5
 - 1.2 Overview of US contributions 7
- 2 Task 2 – Development of ThermCom Software 10
 - 2.1 System layout and boundary conditions10
 - 2.2 Explanation of the ThermCom design tool.....11
 - 2.2.1 General Introduction on Thermal Comfort11
 - 2.2.2 Background of Reduced Order Method for Indoor Air Flow Field Prediction13
 - 2.3 Case studies for the system design in nZEB15
 - 2.3.1 Case Study I: Radiative Panel Heat Exchanger System15
 - 2.3.2 Case Study II: Induction Air Supply Unit.....21
 - 2.3.3 Case Study III: Comparison of Ducted System and Ductless System.....26
 - 2.4 Recommendations on system layout in nZEB36
- 3 Task 3 - Developments of Integrated Heat pumps..... 38
 - 3.1 Background of the IHP Development38
 - 3.2 Variants of the IHP layout.....42
 - 3.2.1 Summary of GS-IHP system development, analyses, and test results.....42
 - 3.2.2 Electric AS-IHP system development, analyses and test results52
 - 3.2.3 Gas engine driven AS-IHP system development summary.....63
- 4 Task 3 – Test Facility for nZEB Technologies..... 72
 - 4.1 Background: Net Zero Energy Residential Test Facility, Gaithersburg, MD USA....72
 - 4.1.1 Objectives for the NZERTF72
 - 4.1.2 Building Characteristics.....72
 - 4.1.3 Thermal and Electrical Load Profiles77
 - 4.1.4 Data Acquisition, Control Systems and Uncertainty.....84
 - 4.1.5 NZERTF Electrical Systems.....89
 - 4.1.6 Cost of NIST NZERTF.....91
 - 4.2 Experience with the NZERTF97
 - 4.2.1 NZERTF Energy Efficiency Results.....97
 - 4.2.2 Indoor Air Quality and Comfort.....107
 - 4.3 Conclusions of field experience with the NZERTF110
- 5 Conclusions and Outlook.....112
 - 5.1 ThermCom Software112
 - 5.2 Integrated Heat Pump (IHP) systems112
 - 5.3 NIST NZERTF future research and investigations113
- 6 National Publications in IEA HPT Annex 40.....114
- 7 Literature.....115
- Acknowledgements119

1 OVERVIEW OF US CONTRIBUTIONS IN ANNEX 40

1.1 Background of nZEB and developments in the USA

As documented in the U.S. Task 1 report for Annex 40 (Baxter and Sikes 2013) the United States is committed to reducing energy consumption in new and existing buildings and has set aggressive goals for doing so. The U.S. Department of Energy (DOE) Building Technology Office (BTO) has set a strategic goal to develop and demonstrate by 2020 how cost-effective strategies can reduce building energy use by 50%, for both new and existing homes, compared to a 2010 baseline (Risser 2013). Furthermore, Presidential Executive Order 13514 stated that the federal government must lead by example when it comes to the design, construction, maintenance, and operation of high performance sustainable building in sustainable locations. A key element of achieving these and other goals is to develop appliances, including heat pumps that are as efficient as possible.

Government-sponsored programs and non-profit organizations, such as ENERGY STAR and LEED, have played a pivotal role in developing certifications and rating systems in the United States that aid homeowners and contractors in building and retrofitting low energy, high performance buildings. As demand for nearly- and net-zero energy buildings (nZEB) continue to ramp up, guidance from the programs, especially with regards to individual components and appliances incorporated into the building, will likely increase.

Market Status of nZEB in US. Green building practices that would be implemented into nZEBs (e.g., high-efficiency HVAC systems, solar photovoltaic systems, glazing systems) have become more prevalent in new building construction in recent years, largely due to consumer incentive programs and the introduction of stricter government regulations. The states of California, Massachusetts, and Oregon are among the most proactive in regards to strategic plans and policies for nZEB developments. Although the market is growing, nZEBs currently comprise only a small fraction of the overall building construction industry in the United States. However, they are no longer constrained to just “demonstration” homes. The following sections summarize the 2012 commercial and residential nZEB-like building market status in the U.S. as reported by Baxter and Sikes (2013).

Commercial buildings. As part of a 2012 research report published by New Buildings Institute, the Zero Energy Commercial Building Consortium, and NASEO, the number and location of existing zero-energy commercial buildings were examined. Out of a total of 99 buildings identified in the United States, 21 were “zero energy buildings” (ZEB) (see Figure 1.1), 39 were ZEBs under construction or had limited data to verify zero energy performance, and 39 were classified as “zero energy-capable” (ZEC) buildings, meaning they could be zero energy if final steps were taken to implement on-site renewable generation. The assessment also concluded that the location of commercial ZEBs was quite diversified across climate zones (New Buildings Institute 2012).

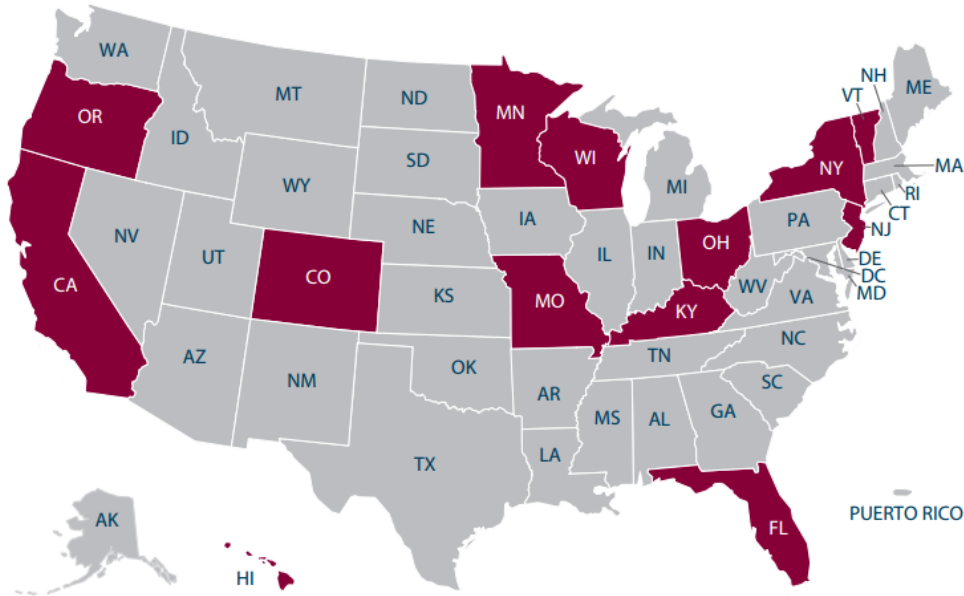


Fig. 1.1. Geographic Distribution of 21 Current Commercial ZEBs Considered in New Buildings Institute Study (2012)

While most existing commercial ZEBs are small buildings, less than 1,400 m² (15,000 ft²), projects are expanding in size and building type, including office buildings and K-12 schools. This conclusion is supported by combining the New Buildings Institute study's ZEBs with the ZECs for a total of 60 projects and observing the breakdown of building types shown in Table 1.1.

Table 1.1. Breakdown of Combined ZEB and ZEC Building Types in New Buildings Institute Study (2012)

Type	Size (total square feet)						Total
	1k - 5k	5k - 10k	10k - 25k	25k - 50k	50k - 100k	> 100k	
Assembly	6	4	5	2			17
Higher Ed	2		4	1			7
K-12		1	1		6	2	10
Mixed-Low Use	2		1				3
Multi-Family		2	1			1	4
Office	1	2	3		1	1	8
Office-Mixed	1	2	3	2			8
Other	1		1		1		3
Total	13	11	19	5	8	4	60

Residential buildings. In the U.S. the most recognizable high-efficiency home market indicator is the ENERGY STAR program (<http://www.energystar.gov/>) for new homes (Energy Star 2013a). Maximizing the energy efficiency of a home (or any building) is important to facilitate reaching the nZEB performance level. Recent estimates of cost and energy savings for the latest (Version 3) ENERGY STAR home criteria indicate that monthly

energy cost savings can exceed investment costs by 5-65% depending on U.S. location (Energy Star 2013b). To date, over 1,435,000 ENERGY STAR-certified homes have been built, including more than 101,000 built in 2012. According to ENERGY STAR, the construction of these 101,000 new homes is the equivalent of:

- Eliminating the emissions from nearly 50,000 vehicles,
- Saving nearly 140 million kg (300 million pounds) of coal,
- Planting nearly 33,000 ha (82,000 acres) of trees, and
- Saving the environment 267 million kg (587 million pounds) of CO₂.

An average national market presence of ENERGY STAR certifications in the new homes sector reached 26% in 2011. The market index compares the number of ENERGY STAR-certified homes built to the number of new privately owned single-family homes permitted in each state and the District of Columbia. In 2008, 15 states had exceeded the average ENERGY STAR Certified New Homes Market Index of 26%, with Arizona topping the list at 54% (U.S. EPA 2013). As shown in Figure 1.2, Texas had the largest overall number of new ENERGY STAR certified homes with almost 30,000 followed by North Carolina and Arizona with more than 5,000 each.

2011 ENERGY STAR Certified New Homes Market Indices for States

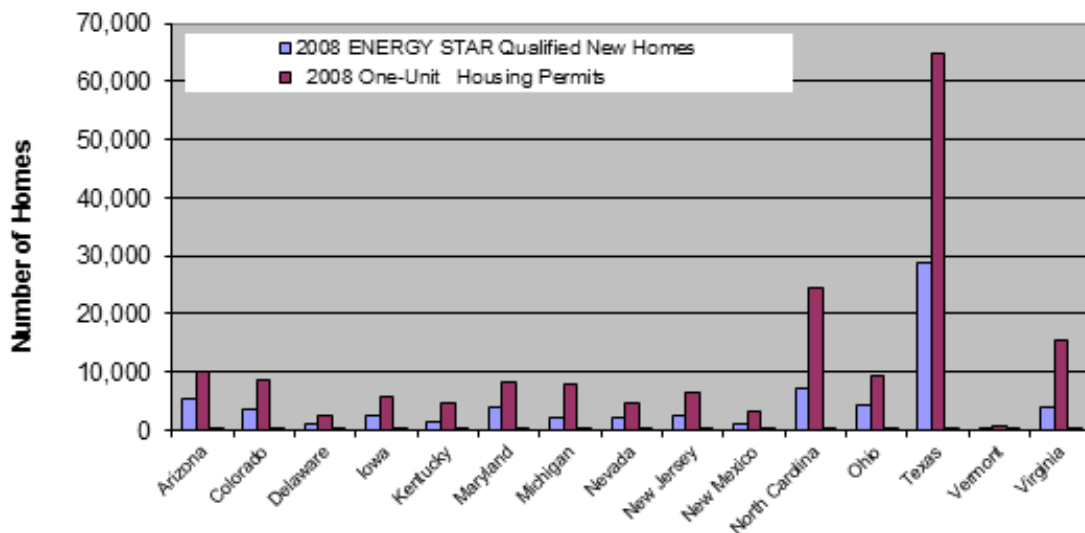


Fig. 1.2. States with an ENERGY STAR Certified New Homes Market Index of 26% or More

1.2 Overview of US contributions

The United States contributions to the Annex work are primarily to Tasks 2 and 3. Detailed summaries of the contributions are presented in the following three sections of this report.

- Task 2: Assessment of system technology: Professor Reinhard Radermacher, Dr. Jiazhen Ling, Professor Yunho Hwang, and Dr. Vikrant Aute at the University of Maryland have been leading the development of the ThermCom software package. ThermCom is primarily a thermal comfort model, but it is designed to facilitate design of more efficient heating and cooling distribution systems enabling a heat pump to operate with the lowest temperature lift possible thereby improving its system efficiency and reducing energy use. Section 2 of the report describes the development in some detail and presents Case studies of three different thermal distribution system concepts.
- Task 3: Technology development and field monitoring:

- Van Baxter and a team from Oak Ridge National Laboratory (ORNL) and several manufacturer and other private sector partner companies have been engaged in development of a number of integrated heat pump (IHP) concepts through field evaluation stage. Development status to-date of electric-driven ground-source and air-source IHP systems and a gas engine driven air-source IHP is reported in Section 3.
- Dr. Vance Payne and a team from the National Institute of Standards and Technology (NIST) have designed and constructed a 252 m² (2,715 ft²) Net Zero Energy Residential Test Facility (NZERTF) on the NIST campus in Gaithersburg, Maryland. (See Figure 1.3 for an overview of NZEB features in the NIST test residence.) Section 4 of the report provides a detailed summary of the NZERTF design, first year test results, and future research for this facility.

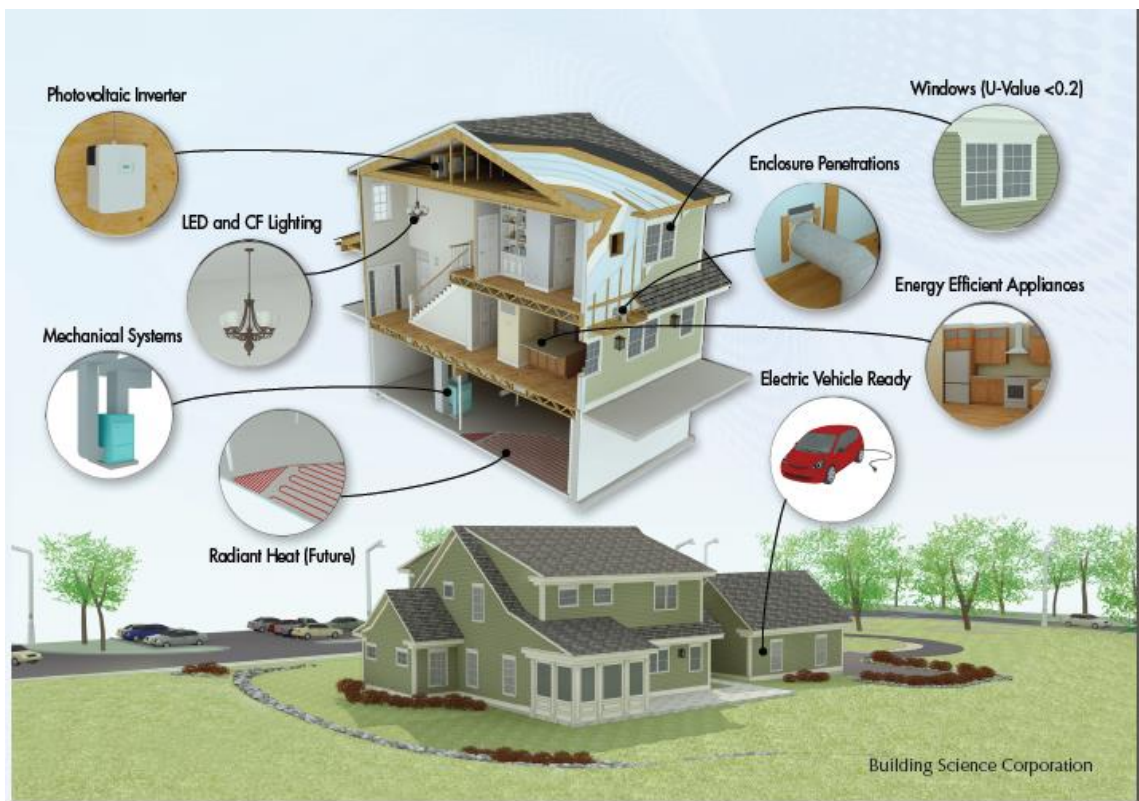


Fig. 1.3. Overview of Key NZEB Features at the NIST NZERTF (NIST 2012)

Task 4: Integration of nZEB into the Energy System: The US did not contribute directly to this Annex 40 Task. However we are also a Participant of HPT Annex 42 (Heat Pumps in Smart Grids). The US Annex 42 Task 1 report (Baxter et al 2014) provides a summary of the status of US energy grids (electric and gas), a brief review of Smart Grid projects underway in the US, and a brief review of the Smart-Grid-readiness of current US heat pump products. One of the major activities underway vis-à-vis heat pumps are the efforts of the Air-Conditioning, Heating, and Refrigeration Institute (AHRI) to establish standard practices for utility demand response performance and communication specifications for smart or connected variable capacity unitary HVAC equipment (including heat pumps). They first established a working group (the Smart or Connected Equipment Ad Hoc Committee) in late 2011 following DOE's August 5, 2011 request for information (RFI) regarding the treatment of smart appliances and equipment in future energy conservation standards and test procedures within DOE's appliance standards program, as well as in the test procedures for the ENERGY STAR Program. The Ad Hoc group noted a number of critical requirements for "smart" systems and equipment manufactured by AHRI member companies. Among these are 1) system owners must have capability to override demand response (DR)

requests received from the grid; and 2) grid/equipment communication standards will be needed to enable the equipment to communicate its demand response capabilities to the utility and to enable utilities to design meaningful DR programs. The recommendations of the Ad Hoc group were compiled in a white paper issued in 2013 (AHRI 2013). Subsequently a proposed framework document was issued in 2014 (AHRI 2014) to establish an AHRI Standard on performance and communication specifications for smart/connected variable capacity equipment. A technical committee has been established to draft this standard.

2 TASK 2 – DEVELOPMENT OF THERMCOM SOFTWARE

2.1 System layout and boundary conditions

The following sections in this report focus on applying computational fluid dynamics (CFD) and reduced order method to conduct thermal comfort analysis of different air conditioning/heat pump systems. Detailed system layouts will be presented in the case study sections.

The first system is radiative panels. This system is similar to chilled beam and heated floor system products. A heated or chilled working fluid, typically water, flows at the back of aluminum panels through serpentine shaped plastic tubes. Copper tubes can also be used but it costs more. The purpose of those tubes is to make the aluminum panel have a uniform surface temperature that is capable of providing sensible cooling/heating to the space. It should be noted that, those panels are not meant to provide dehumidification because this will result in condensation on the heat exchanger surface. The heat exchanger utilizes radiation and natural convection to deliver cooling/heating. The main advantage of this heat exchanger compared with chilled beam/heated floor systems is ease of installation. There is no need to open the floor or ceiling to install the heat exchanger. It can be hung against a wall and is capable of effectively delivering both heating and cooling.

The second system is called induction air supply unit. It is typically installed in the ceiling. Fresh air is supplied through the middle of the unit. Due to the bernoulli law, the flow of fresh air will result in a negative pressure region. Therefore, room air can be induced into the supply and mixes with the conditioned fresh air. An optimum mass ratio of fresh air to induced air is around 40-60. Due to the induction process, fan power is reduced. The mixing process also preheats/precools the fresh air supply making it more thermally comfortable to occupants. The air supply unit has a relatively larger surface area to allow for a comfortable air velocity. This also prevents draught being created underneath the supply unit.

The third thermal comfort study focuses on the thermal comfort comparison between ducted and ductless air distribution systems. In North America, centrally ducted air systems predominate for residential space heating and cooling distribution. While in East Asia, ductless systems dominate the residential market. Due to the complication of the two systems and time frame of the report, the reduced order method was not applied to this comparison. Only CFD calculations are provided.

Except for the radiant heat exchanger case, the air outlet for each case is modeled as the velocity inlet boundary condition. For the last two systems, supply air is added to the space. In order to ensure the mass balance and avoid over-pressurize the space, an undercut is added in the model as the discharge air outlet. It is assumed to be located underneath the door. The undercut is modeled as a pressure outlet condition. For the walls, floor and ceiling, they are modeled as a prescribed temperature boundary condition. It is more common to use adiabatic boundary condition, but in order to calculate the mean radiant temperature, surface temperature has to be known. For all models, internal heat source is added to balance the cooling/heating from supply air. For the first two cases, solar radiation through the window is modeled as a constant heat flux boundary condition.

2.2 Explanation of the ThermCom design tool

2.2.1 General Introduction on Thermal Comfort

Energy saving has been a heated topic for air-conditioning/heat pump systems. However, the ultimate purpose of having those systems is to create a thermally comfortable environment for building occupants. Different people may have different thermal sensations for the same environment and therefore thermal comfort is a subjective matter. Nevertheless, numerous literatures have been dedicated to the study of indoor thermal comfort. In 2004, ASHRAE released Standard 55-2004, Thermal Environmental Conditions for Human Occupancy (ASHRAE 2004), to specify the combinations of indoor thermal environmental factors and personal factors that will produce thermal environmental conditions acceptable to a majority of the occupants within the space. An index called the predicted mean vote (PMV) is used to measure a large group of persons' thermal sensation on a seven-level scale which uses +3 to be hot and -3 to be cold. Table 2.1 lists the detailed definition of the PMV index. The seven-level scale is usually enough to describe the thermal sensation in building applications, however higher numbers than 3 and lower numbers than -3 are also found in some literature to describe thermal sensation in extreme conditions, such as the cabin of a car parked in direct sunlight in summer for a long time.

Table 2.1. Thermal sensation based on PMV scale

PMV scale	Thermal sensation
+3	hot
+2	warm
+1	slightly warm
0	neutral
-1	slightly cool
-2	cool
-3	cold

Six primary factors - metabolic rate (met), clothing insulation (clo), air dry-bulb temperature, radiant temperature, air speed and humidity - are included in the standard when defining conditions for thermal comfort. Besides the primary factors, there are a number of other secondary factors affecting comfort in some circumstances. Figure 2.1 plots two thermal comfort zones on a psychrometric chart. Compared with other conventional psychrometric chart, the x-axis in the figure represents operative temperatures instead of dry-bulb temperatures. It is because the operative temperature takes both the dry-bulb temperature and the radiant temperature into consideration. The operative temperature can be calculated from Eq. (2.1). Two different thermal comfort zones are plotted for summer and winter because clothing insulation is different. The boundaries of these two zones are determined by using Eq. (2.2) and Eq. (2.3), which calculate the maximum and minimum operative

temperature ranges of the comfort zones. There is no unanimous agreement on what should be the low side comfort range of humidity, but ASHRAE suggests it should be higher than 2 kg/kg dry air. Air speeds greater than 0.2 ms^{-1} (40 ftmin^{-1}) may be used to increase the upper operative temperature limit for the comfort zone in certain circumstances

$$t_o = \frac{h_r t_r + h_c t_a}{h_r + h_c} \quad (2.1)$$

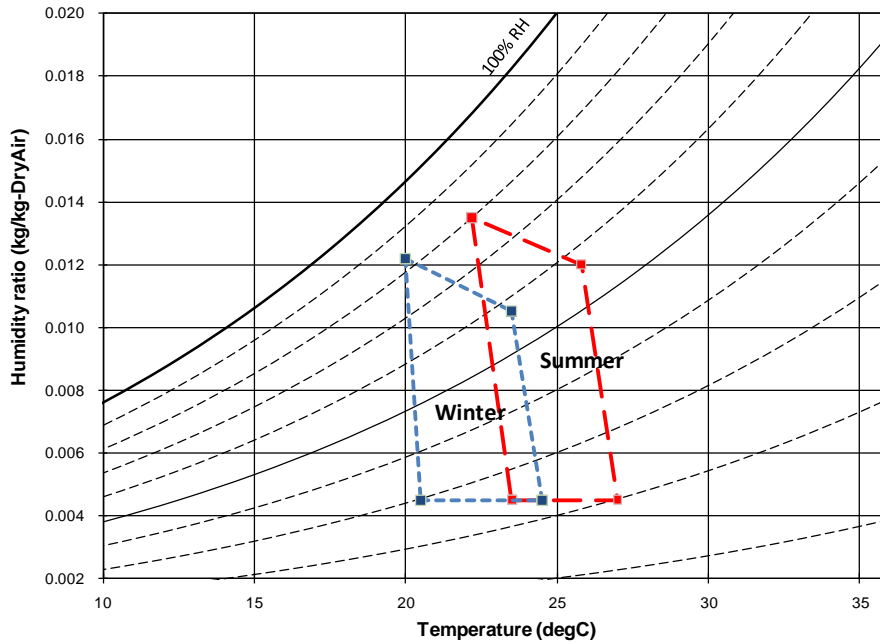


Fig. 2.1. ASHRAE thermal comfort zones for winter and summer

$$T_{min, I_{cl}} = [(I_{cl} - 0.5 \text{ clo}) T_{min, 1.0 \text{ clo}} + (1.0 \text{ clo} - I_{cl}) T_{min, 0.5 \text{ clo}}] / 0.5 \text{ clo} \quad (2.2)$$

$$T_{max, I_{cl}} = [(I_{cl} - 0.5 \text{ clo}) T_{max, 1.0 \text{ clo}} + (1.0 \text{ clo} - I_{cl}) T_{min, 0.5 \text{ clo}}] / 0.5 \text{ clo} \quad (2.3)$$

Where

$T_{max, I_{cl}}$ is the upper operative temperature limit for clothing insulation I_{cl}

$T_{min, I_{cl}}$ is the lower operative temperature limit for clothing insulation I_{cl}

I_{cl} is the thermal insulation of the clothing in question (clo)

Besides ASHRAE Standard 55-2004, the International Standards Organization (ISO) has also established a set of standards to address the thermal comfort issue. ISO standard 7730: 2005, Ergonomics of the thermal environment—Analytical determination and interpretation of thermal comfort using calculation of the PMV and PPD indices and local thermal comfort criteria, describes the PMV (Predicted Mean Vote) and PPD (Predicted Percentage Dissatisfied) indices and specifies acceptable conditions for thermal comfort. ISO 8996:2004, Ergonomics of the thermal environment—Determination of metabolic rate, describes six

methods for estimating metabolic heat production, which are divided into three levels according to accuracy. ISO 9920:2007, Ergonomics of the thermal environment—Estimation of thermal insulation and water vapor resistance of a clothing ensemble, provides an extensive database of the thermal properties of clothing and garments. The properties are based upon measurements on heated manikins where basic (or intrinsic) thermal insulation is measured as well as vapor permeation properties of garments and ensembles.

2.2.2 Background of Reduced Order Method for Indoor Air Flow Field Prediction

To effectively and accurately model indoor thermal comfort, one has to be able to simulate both the mean radiant temperature (MRT) field and the air temperature field. The combination of those two defines the operative temperature as mentioned in the previous section. MRT field modeling requires every surface temperature and view factors between the surfaces and object as inputs. The view factor calculation can be very challenging to calculate especially for irregular surfaces. However, once the room can be simplified to regular walls and no obstacles between walls and occupants, the simulation of indoor radiant temperature field is very straightforward.

The air temperature field modeling on the other hand can be computationally intense. In order to obtain the indoor air temperature field, the CFD method is typically adopted. This method solves the equation set of continuity, momentum and energy equations. Due to the relatively large room scale, the CFD model is typically resulted in a fairly large amount of mesh size. It, therefore, may take hours for CFD to render a solution.

In order to save the computation cost of CFD simulation, a reduced-order method is favored. One common reduced order model is using simple linear curve fitting technique. It is capable of saving a great amount of computation time. Although this method is typically able to capture the general trend of the air temperature field, the method's physical mechanisms are incomplete and it lacks predictive capability (Rambo J., 2006). Therefore, it is useful to develop a new simulation method that requires less computation time compared to CFD simulation and has the capability to make prediction of temperature field in different settings.

Proper orthogonal decomposition (POD) was chosen as the reduced-order simulation methodology to replace the above linear curve fitting. The POD method was first introduced by John Lumley (Berkooz et al. 1993). In other disciplines the same method was called Karhunen-Loève decomposition or principal components analysis. It has several advantages as pointed out by Berkooz et al. (1993). (1) It is statistically based; extracting data from experiments and simulations. (2) Its analytical foundations supply a clear understanding of its capabilities and limitations. (3) It permits the extraction of the results.

In short, the method seeks to decompose a large degree of freedom system into a series expansion:

$$v(x,t) = \sum_{i=1}^m a_i(t)\phi_i(x) \quad (2.4)$$

where v can be any studied variable, such as velocity, temperature, etc.

ϕ is a family of modal basis of v .

a is the coefficient for the expansion, usually a function of time.

The search for good bases is the first step of constructing the expansion. A good set of bases makes the expansion efficient in terms of minimizing m . In order to make the basis to be optimal, it is equally the problem of finding a set of basis that is "most similar" to v . This can be explained from Figure 2.2. Assuming u is the vector to be decomposed while ψ_1 , ψ_2 and

ψ_3 are the different candidates of POD basis φ , neither ψ_1 or ψ_2 can represent u unless additional bases were introduced to offset their horizontal components. For ψ_3 , it is most similar to u in the sense that no additional basis is necessary. Only a coefficient is needed to adjust the magnitude of ψ_3 to match u .

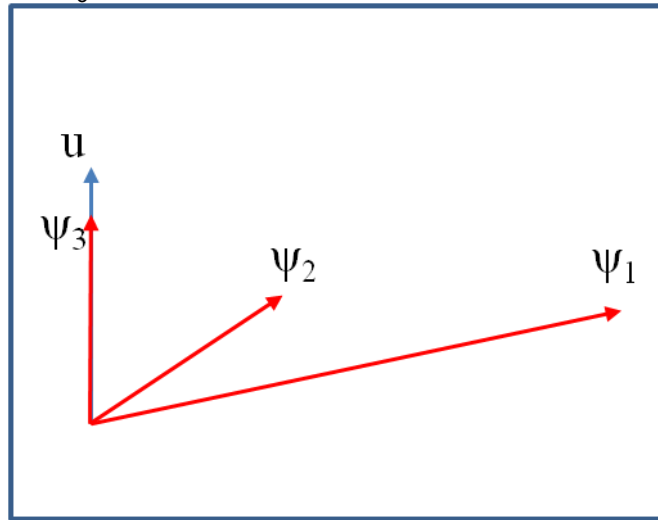


Fig. 2.2. Indication of the search for the optimum basis of u

Thus, it is the same problem as to solve the following equations and to find φ :

$$\max \frac{|(v, \psi)|^2}{(\psi, \psi)} = \frac{\langle |(v, \varphi)|^2 \rangle}{(\varphi, \varphi)} \quad (2.5)$$

The parentheses in the equation represent inner products. When the v and ψ are in the same direction the inner product of the two reaches maximum. If those two are perpendicular to each other, the inner product reduces to zero.

In some literatures, it is also common to use the following expression. One of the advantage of this expression is to produce normalized basis:

$$\max \langle |(v, \varphi)|^2 \rangle - \lambda(|\varphi|^2 - 1) \quad (2.6)$$

It is essential to have a restriction on the normalization in this extreme calculation. In Figure 2.2, ψ_3 is the worst basis of the three, however, without the normalization, it still can be the maximum of inner product due to its large magnitude.

For simplicity, several steps of extreme computing are skipped. For those who are interested in them, please refer to the spectral theory (Riesz and Nagy, 1990).

It turns out that the base functions (φ) are the eigenfunctions of the integral equation (Hung and Tran, 1999):

$$\int C(x, x') \varphi(x') dx' = \lambda \varphi(x) \quad (2.7)$$

where the kernel C is given by:

$$C(x,x') = \frac{1}{N} \sum_{i=1}^N v_i(x)v_i(x') \quad (2.8)$$

Therefore, in short, the search for POD bases can be divided into two steps: construction of the kernel C and calculation of eigenvectors of the C .

Before we start to apply the POD to our air temperature simulation, two questions remain to be answered. How can one guarantee that the series of expansion covers the entire span of u ? How can one prove that the series of expansion is the optimal one?

Completeness

By observing the kernel C , it is clear that the matrix is non-negative. Therefore, all the eigenvalues must be non-zero, i.e., $\lambda_i \geq 0$. Those eigenvectors corresponding to zero eigenvalues do not contribute to the entire kinetic energy of the space. The entire system space is hence reduced to be only formed by eigenvectors corresponding to eigenvalues. There is no piece of information of u missing from the process. More detailed explanation can be obtained from the propositions 2.1 and 2.2 in Berkooz et al. (1993).

Optimality

The POD basis set is optimal for modeling or reconstructing v . Proposition 2.3 in Berkooz et al. (1993) was considered as the basis to the claim.

Proposition 2.3: Let $v(x,t)$ be an ensemble member square integrable on Ω for almost every t and $\{\varphi_i, \lambda_i\}$ be the POD orthonormal basis set with associated eigenvalues. Let

$$v(x,t) = \sum_i a_i(t)\varphi_i(x) \quad (2.9)$$

be the decomposition with respect to this basis, where equality is almost everywhere. Let $\{\psi_i\}$ be an arbitrary orthonormal set such that

$$v(x,t) = \sum_i b_i(t)\psi_i(x) \quad (2.10)$$

Then the following holds:

1. $\langle a_i(t)a_j^*(t) \rangle = \delta_{ij}\lambda_i$, i.e. the POD coefficients are uncorrelated.
2. For every n we have $\sum_{i=1}^n \langle a_i(t)a_i^*(t) \rangle = \sum_{i=1}^n \lambda_i \geq \sum_{i=1}^n \langle b_i(t)b_i^*(t) \rangle$

This implies that, among all linear decompositions, this is the most efficient in the sense that, for a given number of modes the projection on the subspace used for modeling will contain the most kinetic energy possible in an average sense. In additional, the time series of the coefficient $a_i(t)$ are uncorrelated.

2.3 Case studies for the system design in nZEB

2.3.1 Case Study I: Radiative Panel Heat Exchanger System

In a vapor compression system, as the temperature difference between heat absorption and heat rejection processes decreases, the coefficient of performance (COP) of the system generally increases. It is caused by the fact that the reduced temperature difference helps decrease the pressure lift of the compressor thus decreasing the power input to the compressor. To reduce the temperature lift, one can increase the evaporating temperature or decrease the condensing temperature or both. However, for conventional vapor compression air-conditioning systems there is an upper limit to which one can increase the evaporating

temperature so as to maintain sufficient dehumidification. Use of separate sensible and latent cooling technology (SSLC) can eliminate this restriction (Ling *et al.*, 2010). Despite the encouraging energy savings reported in the literature, the design of the indoor heat exchanger (HX) in the SSLC system remains a challenge. As the refrigerant evaporating temperature increases, the supply air temperature usually increases for a given HX. Consequently, the air mass flow rate has to increase to maintain the system capacity. The increased air flow rate leads to an increased fan power consumption and may offset the power savings by the compressor. In short, how to design an indoor HX that minimizes the fan power demand is the challenge. There are various HX designs which address such a challenge, and among those, chilled ceiling panels and heated floor systems are under the most consideration. For both products, the heat transfer mechanism between the working fluid and indoor air is natural convection and radiation, and therefore, the fan power demand is almost zero. Moreover, the enlarged heat transfer area of those products provides radiant cooling or heating to the occupants so that both products may provide better thermal comfort than conventional indoor HXs. However, the installation of the two systems requires an overhaul of the existing ceiling and floor and hence cannot be done without a significant impact to residents (see Figure 2.3). For the purpose of designing a similar product with easier installation, a novel radiative HX is introduced. The radiative HX has a similar structure to the chilled ceiling panels, which include serpentine-shaped tubes fixed on metal sheets. The tubes circulate a working fluid such as water that serves the as heating/cooling source and conducts heat to/from the metal sheets. The metal sheets condition the space air through both natural convection and radiation. An attractive feature of the radiative HXs is that instead of installing them over the ceiling or under the floor, the HX can be simply installed against walls (see Figure 2.4). This installation method has a two-fold benefit: easier installation and capability of providing both heating and cooling. This section discusses the modeling of the radiative HXs so that it can be used as a tool to evaluate the thermal comfort in a zone equipped with such HXs.



Fig. 2.3. Picture of piping for heated floor system during installation (Olesen, 2011)



Fig. 2.4. Picture of the radiative HX installed in an office setting

Radiative HX Thermal Comfort Modeling

The objective of the simulation tool development is to evaluate the thermal comfort condition of a space conditioned by a radiative HX system. In the modeling, the radiative HX is assumed to control the temperature of the entire wall being installed. The modeling includes two major efforts: the simulation of operative temperature (OT, or t_o) field and the evaluation of ASHRAE's thermal comfort criteria. According to the ASHRAE standard 55 (2004), OT is a combination of MRT and air temperature. In the case of applying the radiative HX, OT calculation can be simplified as the arithmetic mean of MRT and air temperature (Equation 2.11). The indices Predicted Mean Vote (PMV) and Predicted Percentage Dissatisfied (PPD) are used to quantify the thermal comfort criteria. The following subsections provide detailed discussions of the two aforementioned modeling efforts.

$$\begin{aligned} t_o &= (h_c t_a + h_r t_r) / (h_c + h_r) \text{ for high air velocity} \\ t_o &= (t_a + t_r) / 2 \text{ for low air velocity} \end{aligned} \quad (2.11)$$

Figure 2.5 describes the radiation model adopted in the study. The room is assumed to be a rectangular shape with four walls (front wall is not shown), a ceiling and a floor. One wall is assumed to have the radiative HX (left wall in the Figure 2.5). It is assumed that the HX covers the entire wall and is maintained a constant temperature. It should be noted that a later experiment demonstrated a 2K temperature difference between inlet and outlet water flow (Koepke, 2011), therefore the assumption of a constant temperature profile is a simplification of the real case. Other walls may have different temperatures, and so may the ceiling and the floor. The window surface usually has different temperature compared to the wall where it is located, which is mainly due to the solar radiation. Equation 2.12 (Arora, 2000) is then applied to calculate the window temperature. It should be noted that the solar incidence in the equation varies with solar angles and window orientation. Therefore, local solar angles such as solar azimuth angle, solar altitude angle should be identified beforehand. As all surface temperatures (wall temperatures, ceiling and floor temperatures, window temperature etc.) are obtained, the MRT can be evaluated by the summation of the view factors between the occupant and individual surface multiplied by the surface temperature. For simplification, the occupant in the room is simplified to be a sphere. Dunkle (1963) defined the equivalent sphere radius of both a standing person and a sitting person. However, since the sphere's radius is infinitesimal compared with the room dimension, the sphere was further simplified to be a dot. Since occupants can move inside the space, the evaluation of their thermal comfort requires calculation of MRT everywhere inside the space, which means that an MRT field has to be obtained.

$$\alpha_D I_D + A\alpha_d I_d = A[h_i(t_g - t_i) + h_o(t_g - t_o)] \quad (2.12)$$



Fig. 2.5. Adapted model for radiant temperature field

The other component of OT calculation is the air temperature simulation. The technique of computational fluid dynamic (CFD) is utilized for air temperature field simulation inside the space. A commercially-available CFD (ANSYS, 2006) package was chosen for the modeling. As an example to facilitate initial research, a 2D square was assumed to represent the vertical middle inter-section plane of the space. It has one cold side (left side) of 20°C which can be assumed as a case of the radiative HX filled with cold water to provide cooling, and one hot side (right side) of 35°C which can be assumed as a case of hot window by direct solar radiation. The square has a mesh of 240 by 240 quad cells with enhanced mesh density in the boundary layer to capture the complicated flow characteristics. To be specific, the boundary layer has the first row of 1 mm and the growth of 1.15, i.e., the entire depth of the boundary layer is 20 mm. The turbulence model used in the model is k- ω Shear Stress Transport (SST) model. The velocity (streamline) and temperature field are demonstrated in Figure 2.6.

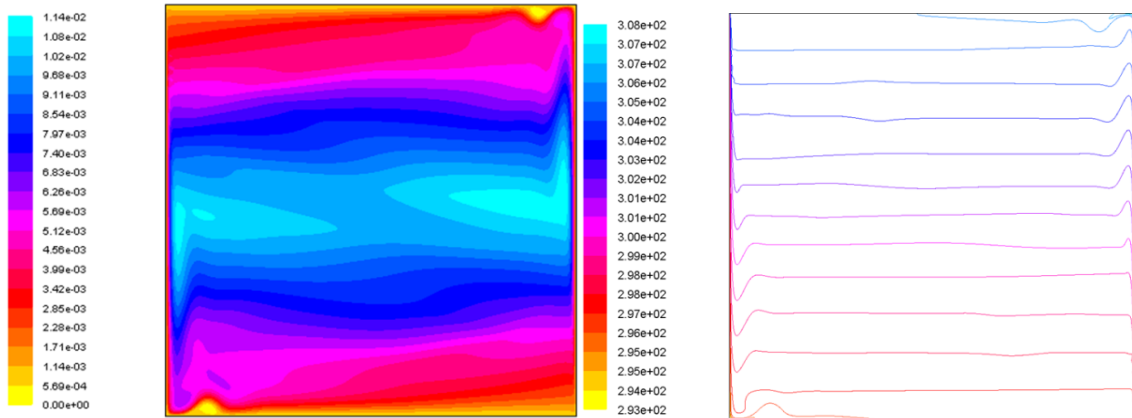


Fig. 2.6. The streamline (velocity, left) and air temperature (right) fields in the studied place

The flow chart of the POD method is shown in Figure 2.7. and Eqn. 2.13.

$$v(x, t) = \sum_{i=1}^m a_i(t)\varphi_i(x) \quad (2.13)$$

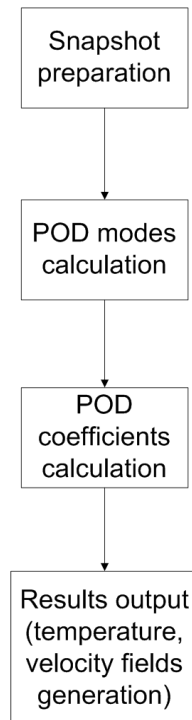


Fig. 2.7. Flow chart of POD method

The basis functions (φ) are the Eigen functions of the integral equation (Ly and Hein, 2001):

$$\int C(x, x')\varphi(x') dx' = \lambda\varphi(x) \quad (2.14)$$

where the kernel C is given by:

$$C(x, x') = \frac{1}{N} \sum_{i=1}^N V_i(x)V_i(x') \quad (2.15)$$

For the current problem, in order to obtain the POD modes for the air temperature field, a technique called “snapshot” was applied to form the matrix C by utilizing the existing CFD simulation results. Nine sets of temperature fields and velocity fields were chosen to form the snapshot. The difference among each snapshot is the different Rayleigh numbers. The CFD software package is used to calculate the eigenvalues of the kernel matrix C. The built-in singular value decomposition (SVD) function was applied to return the eigenvalues and the corresponding eigenvectors. If the eigenvalue is zero meaning that it poses no impact on the system its corresponding eigenvector is neglected. The POD provides the basis of the expansion series. The next step is to find the coefficients in the expansion (Equation 3). A method called Galerkin projection is considered to be a standard approach to obtain the coefficients. The method projects the governing equations on the modal subspace and then solves the governing equations, usually in the form of ordinary differential equations to obtain the coefficients.

PMV and PPD Field Simulation

The previous subsection discusses the simulation of both MRT and air temperature. By simply averaging those two, one can obtain the OT field. However, it is not straightforward to use OT to describe thermal comfort. Therefore, the PMV and PPD fields are also simulated by the software tool. As noted earlier the PMV is a seven-scale system to describe occupant’s thermal sensation from very hot (+3) to very cold (-3). The PPD is its derivative to statistically show what percentage of occupants feel uncomfortable at different PMV scale. Table 2.2 and Figure 2.8 describe the PMV and PPD, respectively, in more detail. To calculate the PMV, Equation 2.16 is used. Most of the many parameters in the equation can be obtained from the ISO standard 7730 (2005). The air temperature and MRT can be calculated by methods summarized in the previous section. The PPD can be calculated based on the Equation 2.17. Figures 2.9 and 2.10 show sample outputs of PMV and PPD from the tool. As shown in the figures, both the left and right sides of the space are affected

by the hot wall and hot window as well as the larger vertical air velocity than that in the middle, so the PMV indices near the walls are between slightly warm and warm. Due to the density difference of air, the cold air remains at the bottom and the hot air remains at the top of the space. Consequently the PMV field shows negative numbers at the bottom and positive numbers at the top of the space. Although the PMV values vary inside the space, most are between -1 and +1 meaning acceptable thermal comfort to most occupants. This is supported by the PPD output, which shows that only a 5% thermal discomfort rate is predicted for most of the space.

$$PMV = [0.303 \cdot e^{(-0.036 \cdot M)} + 0.028] \cdot \{(M - W) - 3.05 \times 10^{-3} \cdot [5733 - 6.99 \cdot (M - W) - p_a] - 0.42 \cdot [(M - W) - 58.15] - 1.7 \times 10^{-5} \cdot M \cdot (5867 - p_a) - 0.0014 \cdot M \cdot (34 - t_a) - 3.96 \times 10^{-8} \cdot f_{cl} \cdot [(t_{cl} + 273)^4 - (t_r + 273)^4] - f_{cl} \cdot h_c \cdot (t_{cl} - t_a)\} \quad (2.16)$$

$$PPD = 100 - 95 \cdot \exp(-0.03353 \cdot PMV^4 - 0.2179 \cdot PMV^2) \quad (2.17)$$

Table 2.2. PMV scale (ISO 7730, 2005)

PMV scale	Thermal sensation
+3	hot
+2	warm
+1	slightly warm
0	neutral
-1	slightly cool
-2	cool
-3	cold

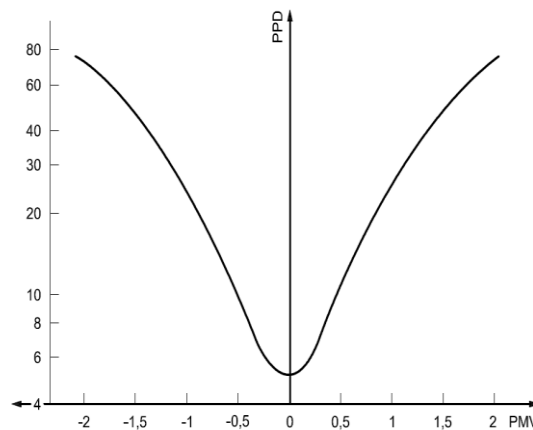


Fig. 2.8. PPD as a function of PMV (ISO 7730, 2005)

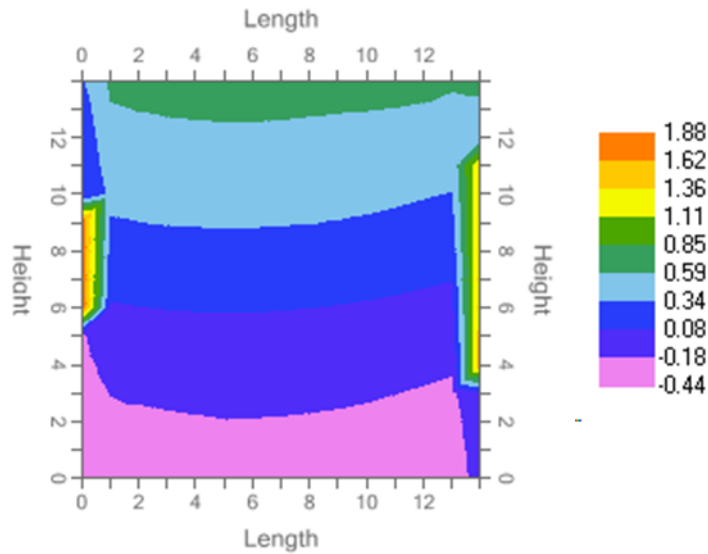


Fig. 2.9. Snapshots of sample PMV output

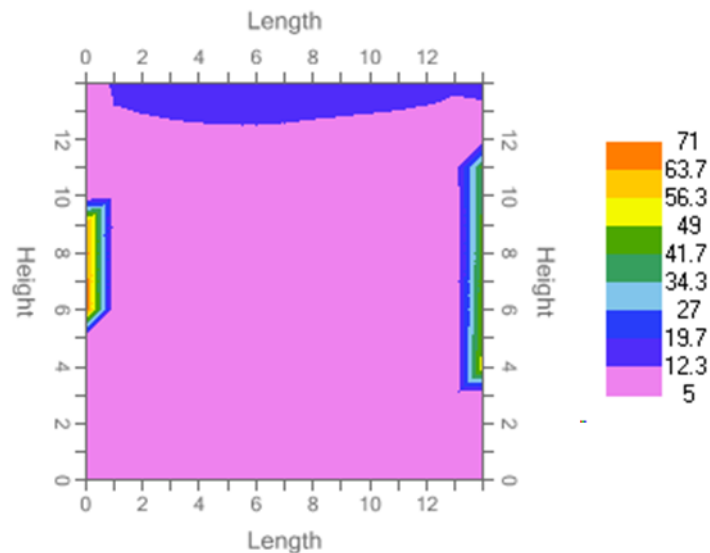


Fig. 2.10. Snapshots of sample PPD output

2.3.2 Case Study II: Induction Air Supply Unit

Introduction

For a heat pump system, the determination of supply air temperature should consider both sensible load and the latent load from space. The refrigerant temperature in the evaporator has to be low enough so that sufficient moisture can be removed. This requires the supply air temperature to be typically lower than the dew point temperature of room air. On the other hand, as the supply air temperature decreases, reheating of the supply air can become necessary to maintain acceptable thermal comfort. The reheat process, if achieved by using an electric heater, will increase the compressor power consumption. An alternative option to obtain the same dehumidification capacity is to increase supply air flow rate. Though this option does not lead to a larger compressor power input, it leads to an increase in fan power consumption.

A novel heat pump system using induced-air supply units is introduced. The schematic of an induced-air unit is shown in Figure 2.11. Fresh air from an air handling unit is sent to the induced-air supply unit. The fresh air has a temperature of 13°C which is lower than that of

traditional units, but because of careful design of heat exchangers (not discussed here for brevity), the evaporating temperature is maintained at 10°C. For the same amount of latent capacity, the 13°C fresh air requires less air flow rate and therefore consumes less fan power. As the fresh air is received from the top, the unit entrains room air through the bottom inlets located at the two sides by induction. Although the fresh air flow is low, the total mixed supply air flow rate is actually higher than that of conventional units. Since the induction does not require any power input, the larger air flow rate does not increase fan power consumption. The amount of induced air is proportional to that of the fresh air supplied and the total air flow is typically made up of 60% room air induced with 40% fresh air supply. The total supply air is sent to the space through the middle part at the bottom of the unit. The surface area of the supply unit is relatively larger than that of conventional outlets (for a rated 300 m³/h supply air flow rate, the unit surface area is 0.3 m²) and the supply air velocity is between 0.2 m/s to 0.9 m/s. The relatively lower air velocity brings the benefit of minimizing the possibility of draught sensations and hence better thermal comfort. Moreover, due to the mixing with room air, the supply air temperature is around 19°C requiring no reheat, and consequently provides occupants with comfortable supply air at no extra fan power penalty.

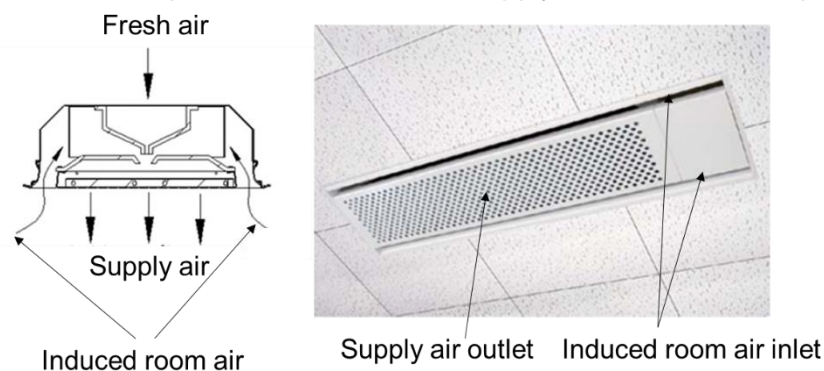


Fig. 2.11. Schematic of induced-air supply unit (left) and the picture of unit after installation (right)

It should be noted that the induced-air supply unit can be used in both heating and cooling cases, and is capable of providing better thermal comfort and lower power consumption compared to traditional systems. However only the thermal comfort analysis is considered in the following sections .

Indoor Air Temperature Calculation

A commercially-available CFD (ANSYS, 2006) package was chosen for the modeling. Several room models with multiple induced-air units are modeled using 3D double precision option. The size of rooms varies depending on the number of supply units. For one- and two-supply cases, the room dimension is 3 m long, 1.5 m wide and 2.7 m high. For three and four supply cases, the room is modeled as 4.5 m long, 3 m wide and 2.7 m high. The supply units are uniformly distributed at the top of the room. Each supply is around 1.1 m in length and 0.6m in width. The CFD mesh size for the smaller room is 500,000 and 1,260,000 for the larger room. Figure 2.12 shows the computational domain for a room with two outlets. The supply unit is modeled as a face with two return air inlets at two sides and supply air outlet in the middle just as shown in Figure 2.11. The Boussinesq assumption (Boussinesq, J., 1897) is applied to enable the simulation of natural convection of indoor air. According to the characteristic length and temperature difference of the model, the Rayleigh number exceeds 10⁹, and therefore the k- ω SST model is enabled as the turbulent viscous model. The conditioned space also receives solar radiation through the outside (window) wall. The solar heat flux is assumed to be 800 W/m². Figures 2.13 to 2.16 show sample results of indoor air temperature profiles and velocity profiles of one supply case at the middle plane of the room in both heating and cooling conditions. The air temperature profile shows a clear stratification due to air density difference, however the temperature difference from floor to a point 1.5

meter high is within 2K. The velocity profile shows a maximum velocity of 0.9 m/s at the supply duct outlet. The bulk air region has a negligible air velocity showing minimal signs of draught. It also can be found that the return air flows back to the supply unit to represent the induction effect.

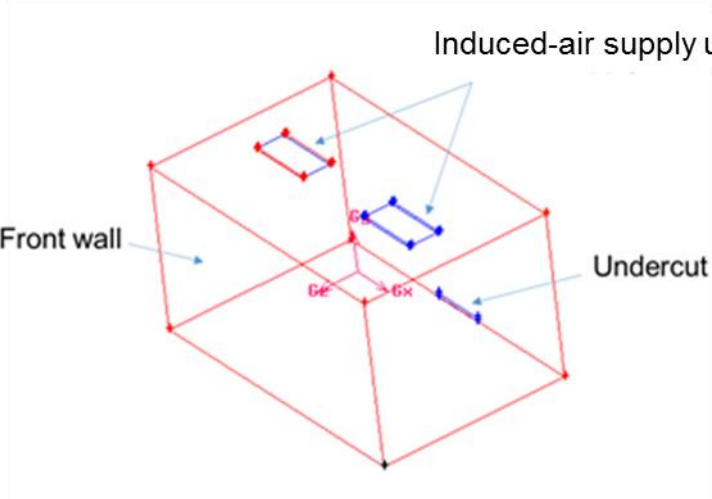


Fig. 2.12. Computational domain for a room with two induced-air supply units

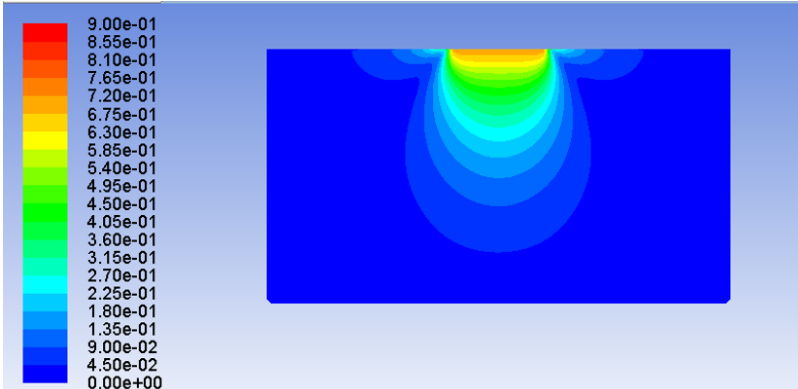


Fig. 2.13. Air velocity (in m/s) profile of one induced-air supply unit (cooling case, middle plane)

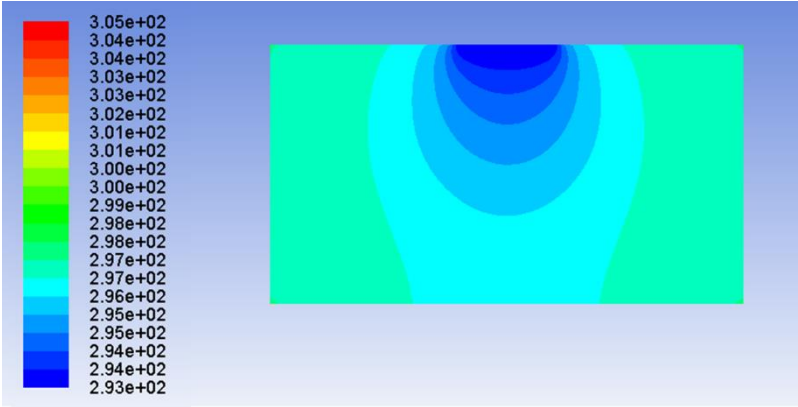


Fig. 2.14. Air temperature (in K) profile of one induced-air supply unit (cooling case, middle plane)

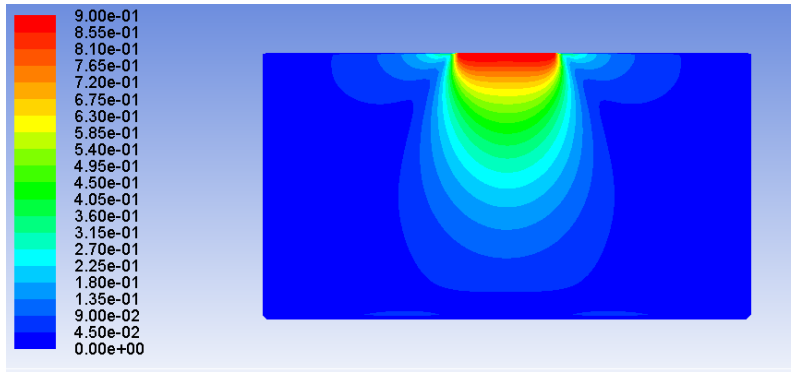


Fig. 2.15. Air velocity (in m/s) profile of one induced-air supply unit (heating case, middle plane)

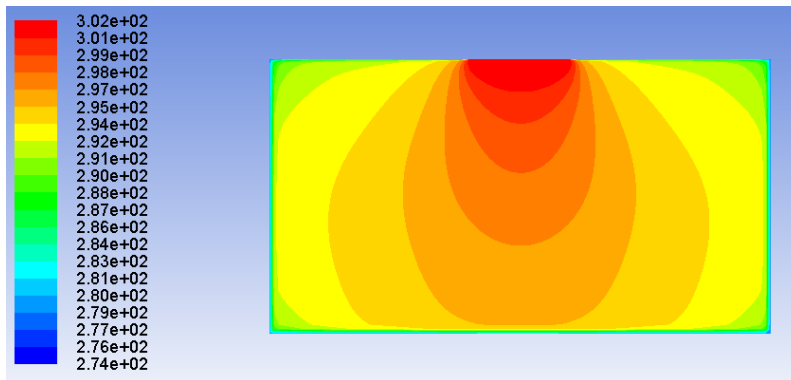


Fig. 2.16. Air temperature (in K) profile of one induced-air supply unit (heating case, middle plane)

Figure 2.17 shows indoor air temperature and velocity profiles in the case of one-supply room. Since it is a reduced-order model, the resolution was downgraded to 16 by 16 by 8. The POD calculation took only ~2 minutes compared to more than 8 hours for a 3D CFD simulation. The significant speed improvement is due because POD conducts interpolation based on CFD snapshots. The validation of the POD model will be discussed in the next section.

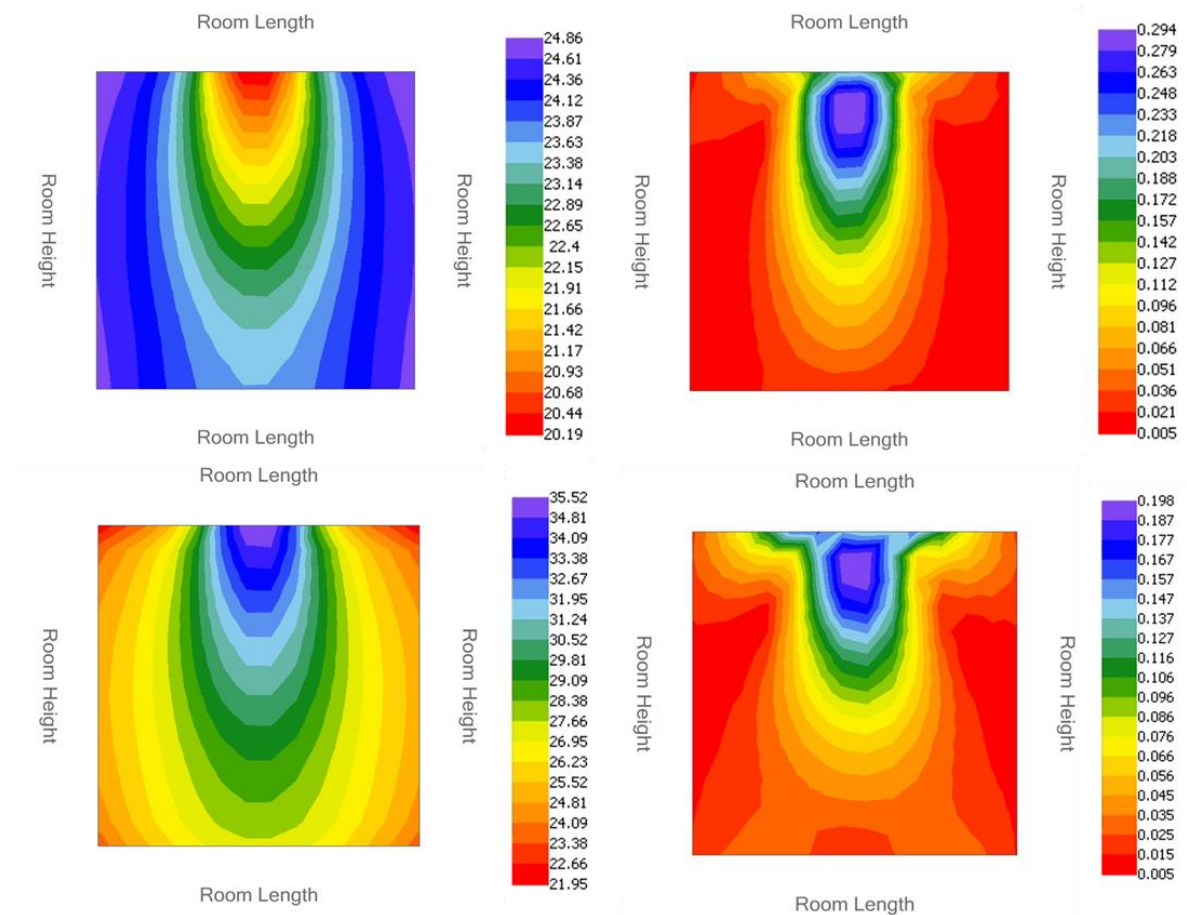


Fig. 2.17. Sample POD results of temperature and velocity profile for the mid-plane - (left top: temperature profile during cooling; right top: velocity profile during cooling; left bottom: temperature profile during heating; right bottom: velocity profile during heating)

Based on the POD outputs of temperature and velocity distributions, the average air temperature and velocity are calculated. The MRT is calculated by using room surface temperatures as well as view angles of the center point in the room to individual surfaces. Figures 2.18 and 2.19 show the PMV and PPD prediction for the room based on one typical weather day in Beijing, China. The typical weather days are defined based on the coldest and hottest days in one year.

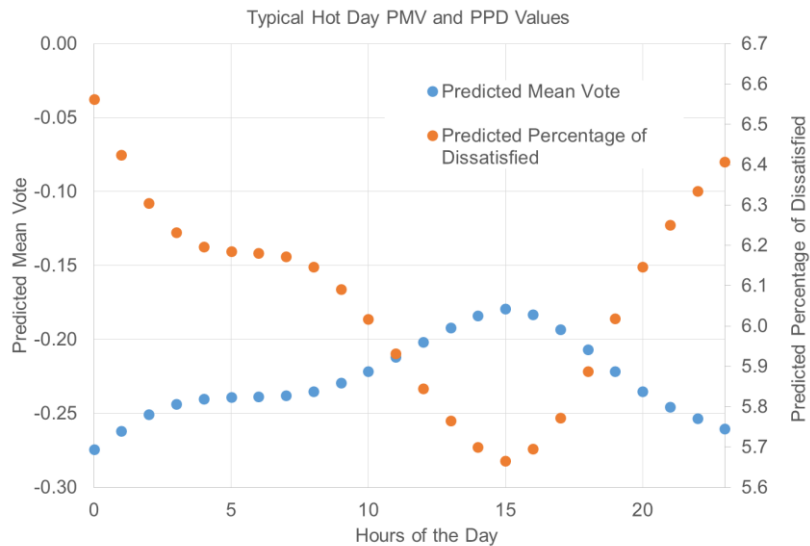


Fig. 2.18. Predicted PMV and PPD for typical hot day

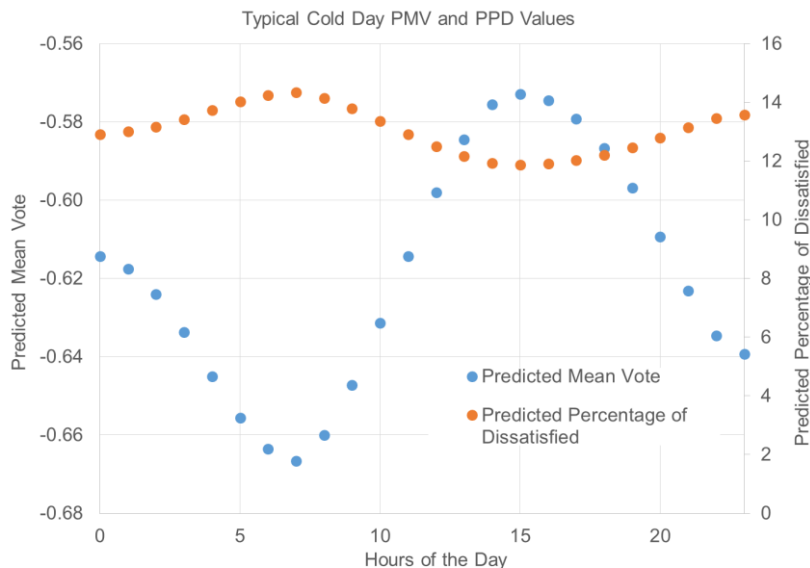


Fig. 2.19. Predicted PMV and PPD for a typical cold day

2.3.3 Case Study III: Comparison of Ducted System and Ductless System

Introduction

In North America, most residential air-conditioning and heat pump systems use centrally ducted air systems to distribute heated and cooled air throughout a home. As shown in Figure 2.20, ducted systems mainly include an outdoor unit and an air handling unit. The outdoor unit hosts the compressor and outdoor heat exchanger and is installed outside of house. The air handling unit is typically installed inside the house such as in an attic or basement (as shown in the figure) and it hosts indoor heat exchangers which may be one slab or two slabs of HXs forming an “A” shape. The air handling unit and outdoor unit are connected using refrigerant pipes. The air handling unit has a blower which draws the return air from the space. The return air flows through the indoor heat exchanger and the processed air is then distributed to multiple rooms through air ducts.

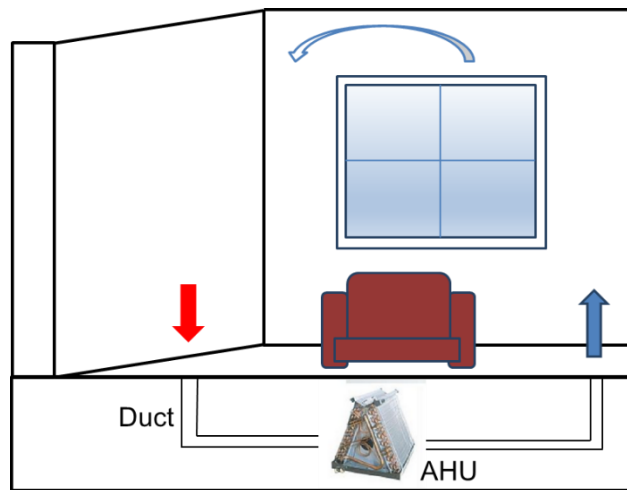


Fig. 2.20. Schematic of a ducted system inside a space

In East Asia countries such as Japan and China, ductless systems are more dominant. The houses in those countries are generally smaller and therefore cannot afford to have multiple air ducts. Ductless systems, as shown in Figure 2.21, typically have one outdoor unit and can have one or multiple indoor units. Each indoor unit has its own indoor heat exchanger and fan. It circulates the air in one room through the indoor heat exchanger and supply the process air to that room. The multiple indoor units are connected with the outdoor unit using refrigerant pipes. No air ducts are required for ductless systems.

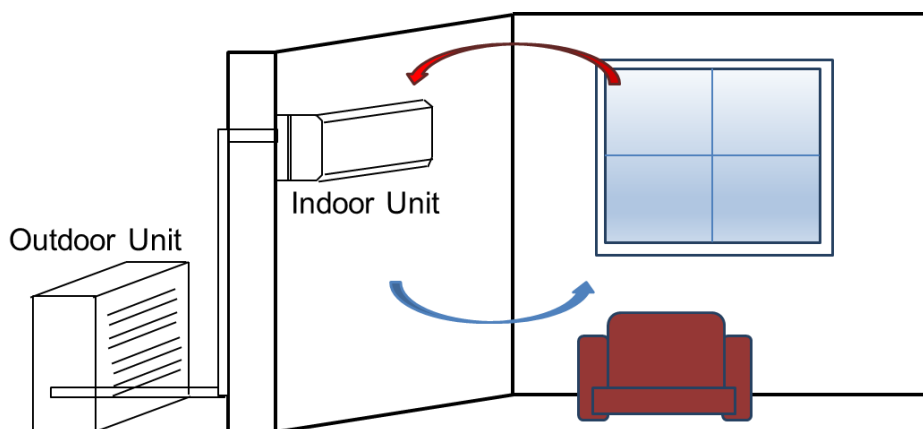


Fig. 2.21. Schematic of a ductless system inside a space

Air Temperature and Velocity Field Simulation using CFD

CFD models were established for both ducted and ductless heat pump systems. For both system, a fixed room dimension is selected as length*width*height = 5 m * 3 m * 2.4 m. Since the focus of the study is indoor thermal comfort, only indoor units were relevant for the simulation. The indoor unit dimension of ductless system was obtained from the measurement of a field test system. The dimension is length*width*height = 0.9 m*0.3 m*0.15 m. To maintain a mass balance in the room, the room air will be discharged through an undercut with an dimension of length*height = 1 m*0.006 m. The total mesh number for the ductless system CFD model is 555,000. The ducted system is assumed to have a floor outlet. In the real case, depending on the locations of room and air handling unit, the air outlet may either be on the floor or on the ceiling. For the simplicity, only one scenario is modeled. The air outlet size is chosen from common grills on the market to be length*width =

0.4 m * 0.4 m. The undercut dimension is the same as the one in the ductless system. Due to the simple geometry of the air outlet, the ducted system CFD model has only a mesh number of 285,000. Figures 2.22 and 2.23 show the geometries of the two systems modeled in Gambit (ANSYS., 2011).

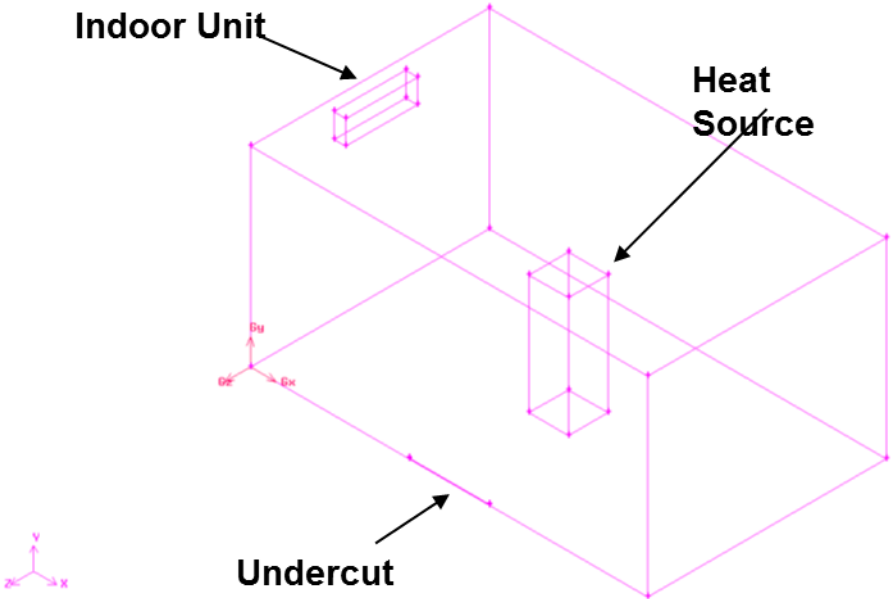


Fig. 2.22. CFD drawing of a ductless system inside a space

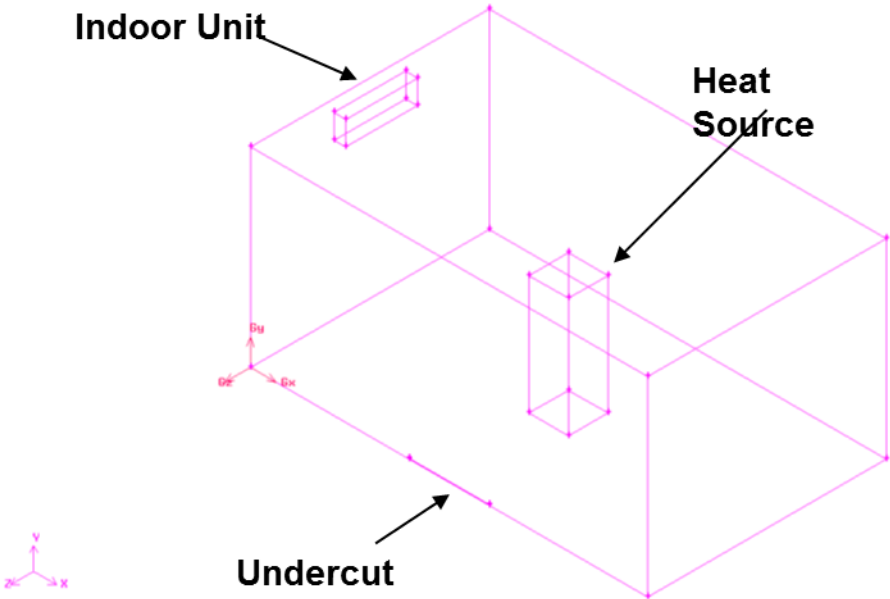


Fig. 2.23. CFD drawing of a ducted system inside a space

Both heating season and cooling season simulations were conducted with various supply air temperatures. In heating, the supply air temperature varies from 35 °C to 45 °C while in cooling, the supply air temperature varies from 12 °C to 18 °C. To maintain the same cooling capacity into the space, the supply air velocity is adjusted according to the supply temperature. Figures 2.24 and 2.25 show the air temperature and velocity comparison results of ducted system and ductless system.

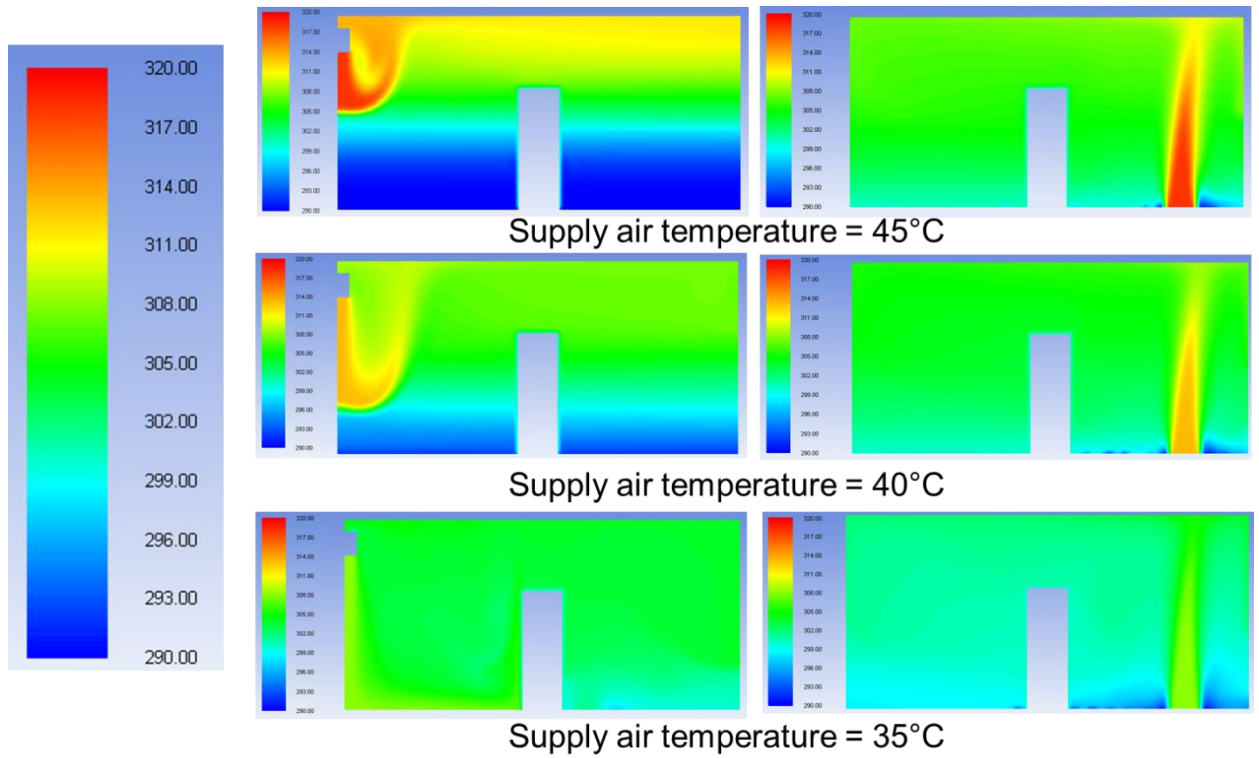


Fig. 2.24. Ducted (rh side) and ductless (lh side) system temperature field comparison in heating cases with different supply temperature

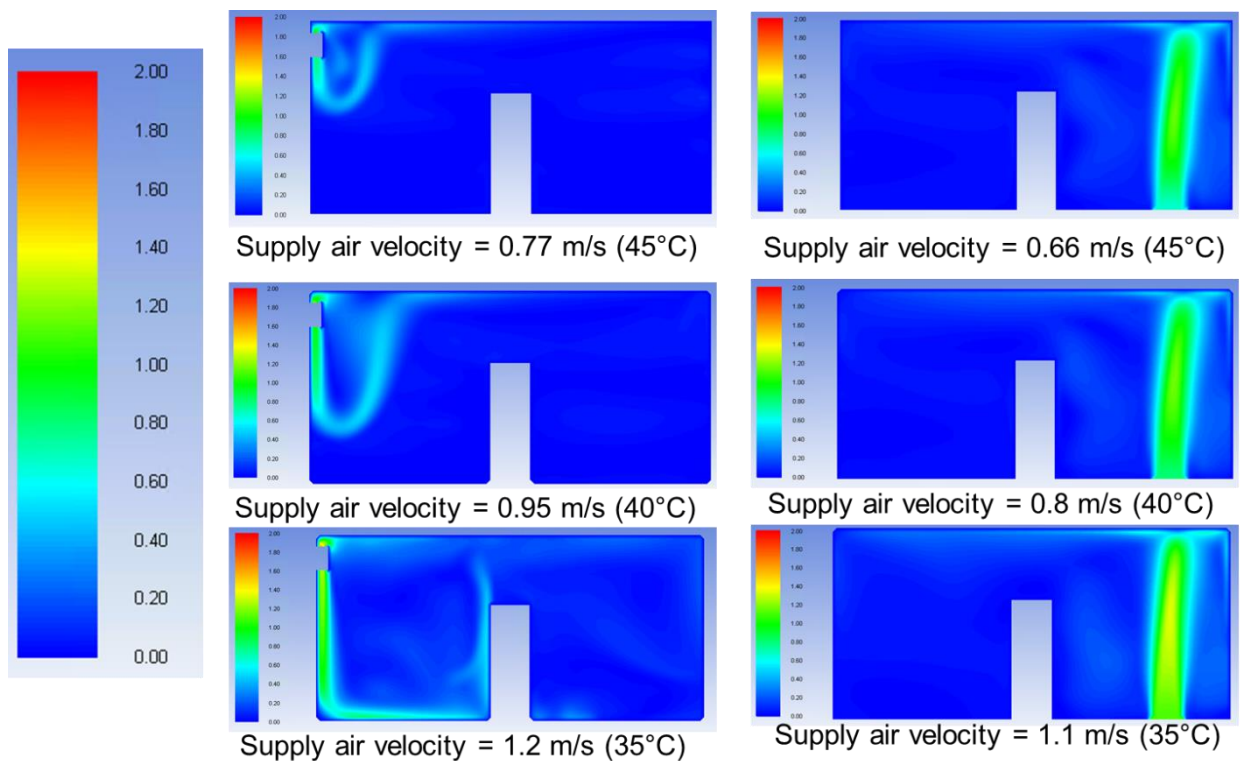


Fig. 2.25. Ducted (rh side) and ductless (lh side) system velocity field comparison in heating cases with different supply velocities (note different velocities for different systems are to keep the capacity to be same)

It is found that in heating, the ductless system shows a greater degree of temperature stratification than does the ducted system. Ductless system with smaller supply air velocity performs better in the sense that the bottom half of the space has a comfortable temperature range but it also shows that less supply air velocity leads to larger temperature stratification. However, it should be noted that, for these analyses, the ductless system is assumed to have a fixed air supply direction of vertical downward. In the real case, the outlet vane can be adjusted to guide the supply air flow to different angles. This may improve the thermal comfort for ductless system. It is also applied to ducted system. The grill can be adjusted so that the air plume is not vertically upward (or the grill can be placed in the ceiling or on a side wall). Figures 2.26 and 2.27 show the air temperature and velocity fields of ducted system and ductless system in the cooling case. It is found that in the cooling case, ducted system with the smallest supply air velocity (lowest supply air temperature) shows a high degree of room temperature stratification. Overall the ductless system provides more effective cooling than does the ducted system. Again, it has to be noted that the different supply angle is not considered.

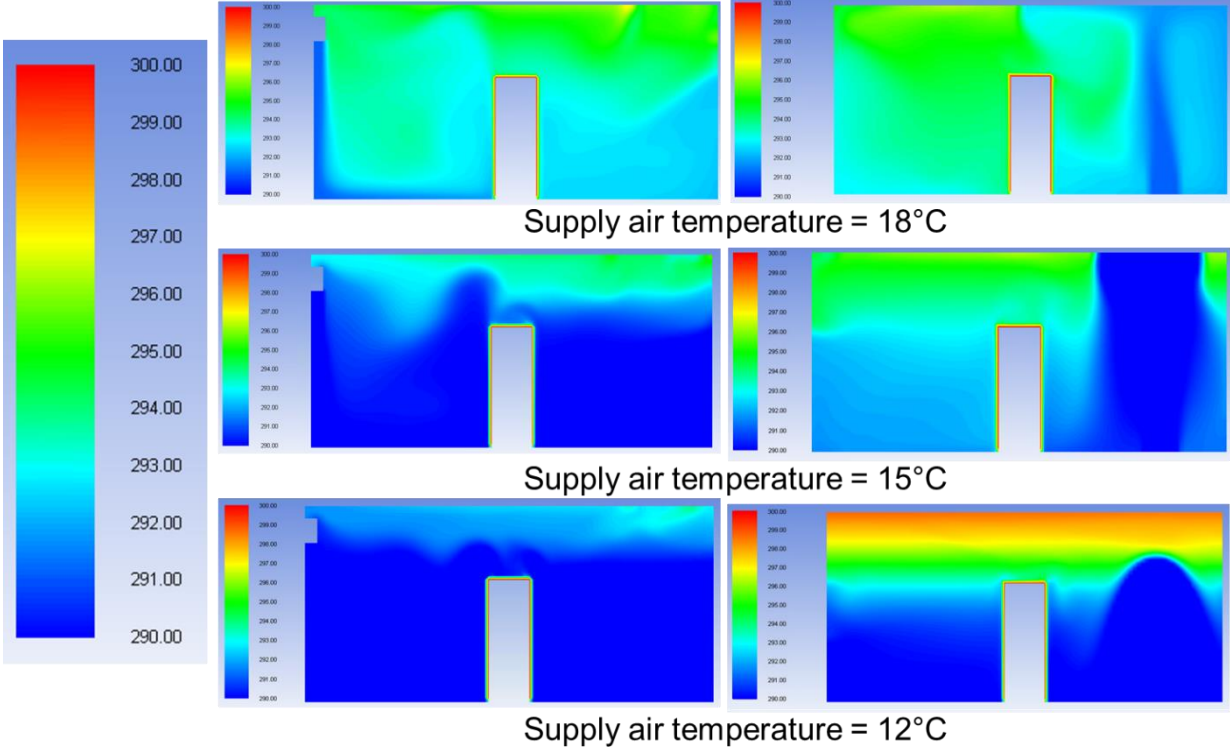


Fig. 2.26. Ducted (rh side) and ductless (lh side) system temperature field comparison in cooling cases with different supply temperature

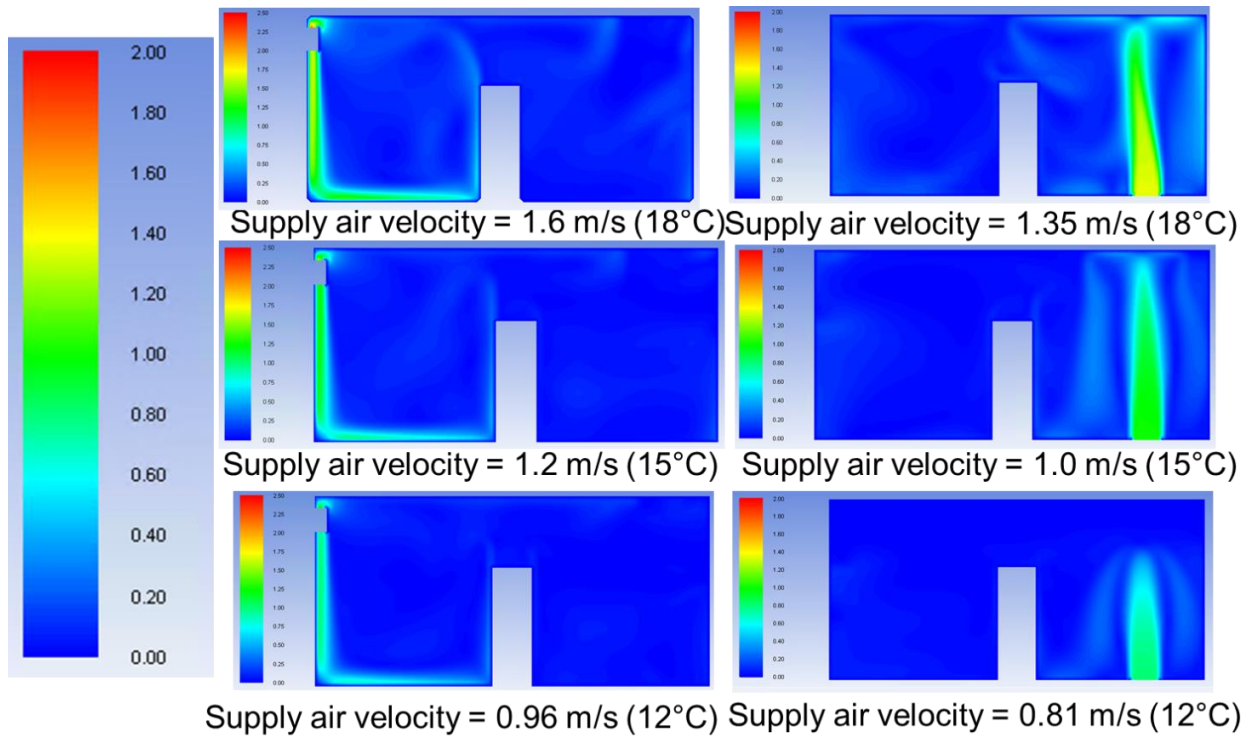


Fig. 2.27. Ducted (rh side) and ductless (lh side) system velocity field comparison in cooling cases with different supply velocities (note different velocities for different systems are to keep the capacity to be same)

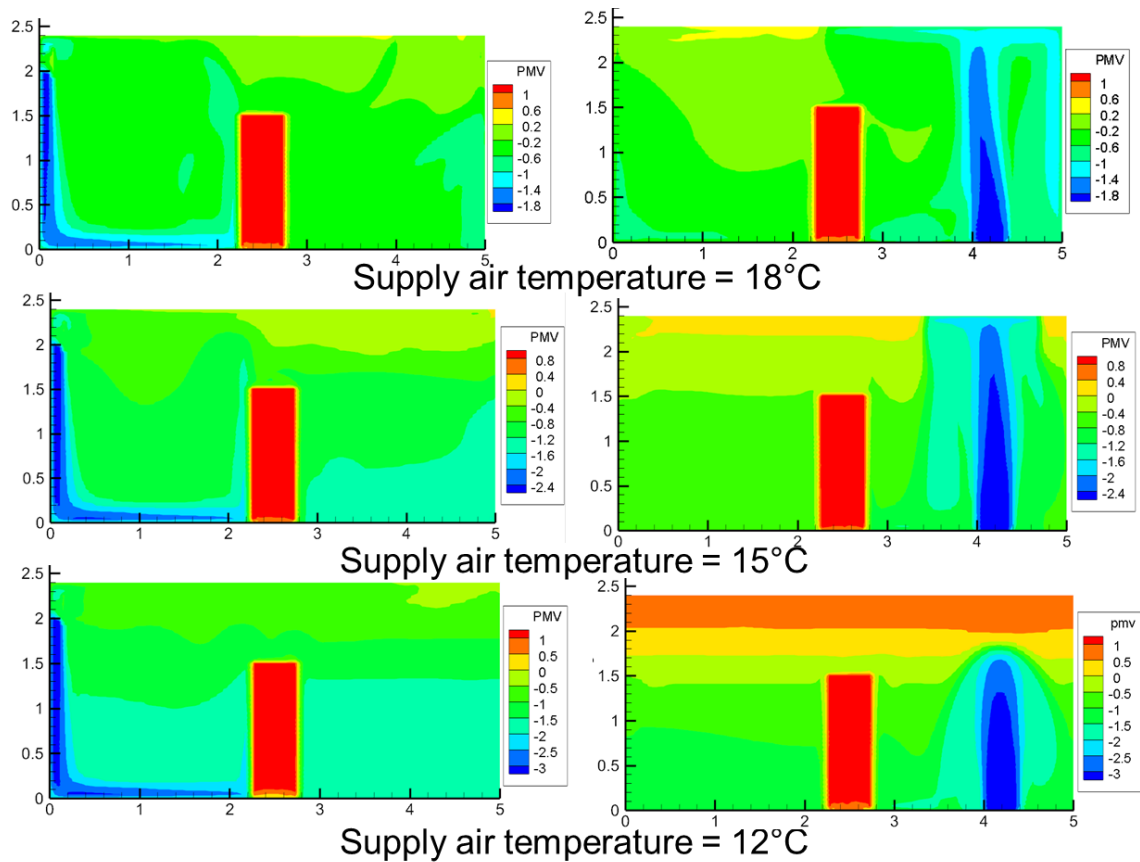


Fig. 2.28. Ducted (rh side) and ductless (lh side) system PMV field comparison in cooling cases with different supply temperature

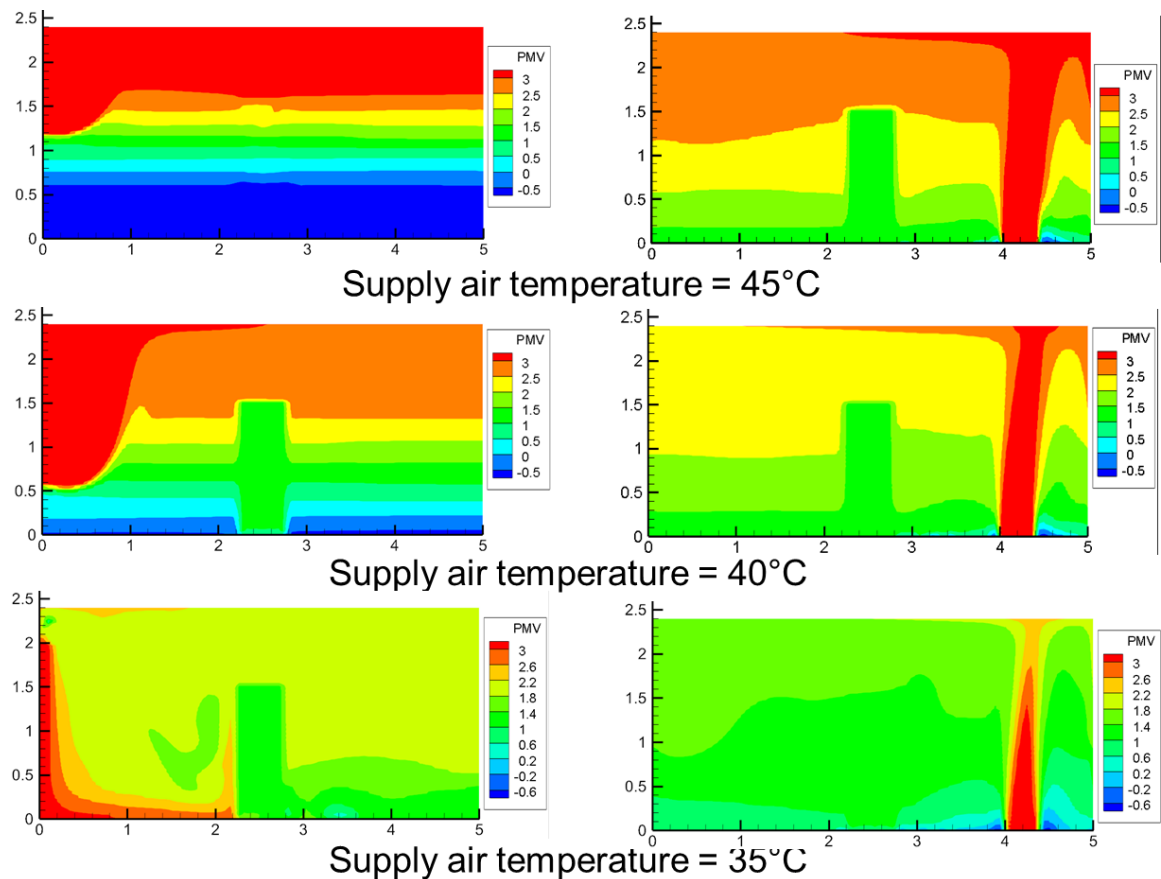


Fig. 2.29. Ducted (rh side) and ductless (lh side) system PMV field comparison in heating cases with different supply temperature

The ASHRAE PMV equation is then applied by using the temperature and velocity fields as inputs. Figures 2.28 and 2.29 show the PMV field of two systems in both heating and cooling cases. Generally speaking, the ducted system with large supply air velocity shows an overall best PMV distribution in heating, while for cooling, the ductless system is better.

Effect of Supply Air Angles for Ductless System

In the discussion above, the supply air angle of the ductless system was assumed to be vertically downward. In the real case, it can actually be changed by adjusting an air discharge vane angle. Additional CFD simulations were carried out by assuming different vane angle settings and the impacts on thermal comfort were evaluated. Figures 2.30 to 2.35 show the ductless system temperature and velocity fields with three vane angle settings, namely 0° (vertically downward), 45° and 80°. For heating the 45° vane setting helps sending the hot air farther into the room. For cooling the 0° and 45° vane position settings have a good thermal comfort in terms of PMV.

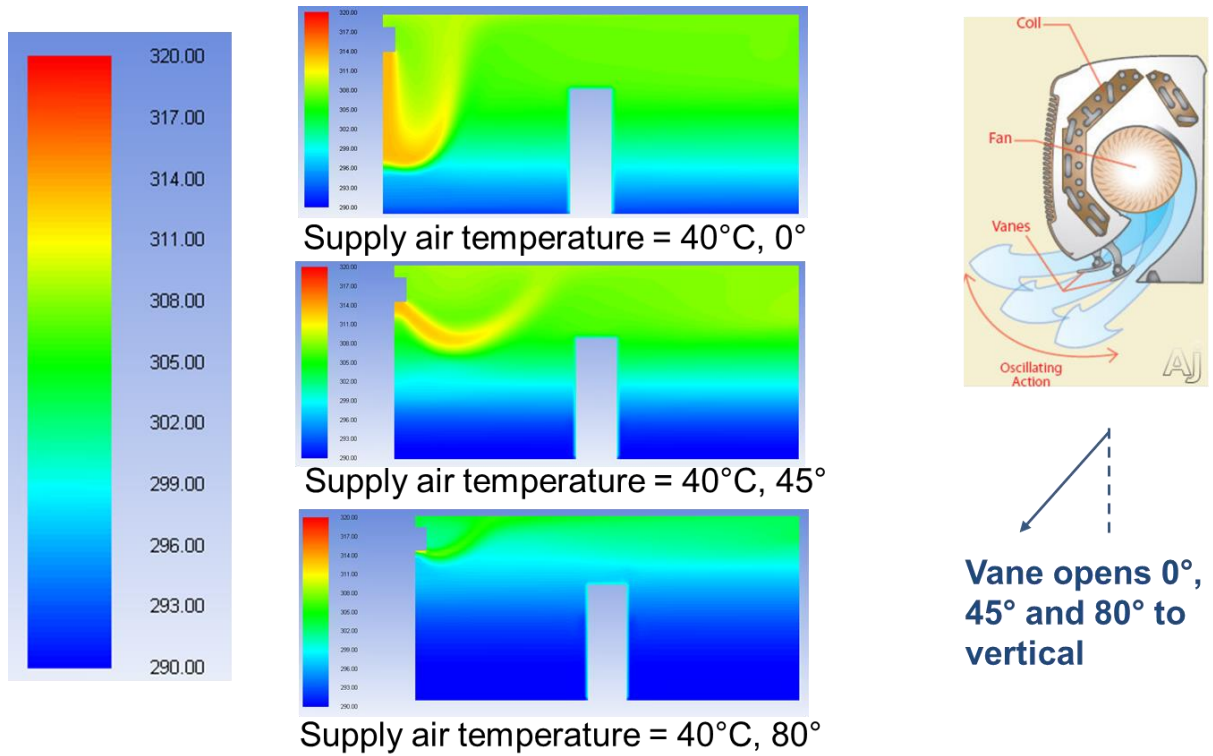


Fig. 2.30. Ductless system temperature field comparison in heating cases with different vane position settings

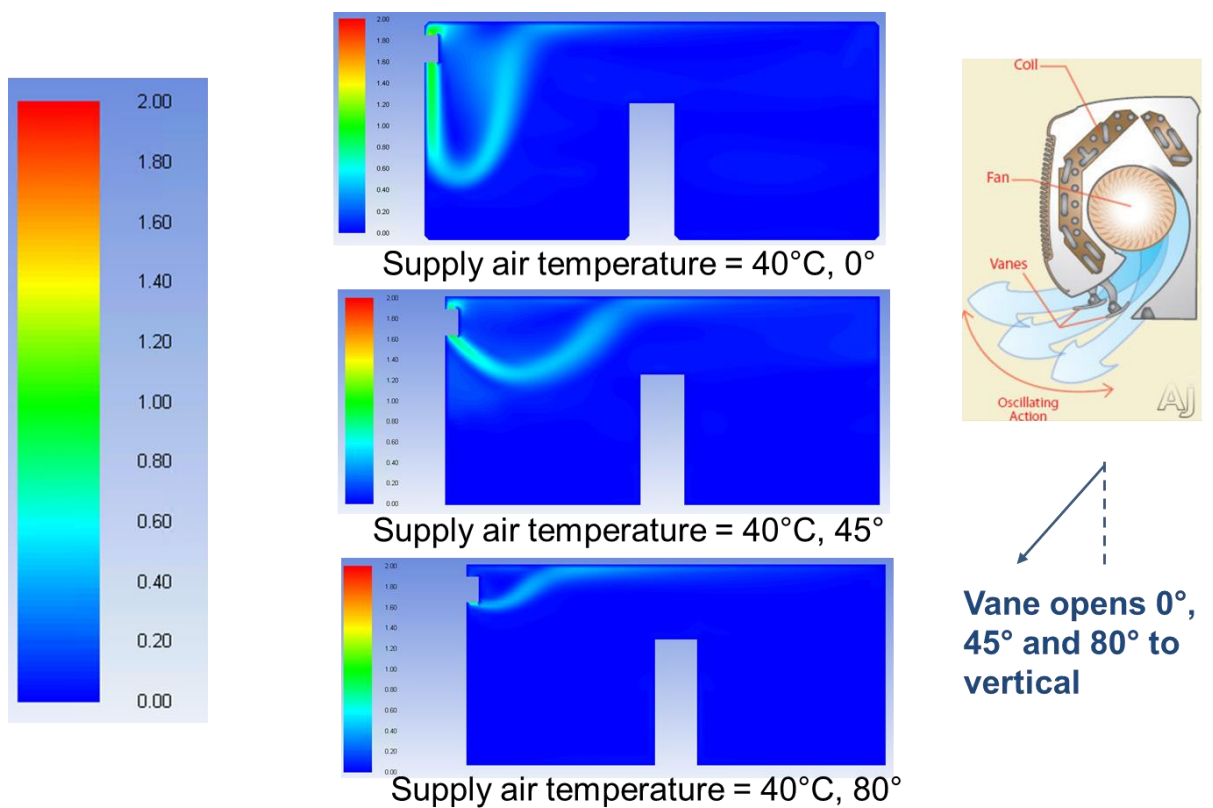
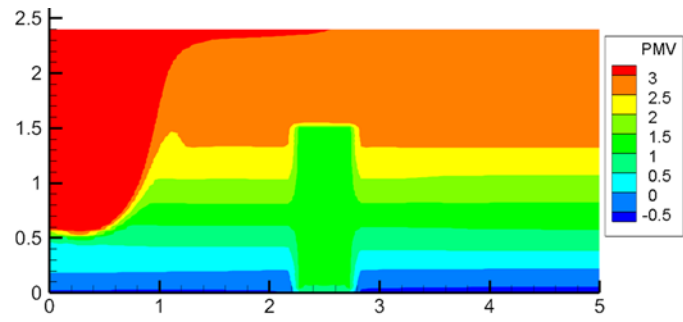
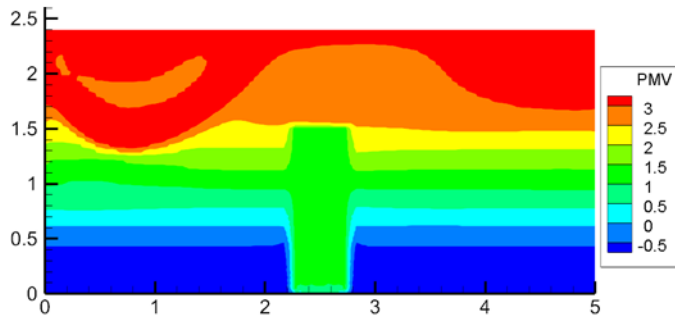


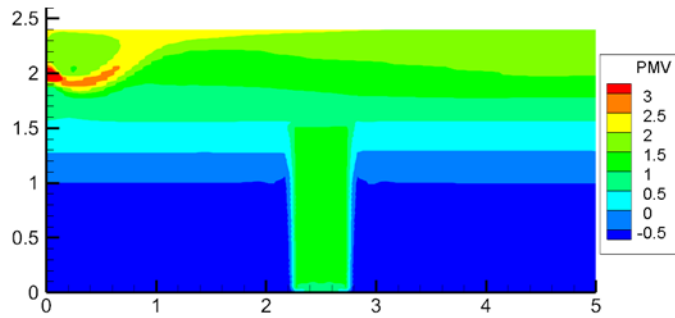
Fig. 2.31. Ductless system velocity field comparison in heating cases with different vane position settings



Supply air temperature = 40°C, 0°



Supply air temperature = 40°C, 45°



Supply air temperature = 40°C, 80°

Fig. 2.32. Ductless system PMV field comparison in heating cases with different vane position settings

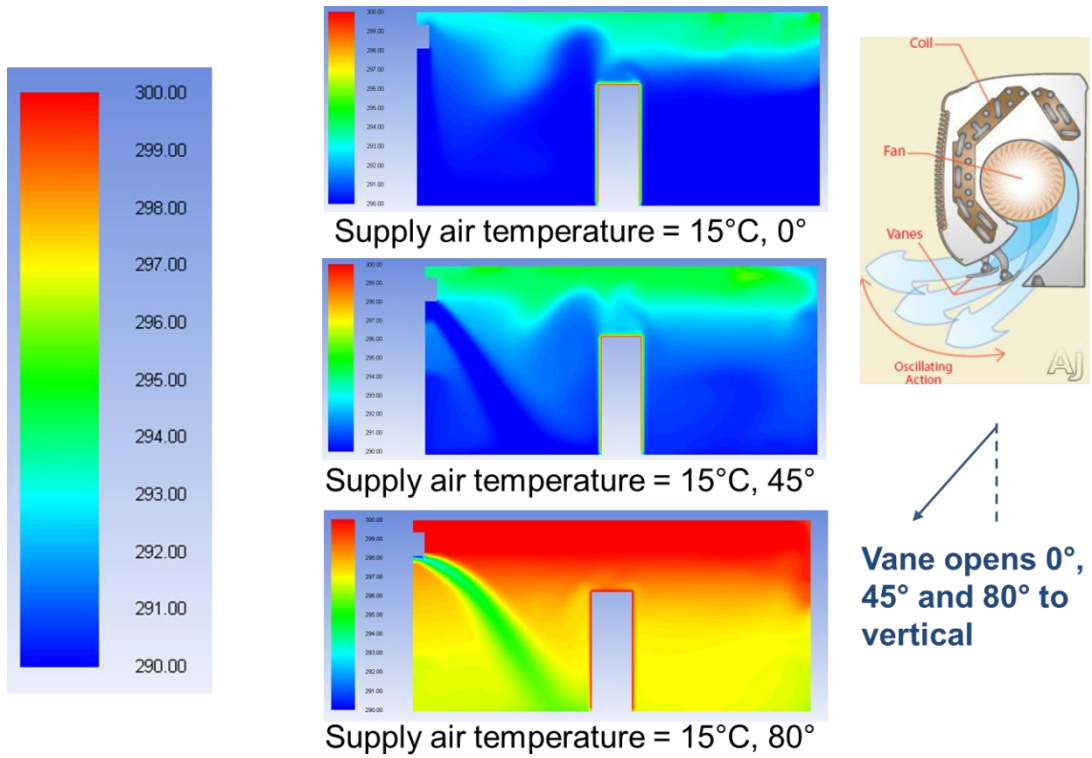


Fig. 2.33. Ductless system temperature field comparison in cooling cases with different vane position settings

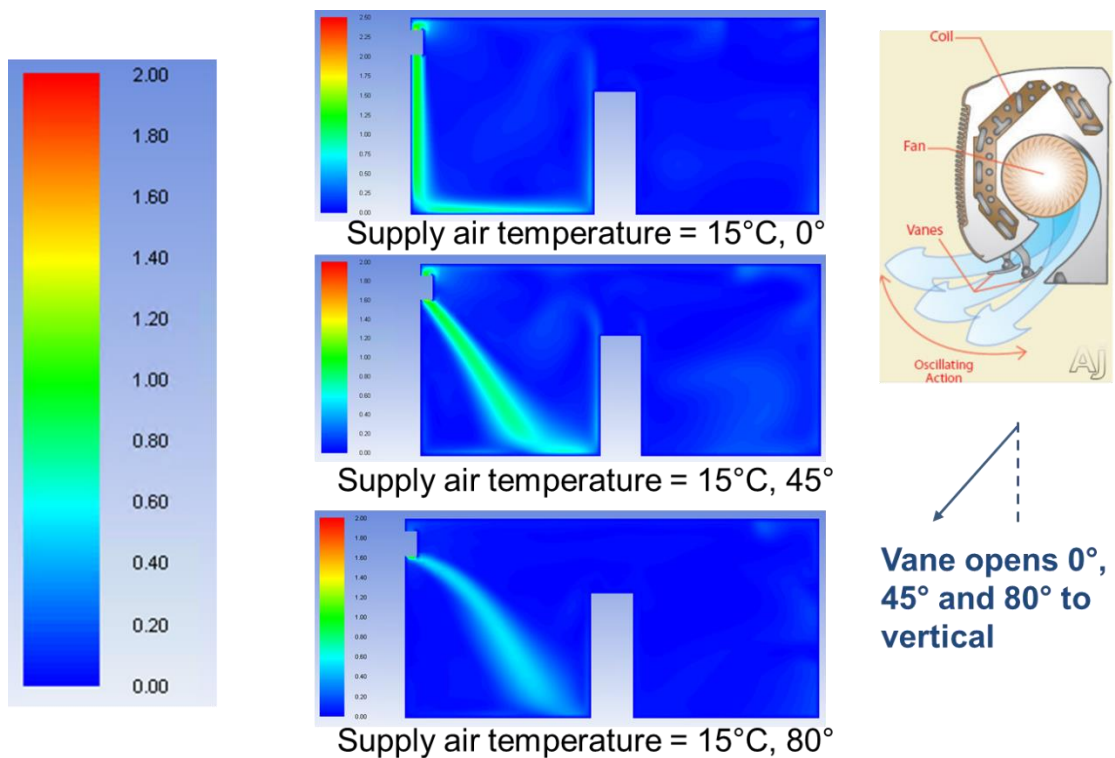
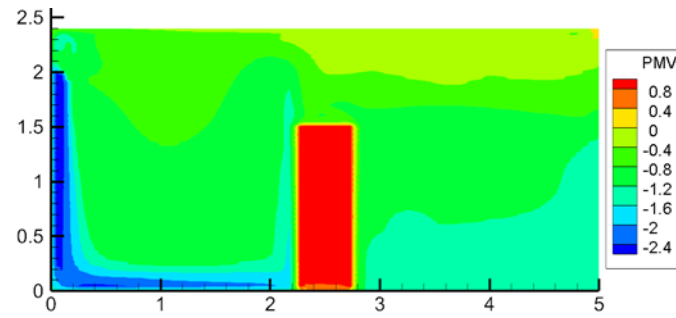
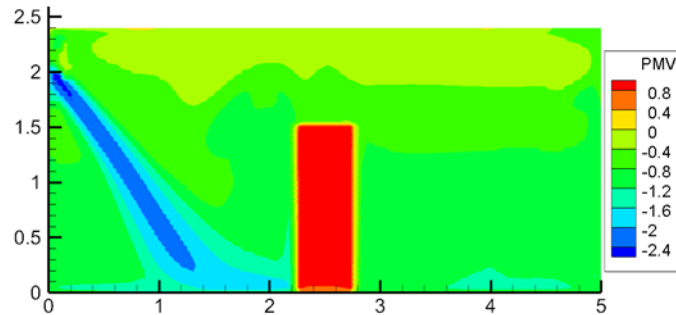


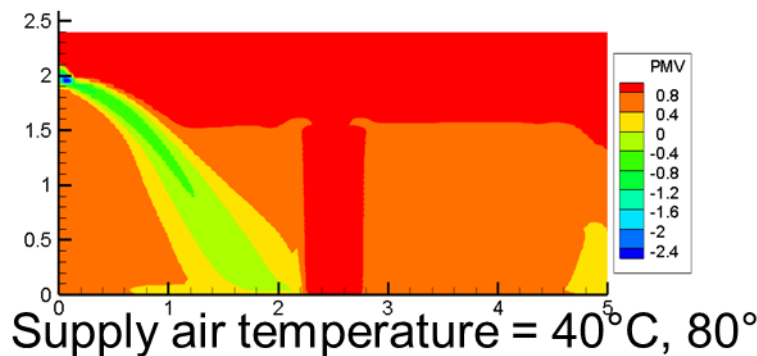
Fig. 2.34. Ductless system velocity field comparison in cooling cases with different vane position settings



Supply air temperature = 15°C, 0°



Supply air temperature = 15°C, 45°



Supply air temperature = 40°C, 80°

Fig. 2.35. Ductless system PMV field comparison in cooling cases with different vane position settings

2.4 Recommendations on system layout in nZEB

Based on the three case studies, it is found that the radiant heat exchanger and induction-based supply unit systems (Cases I and II) are capable of providing improved thermal comfort at low energy consumptions. The major reason is that, for both systems, the room air circulation is driven either by natural convection or pressure gradient. The bulk air circulates at relatively low air velocities and therefore minimizes the chance of draft. To achieve better thermal comfort, it is also important to control the MRT. Conventional systems cannot control the MRT effectively due to the small surface area and view factor between supply air discharge grills or units and occupants. Radiant panels and induction-based supply units have a relatively larger surface area and therefore a larger view factor to occupants. It is proved that with a better control of MRT, the PMV and PPD indices are improved.

With regards to conventional centrally ducted air distribution systems and new emerging ductless systems (Case study III), the thermal comfort evaluation showed significant

temperature stratification in the room. For the ductless system, it is important to adjust the supply air vane angle according to supply air temperature. For a ducted system with air outlets in the room floor, the vertical plume of supply air causes draft sensations and therefore affects thermal comfort. However, the ducted system can provide good thermal comfort in the heating season because the hot supply air flows naturally from bottom to top of the room.

3 TASK 3 - DEVELOPMENTS OF INTEGRATED HEAT PUMPS

3.1 Background of the IHP Development

The U.S. Department of Energy's (DOE) Building Technologies Office (DOE-BTO) has a long term goal to maximize the energy efficiency of the US building stock by year 2030. Maximizing building energy efficiency is an essential facilitating step to enable market uptake of nZEBs including net zero energy homes (nZEH). To achieve this vision, a deep reduction of the energy used by the energy service equipment (equipment providing space heating and cooling, water heating, etc.) is required - 50% or more compared to today's best common practice. One promising approach to achieving this is to produce a single piece of equipment that provides multiple services. ORNL developed a general concept design for such an appliance, called the integrated heat pump (IHP) [Murphy, et al 2007a, b].

The energy service needs of an nZEH include space heating and cooling (SH/SC), water heating (WH), ventilation (V), and possibly dedicated dehumidification (DH) and humidification (H) as well, depending on the requirements of the specific location. These requirements differ in significant ways from those for non nZEH buildings. The high-performance envelope of an nZEH results in much lower SH/SC loads relative to current housing and also makes the house sufficiently air-tight that mechanical ventilation is required to assure adequate indoor air quality. These envelope characteristics mean that the SH/SC loads will be closer in size to the WH load, which is not expected to drop by any significant amount because of an improved envelope. In some locations such as the Gulf Coast area, additional DH will almost certainly be required during the shoulder and cooling seasons.

As noted above, one promising approach to efficiently meeting these needs is with an IHP – a single system based on variable-capacity or variable-speed (VS) heat pumping technology. The energy benefits of an IHP stem from the ability to utilize otherwise wasted energy; for example, heat rejected by the SC operation can be used for WH. Significant energy savings are possible from the higher efficiency operation of the components, the load matching capability of the VS equipment (providing heat exchanger unloading benefits), outdoor-source heat pump water heating, and waste heat recovery in the combined SC and WH mode.

With the greater energy savings the cost of the more energy efficient components required for the IHP can be recovered more quickly than if they were applied to individual pieces of equipment to meet each individual energy service need. An IHP can be designed to use either outdoor air (e.g. air-source IHP or AS-IHP) or geothermal resources (e.g., ground-source IHP or GS-IHP) as the environmental energy source/sink. Schematic illustrations of the AS-IHP and GS-IHP system concepts are given in Figures 3.1 and 3.2, respectively.

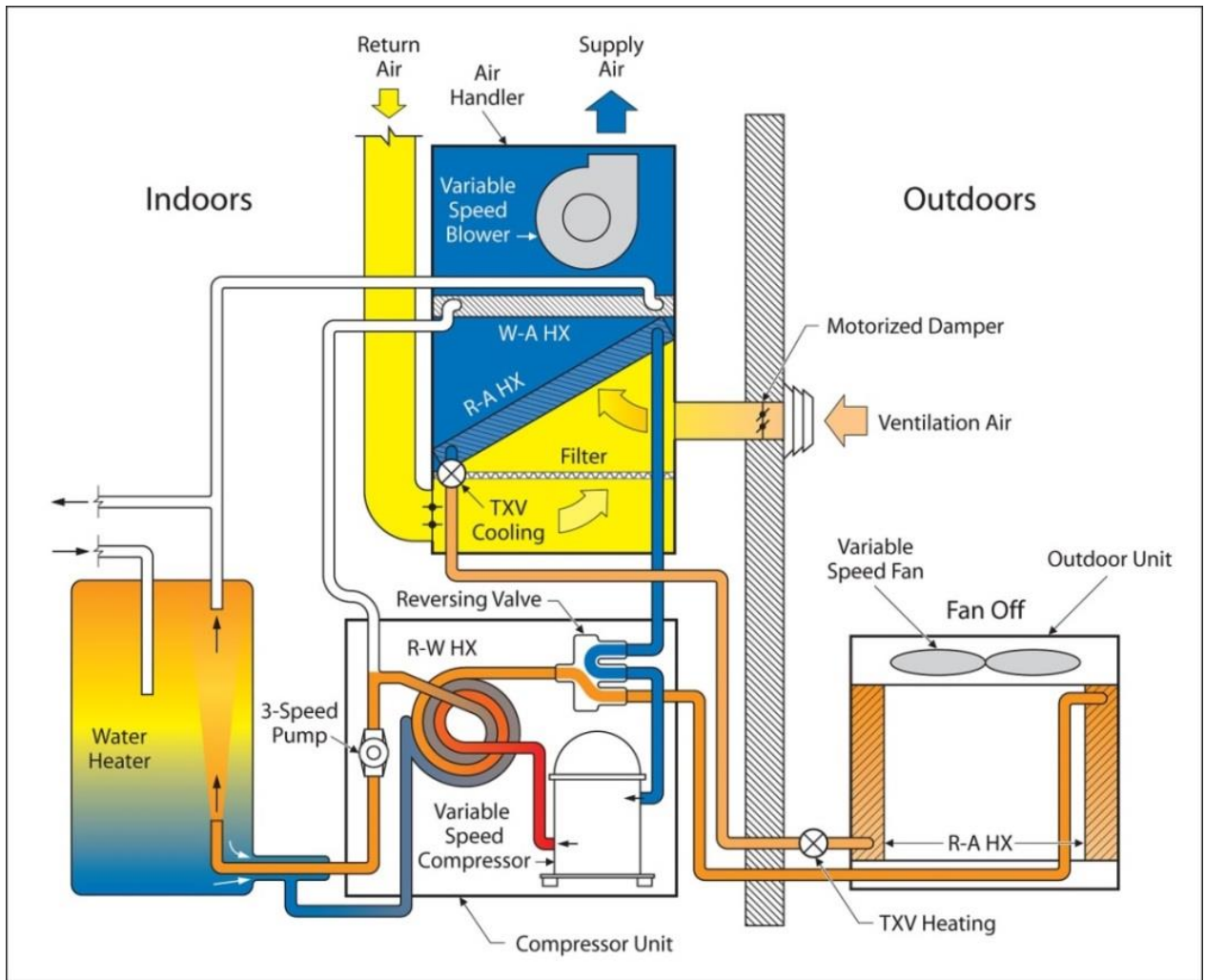


Fig. 3.1. AS-IHP system schematic; SC plus "on-demand" WH mode shown.

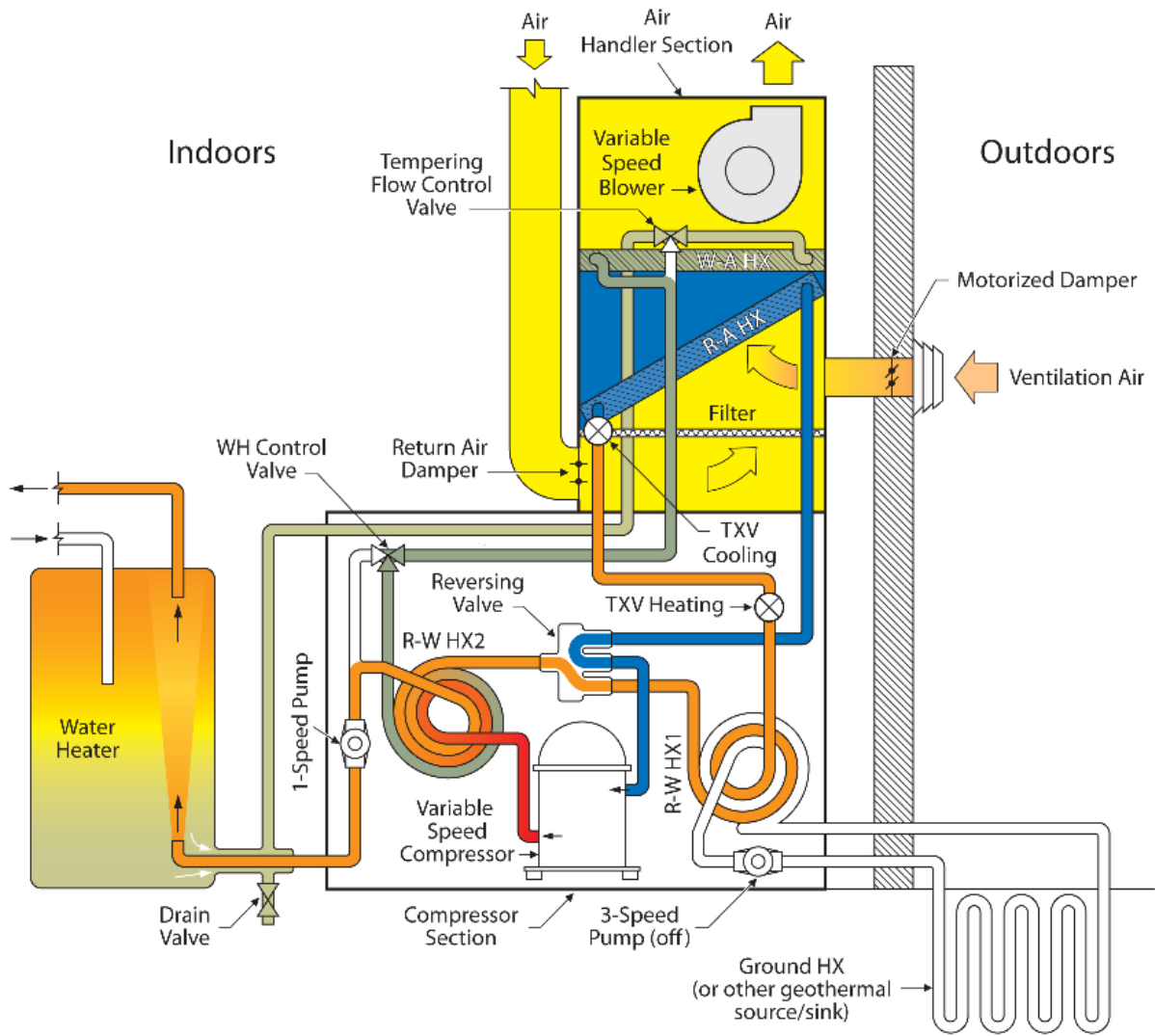


Fig. 3.2. GS-IHP schematic. Dedicated DH and WH mode shown.

Table 3.1 shows the annual loads for a 167m² (1800 ft²) nZEH from TRNSYS (Solar Energy Lab, 2010) simulations reported by Murphy et al (2007 a & b) for five US Climates - corresponding to Building America climate regions (DOE, 2012) of mixed-humid (Atlanta, GA), hot-humid (Houston, TX), hot-dry (Phoenix, AZ), marine (San Francisco, CA), and cold (Chicago, IL). Table 3.1 also shows the nominal design cooling capacity necessary for a heat pump system for these nZEHs.

Table 3.1. Annual SH, SC, WH and demand DH loads for a 167 m² (1800 ft²) nZEH in five US locations

Location	Space heating kWh	Space cooling kWh	Water heating kWh	Demand dehumidification kWh	Heat pump cooling capacity kW, (tons)
Atlanta	4775	5735	3032	158	1.25
Houston	1766	9927	2505	704	1.25
Phoenix	1580	9759	2189	-	1.50
San Francisco	2881	88	3387	42	1.00
Chicago	11475	2550	3807	94	1.25

Tables 3.2-3.4 provide summary results of sub-hourly simulations of the annual performance

of a DOE minimum efficiency (2006 efficiency minimums) baseline HVAC/WH/DH system, an AS-IHP, and a GS-IHP for the five locations. Table 3.2 gives the baseline system results, both for annual energy use and hourly winter and summer maximum peak kW as well as mid-afternoon summer peak kW demand. The baseline system included a fixed capacity air-source heat pump (ASHP) with a rated seasonal cooling COP of 3.8 (SEER of 13 Btu/Wh) and US Region IV seasonal heating COP of 2.3 (HSPF of 7.73 Btu/Wh), an electric water heater with a rated efficiency or energy factor (EF) of 0.90, a 19 l/d (5 gal/d) capacity standalone dehumidifier with a rated DH energy factor (EF_d) 1.4 l/kWh, and ventilation rate per requirements of ASHRAE Standard 62.2 (ASHRAE 2007). Tables 3.3 and 3.4 provide results for the concept AS-IHP and GS-IHP systems, respectively. Control set points were the same for all three systems. For SH/SC, set points were 21.7 °C and 24.4 °C (71 °F and 76 °F), respectively; set point for WH was 49 °C (120 °F); set point for DH was 55% relative humidity (RH). Each system also included a humidifier set to maintain a minimum indoor RH of 30%. The assumed daily hot water use was ~245 l/d (~64.5 gal/d), consistent with the Department of Energy (DOE 2010) daily hot water draw totals for electric resistance and heat pump water heater (HPWH) Energy Factor (EF) ratings testing.

Table 3.2. Estimated annual site HVAC/WH system energy use and peak kW for baseline HVAC/WH system

Location	Heat pump cooling capacity (tons)	HVAC/WH site energy use, kWh	HVAC/WH hourly peak kW demand (W/S/SA)*
Atlanta	1.25	7230	8.6/4.6/2.1
Houston	1.25	7380	6.1/4.4/2.2
Phoenix	1.50	6518	6.1/3.9/2.1
San Francisco	1.00	4968	5.7/5.6/1.6
Chicago	1.25	10773	9.7/6.1/2.4

* W – winter morning; S – summer maximum; SA – summer mid-afternoon.

Table 3.3. Estimated annual site HVAC/WH system energy use and peak kW for AS-IHP system

Location	Heat pump cooling capacity (tons)	HVAC/WH site energy use, kWh	HVAC/WH hourly peak kW demand (W/S/SA)*	% energy savings vs. baseline
Atlanta	1.25	3349	2.2/1.5/1.2	53.7
Houston	1.25	3418	1.9/1.1/1.1	53.7
Phoenix	1.50	3361	2.1/1.7/1.7	48.4
San Francisco	1.00	1629	1.8/1.6/0.8	67.2
Chicago	1.25	5865	7.3/1.6/1.0	45.6

* W – winter morning; S – summer maximum; SA – summer mid-afternoon.

Table 3.4. Estimated annual site HVAC/WH system energy use and peak kW for GS-IHP system

Location	Heat pump cooling capacity (tons)	HVAC/WH site energy use (kWh)	HVAC/WH hourly peak kW demand (W/S/SA)*	% energy savings vs. baseline (%)
Atlanta	1.25	3007	2.0/1.1/1.0	58.4
Houston	1.25	3290	1.8/1.1/1.0	55.4
Phoenix	1.50	2909	1.7/1.2/1.2	55.4
San Francisco	1.00	1699	1.8/1.6/0.6	65.8
Chicago	1.25	5126	6.9/1.7/0.8	52.4

* W – winter morning; S – summer maximum; SA – summer mid-afternoon

Maximum peak demand occurred in the winter for all systems generally during the 6 – 8 a.m. time frame (roughly coincident with winter utility peak periods). The water use schedule assumed for the analysis included a significant draw during that time of day, making electric backup element activity likely (adding to backup electric space heating in the colder locales). Maximum summer peaks are somewhat lower and generally occurred during the 6 – 8 a.m. time period as well for the same reason. Summer hourly peaks during the noon – 7 p.m. time period (roughly coincident with summer utility peak time period) were about 1.6 – 2.4 kW for the baseline system vs. about 0.8 – 1.7 kW for the AS-IHP and 0.6 – 1.2 for the GS-IHP.

The estimated annual energy savings for the AS-IHP exceeded 50% over the baseline system in three locations, closely approached 50% in Phoenix, and achieved ~46% in Chicago. Estimated savings for the GS-IHP concept system exceeded 50% in all locations.

Winter peak kW ranged from about 25 to 75% lower for the AS-IHP than for the baseline. Maximum summer peaks were about 55% to 75% lower, while summer mid-afternoon IHP peaks were ~20 to 60% lower than those of the base system, depending upon location. For the GS-IHP winter peaks were 30-70% lower than for the baseline, summer morning peaks were 70-75% lower, and summer afternoon peaks were 45-70% lower.

3.2 Variants of the IHP layout

As noted above, there are two primary versions of the IHP; a geothermal or ground-source (GS-IHP) and air-source (AS-IHP). ORNL activities have focused on development of four different embodiments of the IHP. One is an electric GS-IHP and the other three are AS-IHPs (two electric driven and one natural gas engine driven). These are described briefly below.

3.2.1 Summary of GS-IHP system development, analyses, and test results

Full details of the GS-IHP concept development can be found in the report by Murphy, et al (2007b). Figure 3.3 shows a conceptual installation. The system uses a variable-speed (VS) compressor, VS indoor blower (for SH/SC distribution), and VS pumps for ground heat exchanger (GHX) fluid circulation and for hot water circulation. A 190 l (50 gallon) WH tank is included. There are a few differences between the GS-IHP system prototypes and the GS-IHP concept reported by Murphy et al (2007b). The concept system included both dedicated DH and H modes (neither of which were included in the prototype system development described below). In addition those analyses were based on a relatively small systems sized for a 167 m² (1800 ft²) very well insulated house with nominal cooling design loads of 1-1.5 tons (3.5-5.3 kW) depending upon location. The prototype system development is a 2-ton (7 kW) nominal size designed for similarly well insulated but larger residences. Note that Figure 3.1 depicts a horizontal GHX installed in the existing home foundation excavation but the system can utilize any geothermal heat source/sink (e.g., vertical bore GHX, ground water, surface water, etc.).

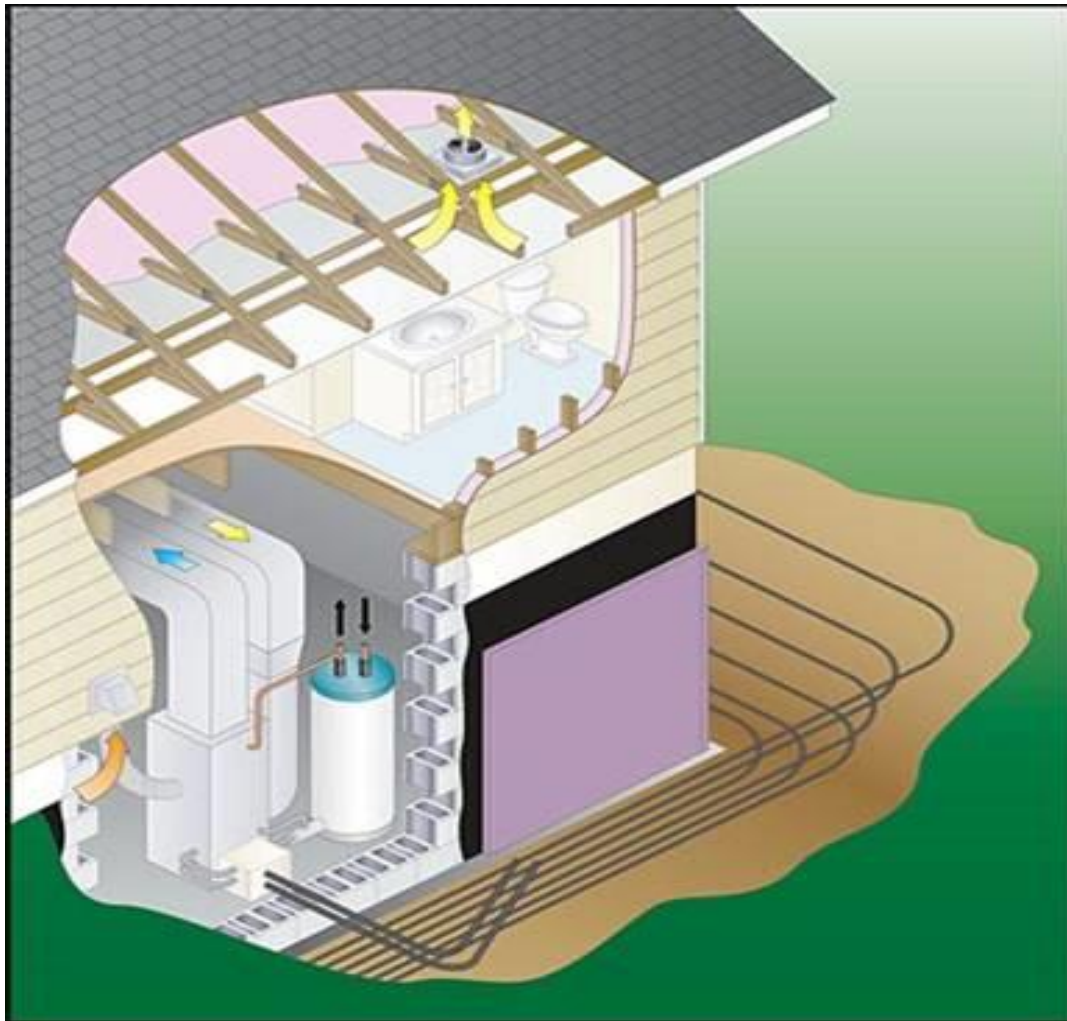


Fig. 3.3. Conceptual installation of residential ground-source integrated heat pump.

Development process and projected GS-IHP prototype performance vs. baseline systems in a well-insulated 240 m² (~2600 ft²) house located in a range of climates. In early 2008 an industry partner, ClimateMaster, Inc. (CM), and ORNL began a series of GS-IHP system design iterations resulting in two generations of GS-IHP prototypes for lab and field testing. Results of the lab tests performed by CM were used to calibrate the variable-speed research version of the DOE/ORNL heat pump design model (HPDM) (Rice 1991; Rice et al, 2005) which was incorporated into the TRNSYS simulation model for estimation of annual performance and energy savings potential. The process is documented by Rice, et al (2013) and Baxter, et al (2013) and summarized in this subsection.

A nominal 2-ton (7 kW) design cooling capacity was selected for system development leading to field testing. CM assembled and lab tested two generations of prototype systems in their laboratory over a wide range of ground-source conditions. ORNL used the detailed lab measurements of refrigerant and source/sink conditions to calibrate the HPDM in each of the four operating modes: SH, SC, SC + WH, and dedicated WH. The HPDM was linked to a publicly available optimization program, GenOpt (Wetter, 2009), to auto-calibrate available heat exchanger (HX) adjustment factors as linear or quadratic functions of compressor speed and/or source/sink temperatures for best match to measured suction and discharge pressures. The test data were also used to determine compressor map power and mass flow corrections, compressor shell heat loss factors, line heat gains/losses and suction superheat levels as similar functions of compressor speed and/or other operating conditions, as well as the indicated active refrigerant charge in each mode. Table 3.5 summarizes the difference

between the calibrated models and CM's lab test data for the final prototype in capacity, compressor power, and compressor-only COP.

Table 3.5. Agreement of Calibrated Models to Prototype 2 GS-IHP Lab Tests

Calibrated Model Results for Prototype 2 GSIHP				
Operation Mode	Calibration Statistics	Capacity	Compressor Power	Compr. Only COP
	(%)	(%)	(%)	(%)
Space Cooling	ave diff.	4.8	1.3	3.5
	std. dev.	2.1	1.9	2.6
Space Heating	ave diff.	4.8	1.4	3.4
	std. dev.	1.2	1	1.4
Dedicated WH	ave diff.	-3.9	-0.9	-3
	std. dev.	3	1.5	3.4

Baseline equipment modeling. To determine the energy savings potential of the GS-IHP design, two baseline cases were also defined. First, a minimum efficiency standard, electric-driven equipment set was defined. This included a 7 kW (2-ton) fixed capacity air-source heat pump with a rated SEER of 13 (cooling SPF=3.8) and US Region IV HSPF of 7.7 (heating SPF=2.3), represented as a function of ambient and indoor conditions based on a manufacturer's published data, and an electric water heater with a rated efficiency or energy factor (EF) of 0.90. This is essentially the same as the baseline system used in the IHP concept development (see IHP Background section above) but without the dehumidifier and humidifier units.

Next a high-efficiency commercially available two-capacity 7 kW (2-ton) ground source heat pump with desuperheater (GSHPwDS) was modeled in HPDM, which was calibrated based on manufacturer's lab data as was done for the GS-IHP case. The two-capacity GSHP has a rated full load cooling COP of 5.4 (EER of 18.5 Btu/Wh) and a rated full load heating 4.0 COP per ISO standard 13256-1 (1998). Part load ratings are 7.6 COP cooling (26 EER) and 4.6 COP heating. Full- and part-load GSHP cooling capacities are 7.80 and 6.25 kW (26.6 and 21.3 MBtu/h) with full- and part-load heating capacities of 5.80 and 4.84 kW (19.8 and 16.5 MBtu/h). The desuperheater function was modeled in TRNSYS as a fixed HX effectiveness based on the manufacturer's test data, pump operation logic, and recommended control settings for the domestic hot water (DHW) tank element thermostats for a 49°C (120°F) set point. The ground and DHW loop pumps were typical single-speed induction-motor designs used by the manufacturer.

GHX modeling. The GHX configuration for both the GS-IHP and GSHPwDS was modeled in TRNSYS as two vertical bore loops connected in parallel. Soil properties were assumed or measured for the 5 U.S. locations. Ten-year sizing runs were made at multiple bore lengths for each system and used to determine the required length to stay within the minimum (winter) and maximum (summer) 10-year design EWTs. (As the minimum and maximum EWTs are approaching asymptotic values at 10 years of operation, 20-year values would be only slightly higher.)

Table 3.6 shows the assumed soil characteristics and grout types for the 5 U.S. locations, the loop fluid, the min and max design temperatures, and the required bore lengths and specifications.

Table 3.6. TRNSYS 10-year bore sizing results for GSHPwDS and GS-IHP units in reference house in 5 different U.S. locations

Location	Soil Characteristics, Assumed* or Measured ^M		Loop Fluid	Min 10-yr EWT	Max 10-yr EWT	Grout Type	Bore Length / Unit Cap. GSHPwDS	Grout Type	Bore Length / Unit Cap. GSIHP
	k	diffusivity							
	Btu/hr-ft-F [W/m-°C]	ft ² /day [mm ² /s]		°F [°C]	°F [°C]	GSHP	ft/ton [m/kW]	GSIHP	(ft/ton) [m/kW]
Atlanta	1.2 [2.1]	0.90 [0.97]	Water	42 [5.6]	95 [35]	Std	313 [27.1]	Enh	294 [25.5]
Houston	1.2 [2.1]	0.90 [0.97]	Water	42 [5.6]	95 [35]	Std	294 [25.5]	Enh	220 [19.1]
Phoenix	0.8 ^M [1.4 ^M]	1.65 ^M [1.77 ^M]	Water	42 [5.6]	95 [35]	Std	572 [49.6]	Enh	449 [38.9]
San Francisco	1.4 [2.4]	1.02 [1.10]	Water	42 [5.6]	95 [35]	Std	268 [23.2]	Enh	310 [26.9]
Chicago	1.4 [2.4]	1.02 [1.10]	20% PG	30 [-1.1]	95 [35]	Std	233 [20.2]	Enh	299 [25.9]

*per soil property data on GEOKISS site (<http://www.geokiss.com/res-design/GSHPDesignRec2.pdf>)

Bore Specifications:
 Number of Bores = 2
 Bore Diameter = 4.5"[11.4cm], Borehole Separation = 15'[4.57m], Nominal HDPE Pipe Size = 0.75"[1.9cm]

Grout Conductivity Assumptions:
 Standard grout, 0.4 Btu/hr-ft-°F [0.69 W/m-°C]
 Enhanced grout, 0.9 Btu/hr-ft-°F [1.56 W/m-°C]

Standard grout was assumed for the conventional 2-capacity GSHPwDS and enhanced grout for the GS-IHP. Enhanced grout was found to more than pay for its higher cost by reducing the required bore length, which was especially beneficial in balanced and cold climates due to the added heat extraction from the ground loop in the winter and shoulder months to meet the domestic hot water (DHW) load. In Atlanta, the required bore length for the GS-IHP with the enhanced grout was 33% less than for standard grout; however, the annual energy use for the GS-IHP was found to be nearly the same regardless of grout used since both cases stayed similarly within the minimum and maximum loop design temperatures. Had standard grout been used for the GS-IHP Atlanta case however, 25% more bore depth was predicted to be required than for the 2-capacity GSHPwDS case.

The relative bore depth requirements between the GS-IHP and two-capacity GSHPwDS given in Table 3.6 show a 6% shorter bore for the GS-IHP in Atlanta, 22 and 25% less depth needed in Phoenix and Houston, and 16 and 28% longer bores needed in San Francisco and Chicago.

System control set points. For SH/SC, indoor set points were 21.7 °C and 24.4 °C (71 °F and 76 °F), respectively; the set point for WH was 49°C (120 °F). The system's DHW controls for heat pump WH operation for the analysis were set to operate until the lower tank temperature was 49°C (120°F) and the upper electric element was set to minimize electric element use while maintaining the upper tank delivery temperature above 41°C (105°F). The assumed daily water use schedule shown in Figure 3.4 includes discrete tempered (@ 41°C) and untempered (@ 49°C) hot water draws totaling ~245 l/d (~64.5 gal/d).

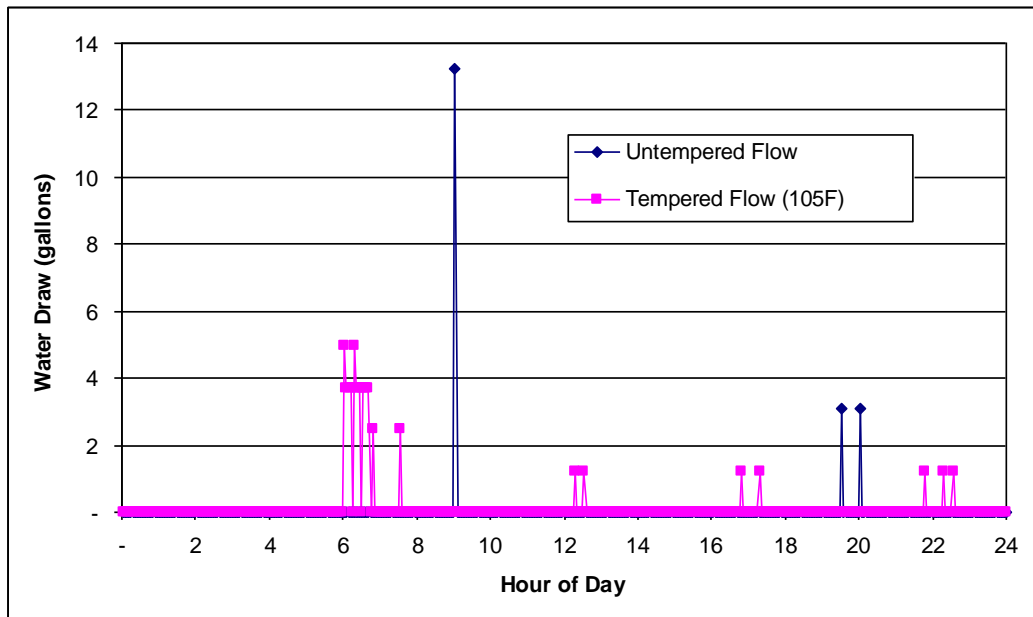


Fig. 3.4. Assumed daily hot water draw schedule from DHW tank

Performance simulation results. Predicted total annual energy savings for the GS-IHP prototype 2 design are shown in Table 3.7 based on TRNSYS analyses in five Building America locations. The predicted energy savings range from 57.2% to 61%. Average savings are 58.7% over the 5 climates.

Electric resistance energy use for space and water heating is predicted to be essentially eliminated in all but the northern climate case, where it was reduced by 97.4%. Water heating savings relative to resistance units range from 68 to 79%.

Table 3.7. Energy Use and Savings for Prototype 2 Relative to Minimum Efficiency Equipment Suite in Residential 2-ton (7 kW) Cooling Application

Operation Mode	Equipment Options				
	ASHP	2-Capacity GSHP w DS		Variable-Speed GSIHP	
	Energy Use, kWh (I ² R)	Energy Use, kWh (I ² R)	% Savings From Base	Energy Use, kWh (I ² R)	% Savings From Base
Atlanta					
space heating	2388	1660	30.5%	1155	51.6%
resistance heat	(93)	(5)		(6)	
space cooling	1608	1177	26.8%	754	53.1%
water heating	3293	2672	18.8%	848	74.3%
resistance heat	(3293)	(2524)		(3)	
ventilation fan	189	189		189	
totals	7479	5699	23.8%	2946	60.6%
Houston					
space heating	1102	754	31.6%	495	55.1%
resistance heat	(6)	(0)		(1)	
space cooling	2548	2154	15.5%	1542	39.5%
water heating	2813	2030	27.8%	619	78.0%
resistance heat	(2813)	(1876)		(0)	
ventilation fan	189	189		189	
totals	6653	5128	22.9%	2845	57.2%
Phoenix					
space heating	762	542	28.9%	306	59.9%
resistance heat	(0)	(0)		(0)	
space cooling	3450	2756	20.1%	1921	44.3%
water heating	2470	1731	29.9%	510	79.4%
resistance heat	(2470)	(1575)		(0)	
ventilation fan	189	189		189	
totals	6871	5218	24.1%	2926	57.4%
San Francisco					
space heating	1366	1142	16.4%	813	40.5%
resistance heat	(0)	(0)		(0)	
space cooling	23	4	83.9%	10	57.0%
water heating	3766	3405	9.6%	1070	71.6%
resistance heat	(3766)	(3330)		(0)	
ventilation fan	189	189		189	
totals	5344	4741	11.3%	2082	61.0%
Chicago					
space heating	6448	4052	37.2%	3139	51.3%
resistance heat	(1268)	(95)		(41)	
space cooling	651	333	48.8%	251	61.5%
water heating	4140	3309	20.1%	1309	68.4%
resistance heat	(4140)	(3108)		(101)	
ventilation fan	189	189		189	
totals	11429	7884	31.0%	4888	57.2%

GS-IHP field performance observations. Both the 1st and 2nd generation prototype IHPs were field tested in a research house in Oak Ridge, TN with simulated occupancy loads (Munk et al, 2014). Figure 3.5 is a photo of the house along with thermal envelope and air infiltration rate details. Figure 3.6 shows the GHX layout (a horizontal trench GHX, part of which was located in existing foundation and utility trenches).

- 2-stories with walkout, unfinished basement (conditioned)
- 344 m² (3700 ft²)
- Wall R_{SI}-3.7
(R_{US}-21)
- Attic R_{SI}-8.8
(R_{US}-50)
- Triple Pane Windows
- 1.24 ACH@50 Pa



Fig 3.5. GS-IHP test house and details

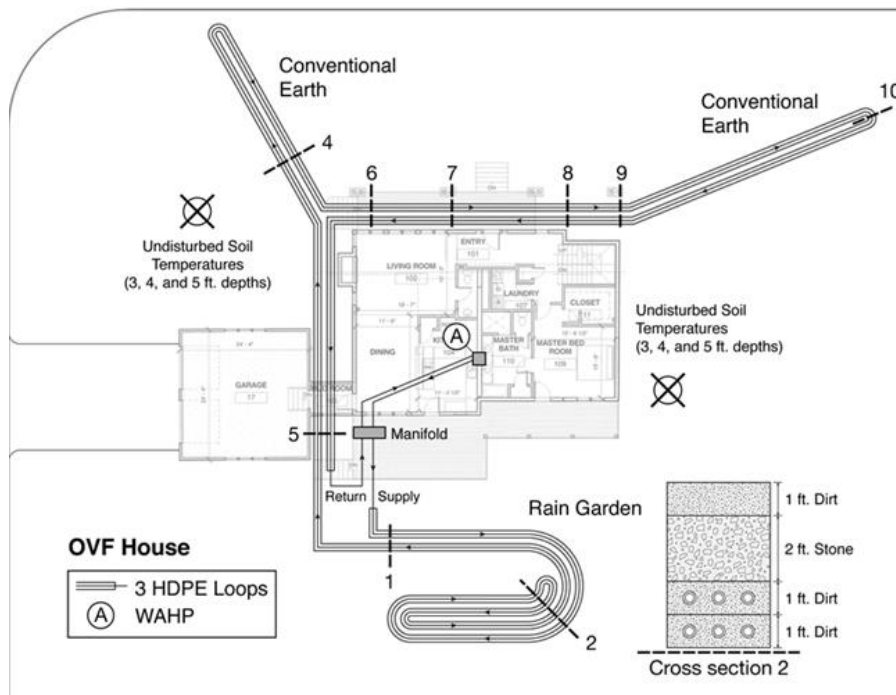


Fig. 3.6. GS-IHP test site GHX layout

The home was split into four zones, upstairs, downstairs living space, master bedroom, and basement, which were all controlled to same set points of 21.7°C for heating and 24.4°C for cooling. The GHX had a total of 796 m of high density polyethylene (HDPE) pipe placed around the foundation of two of the basement walls in addition to two utility trenches and a rain garden in the backyard.

Table 3.8 shows the four operating modes of the prototypes. During the cooling season, the unit can operate in three of the four modes: SC, SC+WH, or WH. If there are coincident space cooling and water heating demands, the unit will run in the SC+WH mode. If there is only a demand for water heating, the unit will run in WH mode. During the heating season, the unit only operates in two of the four modes: SH and WH. There is no combined space heating and water heating mode, so the unit gives water heating priority unless the indoor space temperature falls by a preset number of degrees below the heating set point.

Table 3.8. Prototype GS-IHP Operating Modes

Mode	Heat Source	Heat Sink
Space Cooling	Indoor Air	Ground Loop
Space Heating	Ground Loop	Indoor Air
Space Cooling plus Water Heating	Indoor Air	Domestic Hot Water
Dedicated Water Heating	Ground Loop	Domestic Hot Water

The 1st generation prototype was monitored for the 2011 year (January through December) with details summarized in Baxter et al (2013). Several technical issues were encountered during the year that resulted in frequent interruption of GS-IHP operation. While this limited the extent of the collected performance data, what was available provided invaluable information to CM, enabling them to develop a much improved 2nd generation prototype.

The 2nd generation prototype was installed at the test site on May 7, 2012 with the help of CM personnel. Monitoring of the 2nd generation system took place from June 2012 through January 2013. Since an entire year's worth of data was not able to be collected during the project, approximations were made for months where data was not available so that the annual performance could be estimated. The first step in this process was to fit a sinusoidal wave to the daily average outdoor air temperature (OAT) and daily average entering water temperature (EWT) data. These waveforms were then used to generate average monthly OATs and EWTs for the months without data, Figure 3.7. The load in each mode was then estimated by plotting the monthly delivered output in kWh against the average OAT for the month. A linear fit was applied and, along with the estimated OAT, a delivered load was estimated for months without data. Similarly the COPs for each mode were estimated by plotting the existing data against the average EWT for each month.

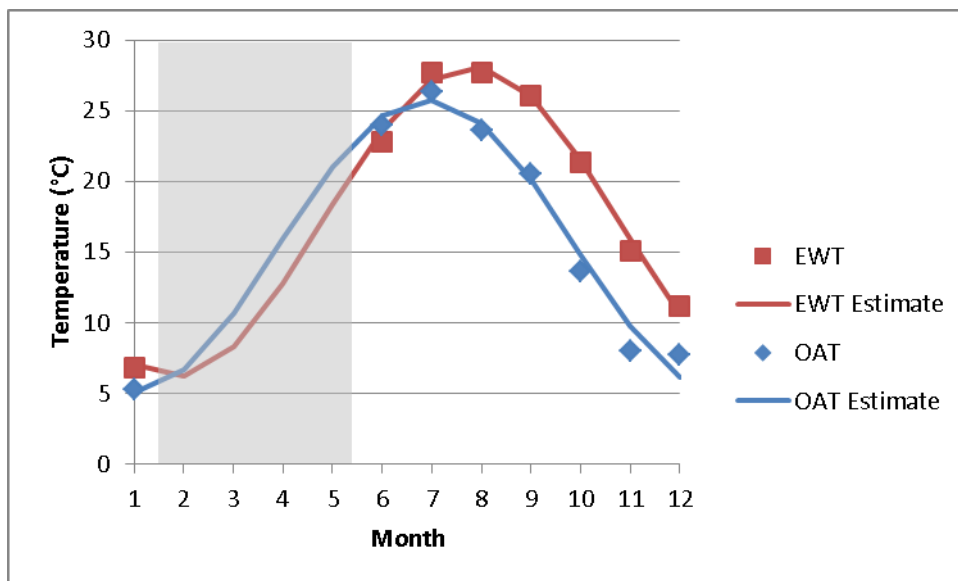


Fig. 3.7. OAT and EWT Measured Data and Estimates (2012-2013)

The estimated annual energy use of the GS-IHP was then compared to that of a baseline system at the same site. The baseline consisted of an ASHP with a rated seasonal cooling COP of 3.8 (SEER of 13 Btu/Wh) and rated seasonal heating COP (in US Region III) of 2.4 (HSPF of 8.3 Btu/Wh), as rated per AHRI 210/240 (AHRI 2008), coupled with an electric resistance water heater. The ASHP rated cooling performance was degraded by 4.7% based on manufacturer's performance data to account for site return air temperatures that were lower than those used to determine the ratings. Results are shown in Table 3.9 below. The space cooling performance for the GSHP is similar to the performance seen from high end ASHPs that have been tested in this climate. However, the water heating COP of 3.8 and space heating COP of 4.1 are very high relative to standalone heat pump water heaters

(HPWH) and ASHPs, respectively. Since the tank losses from the DHW storage tank were not accounted for in the GS-IHP field measured performance, they were also omitted from the baseline equipment efficiency for the performance comparison in Table 3.9 (baseline WH energy factor (EF) of 1.0).

The table shows that the largest percentage and absolute savings come from water heating, at 73.4% and 2007 kWh respectively. The energy savings in the space heating mode come in a close second at 1798 kWh due to both the high efficiency and high heating load (higher than normal for the test site location). The total annual savings when compared to the Baseline equipment is predicted at about 47%, which is very close to the 50% targeted savings for the project. One should note that the actual daily hot water use at the test site was only ~185 l/day vs. the ~245 l/day used for the prototype 2 simulations summarized in Table 3.7. Had the DHW usage at the test site been at the higher level, the annual savings would have been about 50%.

Table 3.9. GS-IHP vs. Baseline Equipment; Estimated Annual Performance Comparison

		GSIHP	Baseline Equipment	Percent Savings Over Baseline
Space Cooling	COP	4.9	3.7	
	Delivered (kWh)	8432	8432	
	Consumed (kWh)	1707	2298	25.7%
Space Heating	COP	4.1	2.4	
	Delivered (kWh)	10524	10524	
	Consumed (kWh)	2539	4337	41.5%
Water Heating	COP	3.8	1	
	Delivered (kWh)	2733	2733	
	Consumed (kWh)	726	2733	73.4%
Total	Consumed (kWh)	4972	9368	46.9%

The HPDM was calibrated against lab data for the 2nd generation unit and used to develop performance maps and these, in turn, were input to the TRNSYS/HPDM (T/H) annual performance simulator along with the site weather data for the 2012 heating and cooling seasons, the site hot water usage averaging ~185 l/d (~49 gal/d), average GHX loop EWTs and water mains temperatures during heat pump operation, and test house specifications to estimate annual performance compared to a baseline minimum efficiency equipment suite (the same baseline suite as described in the Background section minus the dehumidifier and humidifier). The GHX loop EWTs and water mains temperatures for 2012 are shown in Figures 3.8 and 3.9.

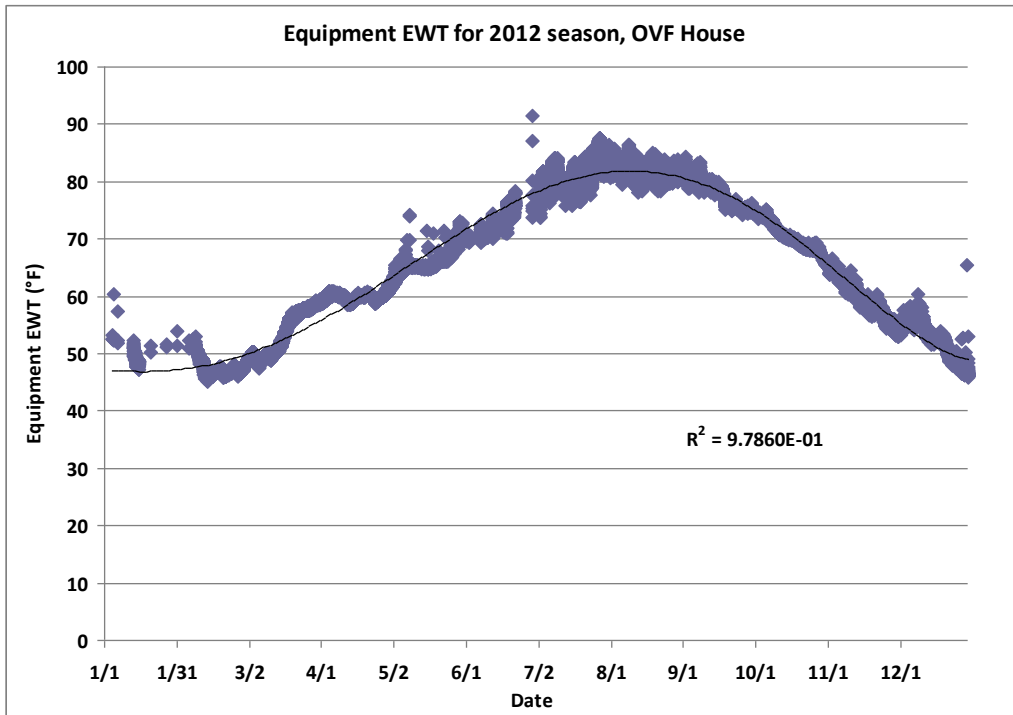


Fig. 3.8. Average return ground loop temperatures during heat pump operation for 2012 season, ZEBRAIalliance house 2 in Oak Ridge, TN

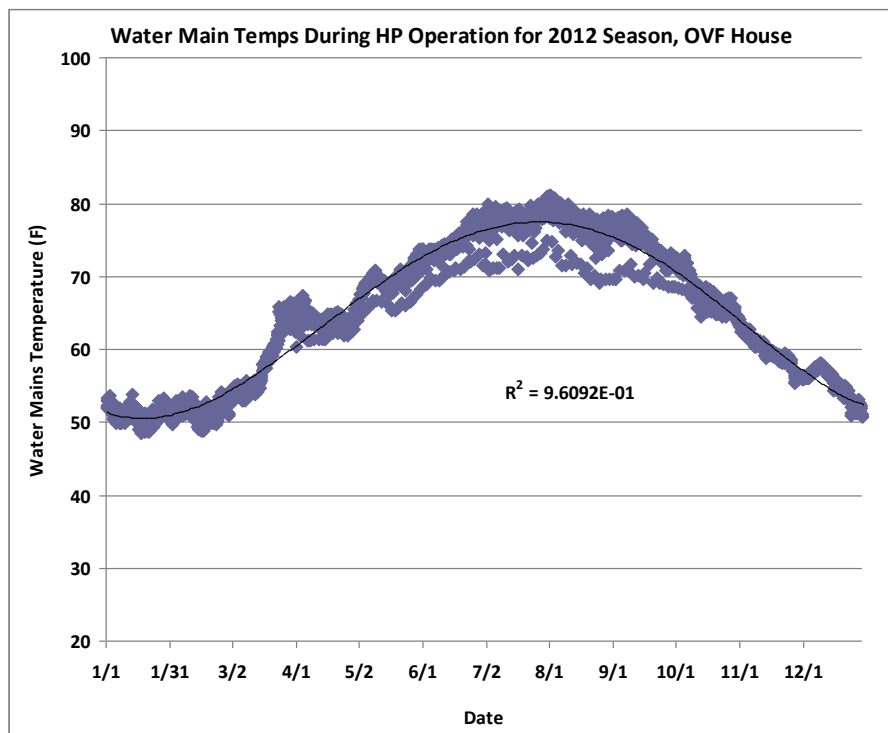


Fig. 3.9. Average water mains temperatures during heat pump operation for 2012 season, ZEBRAIalliance house 2 in Oak Ridge, TN

Results of the T/H simulations follow in Tables 3.10 and 3.11. Table 10 shows the projected energy savings for the 2nd generation prototype where predicted total HVAC/WH savings are 57.8%. Space conditioning savings approach 50% while water heating savings exceed 76%

compared with the baseline electric resistance water heater (WH tank losses were accounted for in the simulation).

Table 3.10. Projected 2nd generation GS-IHP prototype energy savings vs. baseline systems for House 2 in 2012 Season

Predicted Loads and Energy Use by Mode; OVF House, 2012 Season				
Loads from GSIHP Simulation		1-Speed Base	2 nd Generation GSIHP	
Operation Mode	kWh	Energy Use kWh	Energy Use	Reduction from
Oak Ridge, TN				
space heating	8765	3265	1690	48.2%
resistance heat		(127)	(29)	
space cooling	5202	1539	768	50.1%
water heating	2313	2605	610	76.6%
resistance heat		(2605)	(0)	
ventilation fan		109	109	
totals	16280	7519	3177	57.8%

Table 3.11 shows the predicted seasonal COPs (performance factors). Converting the seasonal performance numbers to US SEER and HSPF indices, the GS-IHP had a predicted SEER of 23.1 Btu/Wh and HSPF of 17.7 Btu/Wh.

Table 3.11. Projected 2nd generation seasonal COPs

Predicted Seasonal COPs, OVF House, 2012 Season			
	SC COP	SH COP	WH COP
Baseline ASHP	3.38	2.68	0.89
2 nd Gen. GSIHP	6.77	5.19	3.79

GS-IHP product development status and preliminary payback analyses. A new product based on the beta unit design was announced by CM in 2012 – the Trilogy[®] 40 Q-Mode[™] (<http://www.climatemaster.com/residential/geothermal-heat-pumps/trilogy/>). The unit was formally introduced in a March 2012 press release and was available for order beginning in December 2012. It is available in two nominal SC capacity sizes: 7kW (2 ton) and 14 kW (4 ton).

Preliminary payback analyses for the GS-IHP system concept were reported in Murphy et al (2007b). These analyses were based on the assumption of large quantity production and mature market competition. The simple payback for the GS-IHP vs. the baseline system ranged from 7 to 14 years. These estimates are subject to significant uncertainties primarily related to the GHX installation costs, which can vary widely depending on local site geologic characteristics.

3.2.2 Electric AS-IHP system development, analyses and test results

Full details of the AS-IHP concept development can be found in the report by Murphy, et al (2007a). Figure 3.10 shows a conceptual installation and Figure 3.10 a system schematic. The system uses a variable-speed (VS) compressor, VS indoor blower (for SH/SC distribution), VS outdoor fan, and a hot water circulation pump that may be single-, multi-, or variable-speed. A 190 l (50 gal) WH tank is included. The concept development analyses reported in Murphy et al (2007a) included dedicated DH and H operating modes. none of of the prototype system developments described here include H operation but one does include a dedicated DH mode. In addition those analyses were based on a relatively small (1800 ft², 167 m²) and very well insulated house with nominal cooling design loads of 3.5-5.3 kW (1-1.5 tons) depending upon location. The specific electric AS-IHP developments were of 10.5 kW (3-ton) nominal cooling capacities while the gas engine AS-IHP development was a nominal 17.6 kW (5-ton) size.

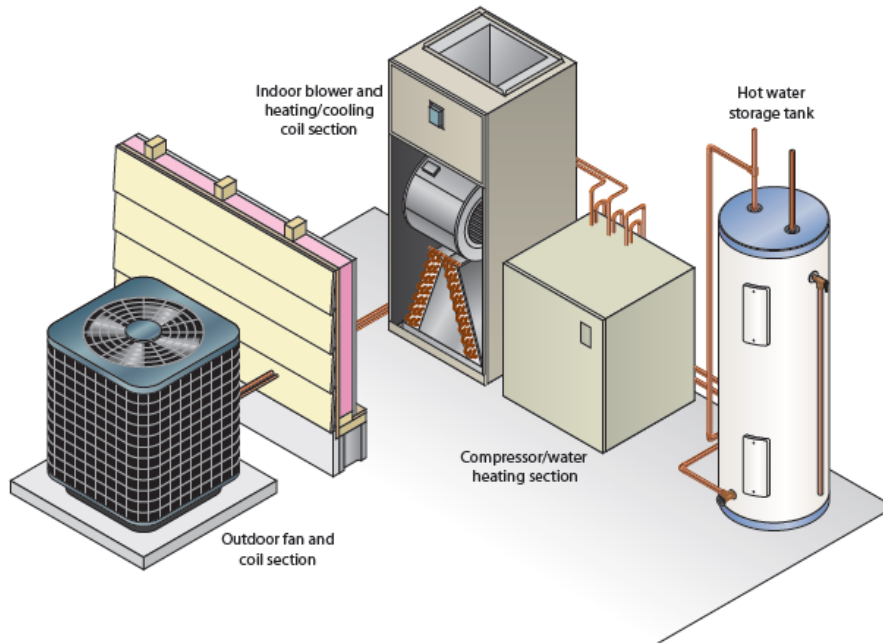


Fig. 3.10. Conceptual installation of the residential air-source integrated heat pump.

Electric AS-IHP 1 – single-compressor or combined system

The AS-IHP concept investigation reported by Murphy, et al (2007a) led to collaboration with an ASHP manufacturer to develop a design suitable for existing residential applications using R-410A refrigerant. A nominal 10.6 kW (3-ton) design cooling size was selected for development. ORNL and manufacturer team members engaged in an iterative process of prototype analyses/design, lab testing, and re-design based on lab results. Three generations of prototypes were developed leading to field testing. The design uses VS compressor, blower, and fan. Dual electronic expansion valves (EEVs) are used to provide a wide range of refrigerant flow control. A double-walled concentric fluted-tube heat exchanger (HX) was used for WH operation with tube-and-fin HXs for the indoor and outdoor coils for the first prototype design. Subsequent prototypes used more compact HX designs for all three HXs.

Expected WH modes of operation included dedicated WH using the outdoor coil as the heat source and combined space cooling (SC) and WH, both of which employed the full condensing (FC) output for WH. Another WH mode used desuperheating (DS) during SC or SH operation. A pump capable of at least two-speed operation was required to meet both FC and DS water flow requirements.

One technical challenge for the AS-IHP system development was refrigerant charge management. This challenge is greater for air-source systems than for ground-source units because outdoor air coils have much larger internal volume than water-to-refrigerant HXs of similar capacity. To deal with this issue, the manufacturer developed a proprietary design to manage charge between operating modes.

Another design challenge is in WH operation. VS compressors typically can operate at maximum condensing temperatures only above a certain speed, with limits on condensing temperature dropping linearly below this speed, illustrated in Figure 3.11. This constraint limits the minimum compressor speed for dedicated WH. In addition, to reach maximum output water temperatures above about 50°C (122°F) while staying within the compressor operating envelope, higher speeds with output capacity of 10.5 kW (3 tons) or more are

required. As such, a pump capable of providing $\sim 1.14 \text{ m}^3/\text{h}$ (5 gal/m) or higher flow is required. Operation in DS-only mode can also provide temperatures above 50°C (122°F).

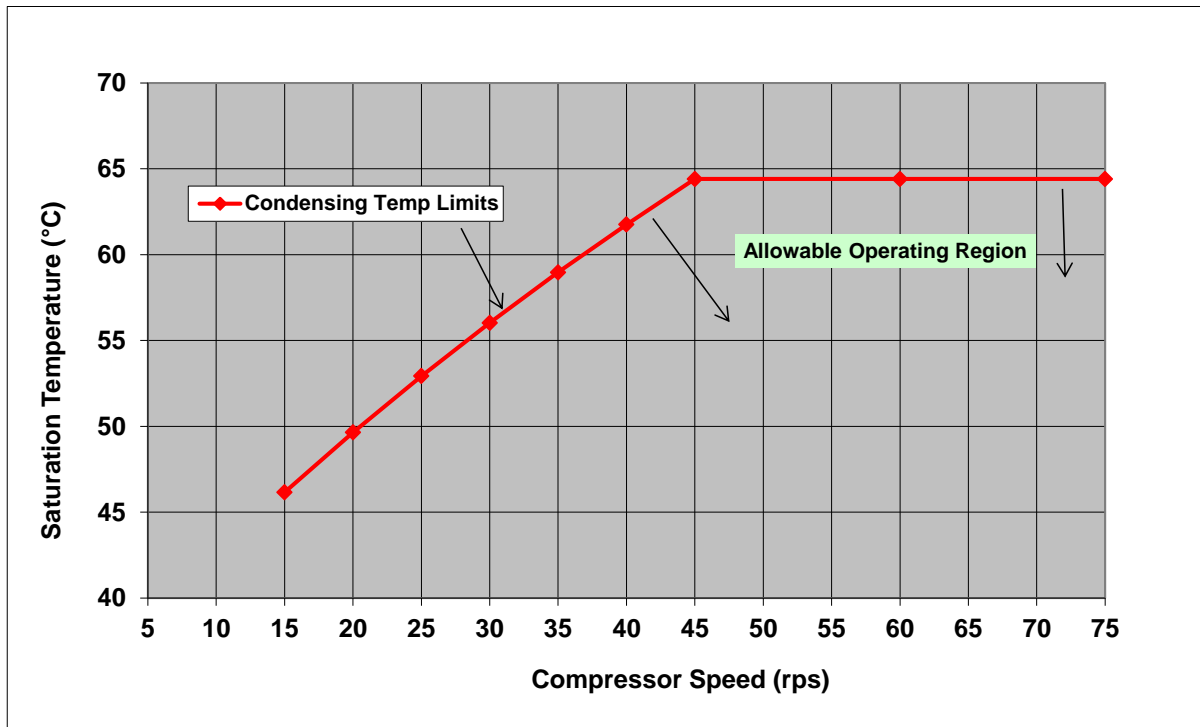


Fig. 3.11. Condensing Temperature Limits Versus Compressor Speed for an Example Rotary Compressor

Development process and projected AS-IHP prototype performance vs. baseline systems in a well-insulated 242 m² (2600 ft²) house located in a range of climates.

Following a similar process as that used for the GS-IHP system analyses, results of the prototype lab tests were used to calibrate the variable-speed research version of the DOE/ORNL heat pump design model (HPDM). In turn, system performance maps generated by the HPDM were used in the TRNSYS/HPDM (T/H) simulation model for estimation of annual performance and energy savings potential. The process is documented by Rice, et al (2014a) and summarized in this subsection.

ORNL used the detailed lab measurements over a wide range of refrigerant, outdoor and indoor air temperature, and entering DHW temperature conditions to calibrate the HPDM in each of the operating modes utilizing the GenOpt program (Wetter, 2009). Once this process was complete, we used the HPDM to generate performance maps (i.e., tables) of capacities, powers, and mass flow rates for each mode as a function of all relevant independent variables, e.g., compressor speed, indoor and outdoor temperature and RH, and entering water temperature (EWT) from the DHW loop. The DS operation was modeled in TRNSYS as a fixed HX effectiveness based on the laboratory test data.

Annual performance analyses were conducted with the T/H model using the same house, climate locations, control set points, and daily DHW use profile and quantity as for the GS-IHP analyses described earlier. For winter operation, thermostat control priority was given to SH with WH limited to DS (and back up electric elements as needed) until the SH heating load was satisfied. This approach provides better control of the indoor space temperature in the winter season than with WH priority control. Dedicated WH (using the outdoor coil as a source) is limited to operation above a specified cutoff ambient, when no SH call is active, and in shoulder months when the ambient is below a specified cutoff. In SC mode, DS WH operation is used first when a WH call is active, until a prescribed water draw is reached, when the unit will switch to combined SC+WH operation with FC output.

Simulation results for the 2nd prototype configuration are shown in Table 3.12 for each location. The entries in red show the portion of the total energy use for that mode that was from resistance heat. Total HVAC/WH energy savings relative to the all-electric baseline unit averaged 52%, ranging from 46-47% in the cold and hot locations to >60% in the mild marine climate. The predicted average space conditioning savings are 42% with average WH savings of 70%.

Table 3.12. Energy Use and Savings Predictions for AS-IHP Lab Prototype 2 Design

Energy Use by Mode, 242 m ² Tight, Well-Insulated House			
Operation Mode	Equipment Performance		
	Baseline	Prototype AS-IHP	
	Energy Use, kWh (I ² R)	Energy Use, kWh (I ² R)	Savings from Base (%)
Atlanta			
space heating	2314	1359	41.2%
resistance heat	(42)	(0)	
space cooling	1566	905	42.2%
water heating	3293	987	70.0%
resistance heat	(3293)	(324)	
ventilation fan	189	189	
totals	7361	3440	53.3%
Houston			
space heating	1062	598	43.6%
resistance heat	(3)	(0)	
space cooling	2498	1480	40.7%
water heating	2728	664	75.7%
resistance heat	(2728)	(121)	
ventilation fan	189	189	
totals	6476	2931	54.7%
Phoenix			
space heating	724	398	45.0%
resistance heat	(1)	(0)	
space cooling	3395	2320	31.7%
water heating	2392	665	72.2%
resistance heat	(2392)	(117)	
ventilation fan	189	189	
totals	6700	3572	46.7%
San Francisco			
space heating	1304	703	46.1%
resistance heat	(1)	(0)	
space cooling	21	11	44.8%
water heating	3676	1126	69.4%
resistance heat	(3676)	(361)	
ventilation fan	189	189	
totals	5189	2030	60.9%
Chicago			
space heating	6287	3974	36.8%
resistance heat	(1037)	(474)	
space cooling	623	340	45.5%
water heating	4110	1545	62.4%
resistance heat	(4110)	(691)	
ventilation fan	189	189	
totals	11209	6048	46.0%

Field performance observations to date. Based on the lab test results and favorable projected energy savings of the 2nd prototype, a 3rd generation field test prototype was fabricated. A one-year field test was initiated in a 223 m² (2,400 ft²) test house (Figure 3.12) in Knoxville, TN in May 2014. Pictures of the field test system are included in Figure 3.13 with the data acquisition system (DAS) shown in Figure 3.14.



Fig. 3.12. Field test site in Yarnell Station neighborhood, Knoxville, TN



Fig. 3.13. Prototype installation; l) indoor sections (hot water storage tank, compressor and water heating module, and indoor fan coil), r) outdoor fan coil section



Fig. 3.14. Field data monitoring system

Cooling season summary. Before the field testing started work was done to set up the test house occupancy simulation. The water draw schedule used at the site is based on the latest Building America water draw generator http://www1.eere.energy.gov/buildings/residential/ba_analysis_spreadsheets.html. Latent, sensible and various building loads are based on the Building America House Simulation Protocols (Hendron and Engebrecht, 2010). Occupancy simulation is accomplished via scheduled operation of small space heaters (to simulate sensible heat), and humidifiers (to simulate latent heat). DHW loads (dishwasher, clothes washer, showers, sinks, etc.) are simulated by operating solenoid controlled water valves according to the programmed schedule. Temperature control set points of 49.0°C (120 °F) for WH and 24.4 °C (76 °F) for space cooling were implemented in the system controls prior to starting data monitoring in May. The primary operating modes experienced during this period were:

- SC only (Ded SC)
- SC + desuperheater (DS) WH (SC+DS)
- SC + FC WH (SC+WH)

Figure 3.15 illustrates the SC and WH monthly average COPs for each mode and average for the entire month for May through September 2014. The average monthly SC COP has ranged from about 5.0 to 5.35 each month while the monthly WH COP has ranged from 3.23-4.75 (ignoring electric element power usage). There was a small amount of backup WH electric element energy consumption during the summer but this was due to control system issues (e.g. control computer failing to reboot properly, etc.). No element usage would be expected in the summer period under the hot water use profile in effect at the test house.

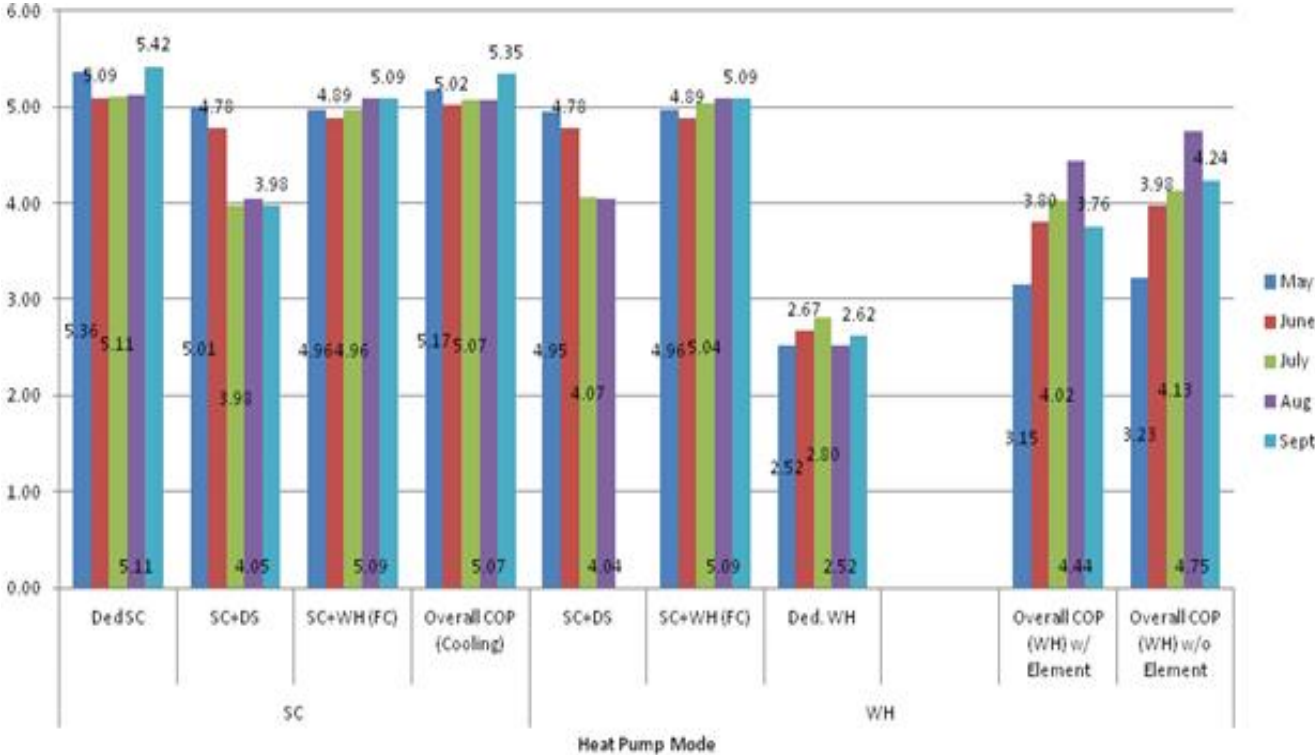


Fig. 3.15. Average monthly SC and WH COPs by mode and overall

The overall average field-measured system cooling season efficiency for the AS-IHP system is given in Table 3.13. Average overall efficiencies by mode (SC and WH) are included as well. Average seasonal efficiencies were 5.14 for SC, 4.39 for WH, and 5.03 for the overall average.

Table 3.13. Cooling Seasonal average COPs

Mode	Energy delivered kWh	Energy use kWh	Average COP
SC	7416	1444	5.14 (SEER = 17.47 Btu/Wh)
WH (no element)	1014	231	4.39
Total/average	8430	1675	5.03

Heating season. Heating season field monitoring began in October 2014 and continued through May 2015. Temperature control set points of 49 °C (120°F) for water heating and 21.7 °C (71 °F) for space heating were implemented in the system controls prior to starting data monitoring in October. System performance data are currently under analysis and review by the manufacturing partner and by ORNL and are not available for reporting at this point. A full annual performance report is expected by late Fall 2015.

Electric AS-IHP 2 – two-box system

ORNL has been engaged in a 2nd AS-IHP system development effort with another manufacturer partner (Lennox Industries). This embodiment of the concept is a two-unit or “two-box” system based on a central high-efficiency ASHP coupled with a prototype water heating/dehumidification (WH-DH) module (see Figure 3.16). The WH-DH module can be integrated with the ASHP unit by a parallel secondary duct loop around the central air handler, receiving a portion of the central return air when the secondary (WH-DH) blower is operating and returning this air to the supply air stream. It also has an optional connection to an outdoor air intake to provide a means for conditioning and circulating ventilation air through the central duct system. A dedicated space DH cycle addresses humidity control and integration of heat pump WH is expedient since the small vapor compression components can perform double-duty. This integrated yet independent operation of the WH-DH unit provides dehumidification of the central return and ventilation air as well as a central heat source for the WH mode. The independent operation is especially useful in the shoulder months which often require dedicated DH, along with WH, but little or no SC or SH. Another significant advantage is that *this IHP approach can be relatively easily applied to retrofit/upgrade applications as well as new construction*, utilizing standard electric water heaters and a wide range of multi-capacity and variable speed ASHPs. In retrofit applications even if the tank is remote from the heat pump indoor section, the WH-DH unit can be located at the WH tank and the system will still retain most or all of the IHP advantages. Details of the development are given in Rice et al (2014b) and summarized here.

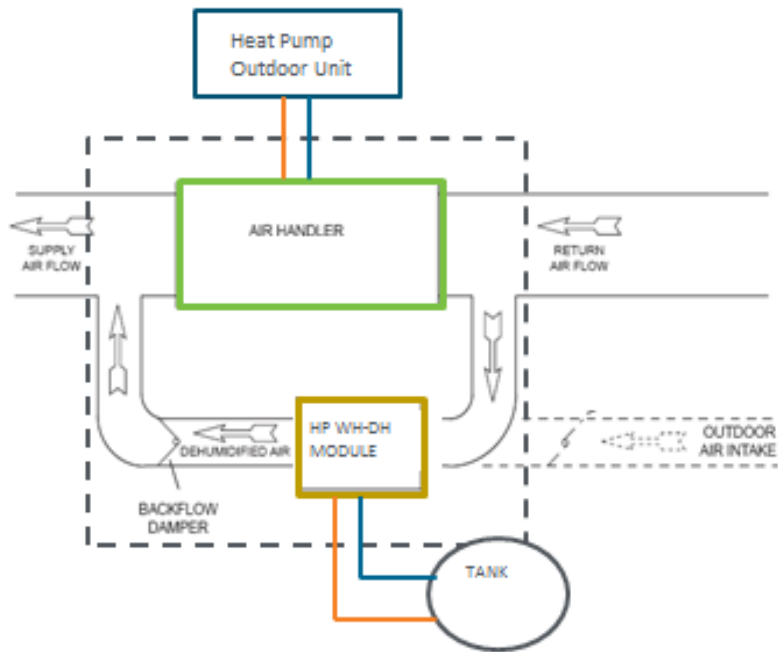


Fig. 3.16. Two-box AS-IHP Concept Schematic

WH-DH module field test prototype design summary. The design of the WH-DH module is based on US Patent 8,689,574 B2 (US Patent Office 2014). Figure 3.17 shows a computer aided design (CAD) drawing of the system concept. Performance goals for the WH-DH unit are to meet or exceed US EnergyStar (<http://www.energystar.gov/>) performance levels for WH and DH modes of operation. For the DH mode, the Energy Factor (EF_d) requirement for EnergyStar rating is >1.85 L/kWh for units with water removal capacity of <35.5 L/d (<75 pints/d or <9.375 gal/d). For WH, an $EF \geq 2.0$ (W/W) is required for EnergyStar designation. The remaining design goal was to provide water heating capacity of ~ 2 kW, about twice that for existing EnergyStar HPWH products.

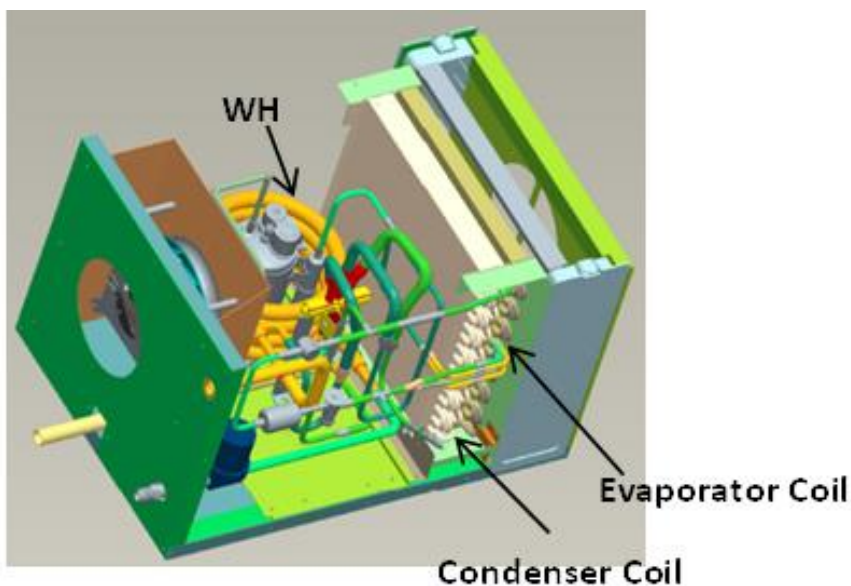


Fig. 3.17. CAD Drawing of 1st Prototype WH-DH Module Layout

Two generations of lab prototypes were assembled by Lennox and tested at ORNL and at Lennox facilities. The initial prototype used an R-410A rotary compressor with ~ 2 kW (~ 7000 Btu/h) cooling capacity and 2.8 cooling COP (9.5 Wh/Btu EER) ratings. Separate condensers

were used for each operating mode -- a 3.5 kW (1-ton) fluted tube-in-tube double-walled water-to-refrigerant heat exchanger (HX) and a three-row fin-and-tube air-to-refrigerant HX, in combination with a common two-row fin-and-tube evaporator. The 1st generation module was tested extensively at ORNL in FY2013 in both the WH and DH modes.

DH mode test results showed an average measured EF_d of ~2.0, exceeding the 1.85 EF goal. WH mode results fell slightly short of the EF goal (1.92 measured vs. the 2.0 goal). High internal heat losses at high entering water temperatures were the primary reason for this shortfall. Based on these 1st generation WH-DH performance test results extended performance maps were developed for each mode using the HPDM (calibrated to the WH-DH lab performance). These maps along with maps (based on published performance data) for a Lennox two-speed ASHP with 5.39 cooling seasonal COP (18.4 Btu/Wh SEER) and 2.67 heating seasonal COP (9.1 Btu/Wh HSPF) ratings were input to the T/H model for annual performance simulation vs. a minimum efficiency electric baseline - ASHP with 3.81 seasonal cooling COP (13 SEER) and 2.26 seasonal heating COP (7.7 HSPF) ratings along with a 0.90 EF water heater and a 1.4 EF_d free-standing dehumidifier. Simulation results (Table 3.14, below) predicted HVAC/WH energy savings for the two-unit AS-IHP system ranging from 33 to 36%, a bit short of the 40% target for this system due primarily to the lower than targeted WH mode performance of the 1st generation WH-DH prototype. The simulations were done for the same house and control set points as used for the GS-IHP and combined system AS-IHP simulations discussed previously but only for the three locations with highest dedicated DH loads.

Table 3.14. Energy Use and Savings Predictions for AS-IHP with Prototype 1 WH-DH Unit Configuration

Energy Use by Mode; 242 m² Tight, Well-Insulated House			
	1-Speed Base	2-Speed w WH-DH Unit, 113 L/s	
Operation Mode	Energy Use kWh (I²R)	Energy Use kWh (I²R)	Reduction from Base (%)
Atlanta			
space heating	2311	1965	15.0%
resistance heat	(18)	(31)	
space cooling	1741	1059	39.2%
water heating	3380	1553	54.1%
resistance heat	(3380)	(488)	
dedicated DH	319	299	6.2%
ventilation fan	189	202	-6.9%
totals	7941	5079	36.0%
Houston			
space heating	995	906	9.0%
resistance heat	(0)	(3)	
space cooling	3035	1975	34.9%
water heating	2813	1169	58.5%
resistance heat	(2813)	(246)	
dedicated DH	1154	1035	10.3%
ventilation fan	189	179	5.6%
totals	8187	5264	35.7%
Chicago			
space heating	6214	4915	20.9%
resistance heat	(916)	(669)	
space cooling	740	402	45.6%
water heating	4218	2122	49.7%
resistance heat	(4218)	(906)	
dedicated DH	154	154	0.0%
ventilation fan	189	169	10.5%
totals	11514	7762	32.6%

A 2nd generation WH-DH prototype was then built and tested by Lennox in 2014. It used the same compressor and DH mode condenser as the first unit. A brazed-plate water-to-refrigerant HX replaced the tube-in-tube design to provide a lighter weight, more compact and easily insulated design. Larger air duct inlet and outlet duct collars were implemented to reduce the static pressure drop in the unit and improve its airflow capability.

DH mode tests of the 2nd generation prototype have shown about a 7% improved DH EF relative to that for the first prototype - ~2.15 L/kWh vs. ~2 L/kWh. We believe this was due to the improved evaporator refrigerant flow distribution and more uniform airflow over the evaporator and condenser from the larger inlet/outlet ducts. WH mode test results showed an EF of ~2.05, thus slightly exceeding the WH performance goal for the project.

Two-box AS-IHP field test system plans. The field test design is generally based on the prototype 2 architecture implementing its operating mode efficiency improvements. Figure 3.18 provides a CAD schematic of the general layout of the field test prototype WH-DH design.

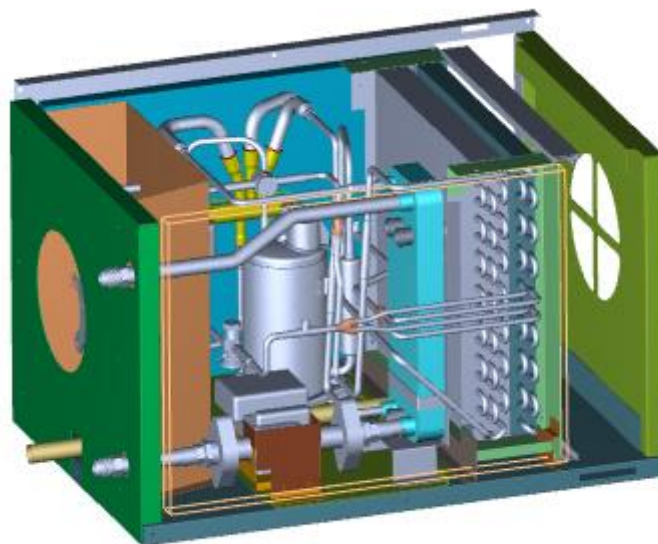


Fig. 3.18. CAD drawing of field test prototype WH-DH module design.

A field test of two-box system began in July 2015 in the test house pictured in Figure 3.12. An artist's concept of the system arrangement is given in Figure 3.19. The ASHP for the field test system will be a new VS ASHP product recently launched by Lennox with nominal 10.5 kW (~3-ton) cooling design capacity. These ASHPs have rated seasonal cooling and heating COPs >5.8 (>20 SEER) and >2.9 (>10 HSPF), respectively. This is at least 8-10% higher than the rated performance of the two-speed ASHP used for the annual performance analyses summarized in Table 3.15 above. Given the higher efficiencies of the VS ASHP and the current WH-DH prototype, we are reasonably confident that the field test system should reach or exceed the 40% annual energy savings project target (average over a range of U.S. climates).

The Lennox VS ASHP can be coupled to a Solar photovoltaic (PV) system (Lennox SunSource[®], Lennox 2013a, b). Rice et al (2014b) investigated how many 275 dc watt solar modules would be needed to offset the annual electrical AS-IHP system energy requirement for each city included in Table 3.15. Annual generation output of the PV modules was estimated per the method reported by Dobos (2013). For Atlanta and Houston 13 modules

and 15 modules, respectively, should be adequate to supply the annual electric power needs of the AS-IHP system. For Chicago, the maximum of 16 solar modules would still leave a shortfall of 2157 kWh. At the time this report is being put together, the rated power of the PV modules has increased to 300W. Use of this PV option is currently not included in the field test plans.

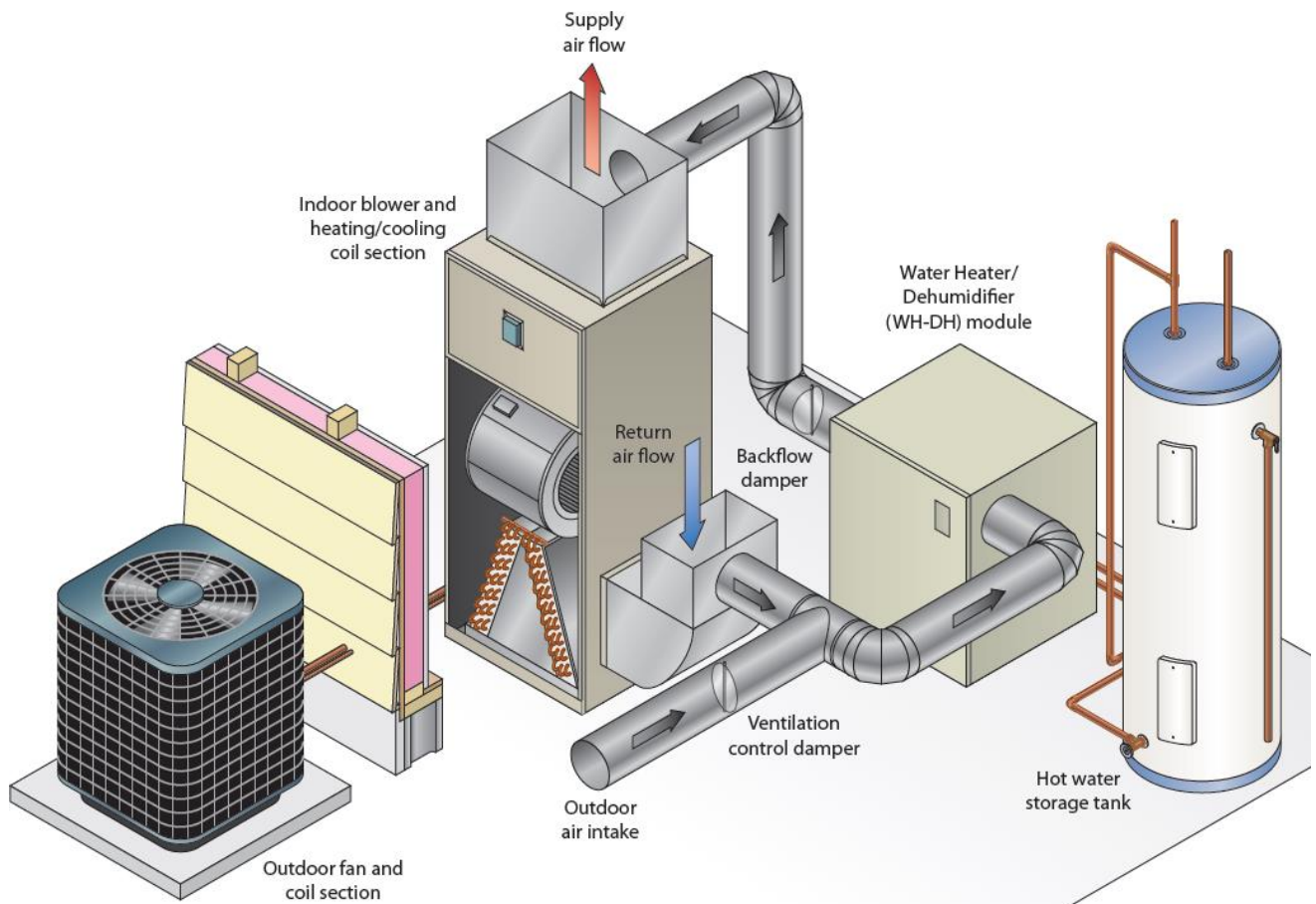


Fig. 3.19. Two-unit AS-IHP field test system arrangement.

3.2.3 Gas engine driven AS-IHP system development summary

Gas Engine-Driven Heat Pumps (GHP) can be an attractive economic choice in parts of the US where the typical engine fuels such as natural gas, propane or liquefied petroleum gas (LPG), can be less expensive than electricity (Mahderekal et al, 2012). Compared to conventional fuel-fired furnace heating systems they are projected to reduce fuel consumption for space heating by 35% and for water heating by 80% (Vineyard 2014). They also significantly reduce summer cooling electric peak demand compared to electric air-conditioning (AC) systems. A GHP can be a more attractive climate control system than conventional single-speed electric heat pumps for a number of reasons, e.g.:

- Variable speed (VS) operation: Typically, the GHP can cycle at minimum speed and modulate between a minimum and maximum speed to match the required load. As a result, the part load efficiency of such a system will be high. Its seasonal operational cost and cycling losses will be lower than those of a single speed system with an on-off control system.
- Engine heat recovery: The engine's waste heat can be recovered to significantly augment SH capacity in winter and to provide DHW heating year-round. Thus, the system's efficiency will be increased.

- As noted already, GHPs rely on natural gas or LPG fuels as the primary energy source. In many regions of the US, these fuels are less costly than electricity for a typical overall HP COP and efficiency of the engine leading to energy cost savings for the building owner.
- By including a generator with the engine, a GHP can produce its own power to run the electric auxiliaries (fans, pumps, etc.). This resource can also be used to generate extra power to charge a battery and provide backup power for essential building needs (refrigerator, lights, etc.) in the event of an electric grid outage. The battery can be used to start the engine, so the GHP could effectively operate independently of the electric grid if necessary (Intellichoice Energy 2014).

ORNL and partners Southwest Gas Corp (SWG, a gas utility company) and Intellichoice Energy (engineering consultancy company), and Marathon Engine Systems (engine and system manufacturer) have been collaborating toward development of a multi-function (or IHP type) gas engine driven heat pump (Vineyard 2014). The system design was based on the needs of the SWG market located in the southwest US (Figure 3.20). This area is a part of the hot-dry climate zone of the US and characterized by very long, very hot summers, but also experiences very cold winters in parts of the area due to elevation.



Fig. 3.20. SWG utility service area.

Figure 3.21 is a schematic of the system. The engine coolant to refrigerant heat exchanger component (approximately in the center of the schematic) is used during winter SH operation to boost the compressor suction pressure and augment SH capacity. DHW heating is provided by heat recovery from the engine coolant via the heat exchanger component in the center right-hand side of the schematic.

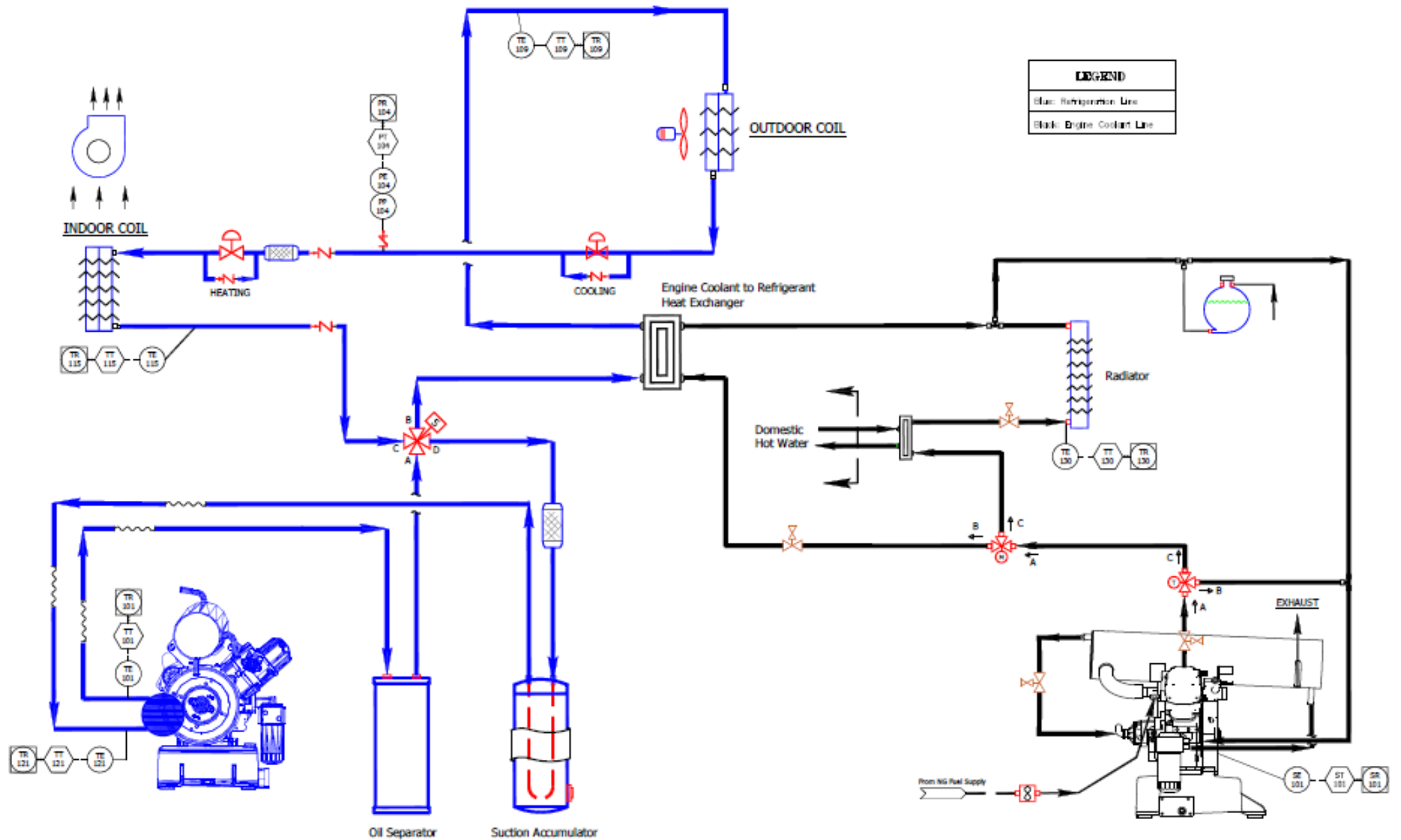


Fig. 3.21. Gas engine AS-IHP schematic; space cooling mode operation shown. Blue lines signify refrigerant flow and black lines engine coolant flow.

Initial, Alpha, prototype. Similarly as for the electric IHP system projects, the gas engine IHP team worked through a number of iterations of prototype design, fabrication and lab testing and field testing. Figure 3.22 is a photo of the first generation, or Alpha, prototype as set up for testing at ORNL. Summary cooling and heating lab test results are given in Figure 3.23 and Table 3.15.



Fig. 3.22. Alpha (1st generation) prototype – lab test set up.

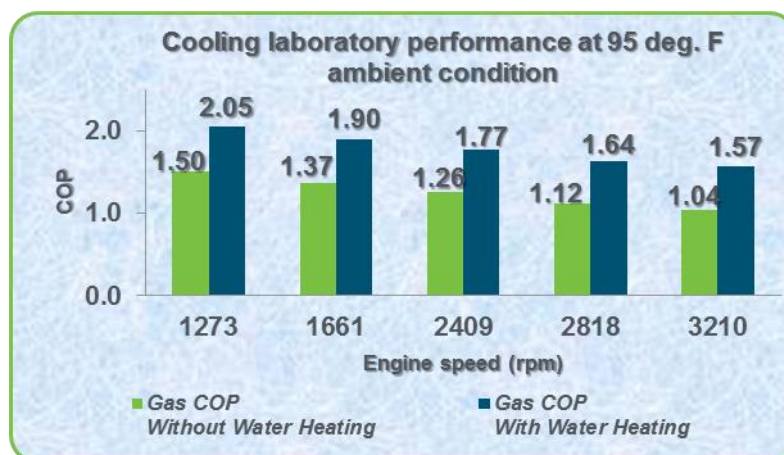


Fig. 3.23. Alpha 1 Cooling COP with and without WH vs. Engine speed (based on gas consumption).

Table 3.15. Alpha prototype lab test summary results vs. project goals; engine rpm ~2400

	Performance target	Test results
Cooling capacity @ 35°C, kW	12.3-18.2	14.4
Cooling COP (gas) @ 35°C	1.3	1.28
Heating capacity, kW @ 8.3°C	14.7-22.0	21.1
Heating COP (gas) @ 8.3°C	1.5	1.48
DHW supply, m ³ /d	0.225	>0.225
DHW supply temperature, °C	60	~60
Ancillary electric loads, kW	0.75-1.0	~0.95

In December 2012, 20 of the Alpha prototypes were installed in occupied homes in the SWG service area. They were monitored through June 2014 (Vineyard 2014; SWG 2014). Figure 3.24 is a photo of one of the systems in Las Vegas. Summary energy cost results for the 2012 test year (for eight systems in the Las Vegas area) are presented in Table 3.16.



Fig. 3.24. Alpha prototype, field test site in Las Vegas area.

Table 3.16. Alpha prototype demonstrated energy costs vs. baseline system at Las Vegas test sites

Site #	2012 baseline energy costs	2013 Alpha prototype energy costs	Savings, %
1	\$3,083	\$2,877	6.7
2	\$3,061	\$2,660	13.1
3	\$2,356	\$2,068	12.2
4	\$1,569	\$1,442	8.0
5	\$3,163	\$2,760	12.7
6	\$3,237	\$2,819	12.9
7	\$3,379	\$2,798	17.2
8	\$3,680	\$3,375	8.3

NOTE – savings expected to be greater in colder locales with greater winter gas usage for space heating.

Table 3.17 presents the gas IHP system cost targets for acceptable market penetration. An overall cost of \$9000 for the system is sought. Assuming the first cost target can be met simple pay back of five years or less could be achieved in locales with high heating loads (Table 3.18). In cooling (AC) load dominated areas, the pay back estimates range from about 7.5 years vs. Minimum efficiency electric AC units to 9 years or more for higher efficiency ACs.

Table 3.17. Component and system cost targets for viable product

Item	Cost for 1000 units
Controls (engine/system)	\$1,000
Recuperator	\$ 600
Compressor	\$ 500
Insulation	\$ 200
Radiator/fan	\$ 450
Drive assembly	\$ 250
Outdoor coil	\$ 800
Cabinet	\$1,300
Alternator/generator	\$ 500
Refrigerant circuit, w/parts	\$1,100
Engine	\$2,300
Total	\$9,000

Table 3.18. Simple payback¹ vs. baseline gas furnace, gas water heater, and electric AC (cooling seasonal COPs of 4.1 and 5.3)

Location	Years for 4.1 AC COP (14 SEER)	Years for 5.3 AC COP (18 SEER)
Elko, NV	3.9	3.7
Las Vegas, NV	7.3	8.9
Phoenix, AZ	7.5	11.7
New York, NY	3.6	3.9
Chicago, IL	4.0	4.1
National average	5.3	5.8

¹Assumes target system cost for 1,000 units of \$9,000 is met

Figure 3.25 presents results of a survey of homeowners who hosted the Alpha prototype field test systems. In terms of system operation and indoor comfort, most responses were either favorable or very favorable. By a small majority, most residents also felt that the DHW performance was improved compared to the baseline gas WH systems they replaced.

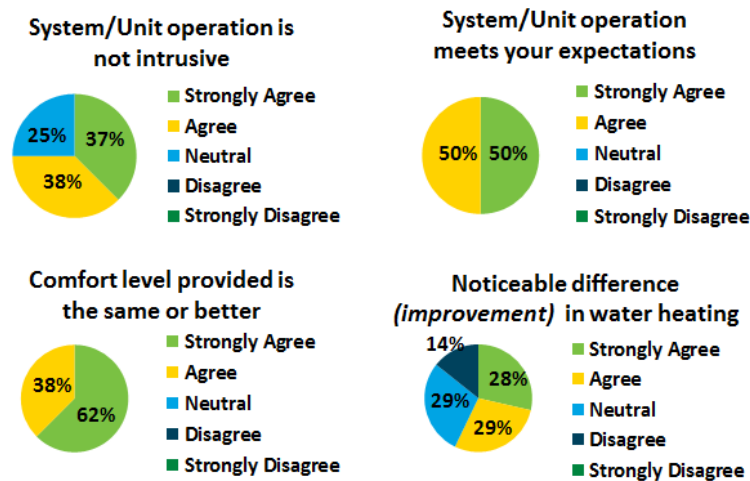


Fig. 3.25. Alpha prototype homeowner survey results (Vineyard 2014).

Beta prototype. Based on the Alpha prototype performance results, the team proceed to development of a next, Beta, generation system. In July 2014 the Beta prototypes were installed at the Las Vegas area field test sites (see photo of one unit in Figure 3.26). The major differences between the Beta and Alpha prototypes were the outdoor coil size increased on the Beta and the fan motor size went from a 0.56 kW electric to 0.25 kW electric motor. The engine operating speeds were also changed. The Alpha I prototype low speed was 1800 rpm and the high speed was 3400 rpm. For the Beta prototype the low speed was increased to 2350 rpm while the high speed setting stayed the same. During peak cooling or heating demands during the 2013 test period, the Alpha unit could not maintain indoor temperature on low speed. For cooling months the indoor temperature would rise and the engine RPM would increase to 3400 RPM. This generally resulted in longer run times when compared to the Beta unit operation in the 2014 summer. For instance during the particularly hot week of July 21, 2014 with site average temperatures ranging from 38.3 to 45.0 °C (and peak temperatures from 46.1 to 55 °C), most of the Beta units generally operated at 2350 RPM (low speed) for over 80% of the time (SWG 2014).



Fig. 3.26. Beta prototype field test unit.

Table 3.19 indicates the Beta units in the 2014 summer ran 35% less time on average than did the Alpha units during the same time period in 2013. In addition to the Beta operating hours being lower than Alpha hours, the overall fuel use by the Beta units averaged ~20% less than that of the Alpha units. While the Alphas had lower fuel use/h (due to the lower speed operation), the Beta units ran less time to achieve the same comfort level results.

Table 3.19. Beta vs. Alpha propane (LPG) prototype field test unit performance

Month	Beta unit runtime, hours (2014)	Alpha unit runtime, hours (2013)	Beta unit propane usage		Alpha unit propane usage	
			Liters	Liters/h	Liters	Liters/h
August	202	353	328.5	1.62	454.6	1.29
September	222	211	355.5	1.60	271.7	1.29
October	52	218	81.9	1.58	280.7	1.29
November	49	25	74.8	1.52	32.2	1.29
Total or avg.	525	807	840.7	1.60	1039.2	1.29

A customer/homeowner survey was also conducted for the Beta prototypes. Overall results indicated the installation, service, and operation of the Betas units met customer expectations. However, a noise issue came up with the Beta units that had not been apparent at the Alpha unit field test sites. Beta unit cabinet enhancements and improvements in the field installation process made a significant improvement in the overall unit vibration and sound pressure levels as compared to the Alpha prototypes. However, the overall noise reduction made it possible for some of the field test site homeowners to now hear a low level sound wave frequency (less than 90 Hz). The same engine parts were used in both the Alpha and the Beta units. Detailed sound analyses revealed that there are three sources of noise: combustion noise, combustion induced mechanical noise and mechanical noise. The induced and mechanical noise concerns have been addressed effectively. Engine combustion (exhaust) noise has also been reduced sufficiently by the current muffler design (Mahderekal 2015).

Beta prototype with power generation capability. Low cost (~\$500) DC generators, rated for 2400 watts, were installed on the prototype for internal (to the unit) and external electric power supply. Figure 3.26 shows the generator installation. A DC to AC transformer was included to convert the 24volt DC generator output to the 120 volt AC output needed by the unit fans and external electric loads.



Fig. 3.26. Prototype with low-cost DC generator option.

Short term (three day long) testing was performed in order to investigate the performance of the unit with low cost power generation. The ambient temperature was set at 35 °C and indoor temperature was set to 26.7 °C with relative humidity of 51%. Figure 3.27 summarizes the performance of the system at different conditions. The internal power generator consistently produced about 1.5 kW for the indoor and outdoor fans. At 1600 rpm and zero external power extraction, the cooling capacity was 18.2 kW (5.2 tons). With extraction of 0.4 kW for external loads, however, the cooling capacity fell to 10.6 kW (3 tons). Further increases in external electric load at 1600 rpm resulted in engine stall.

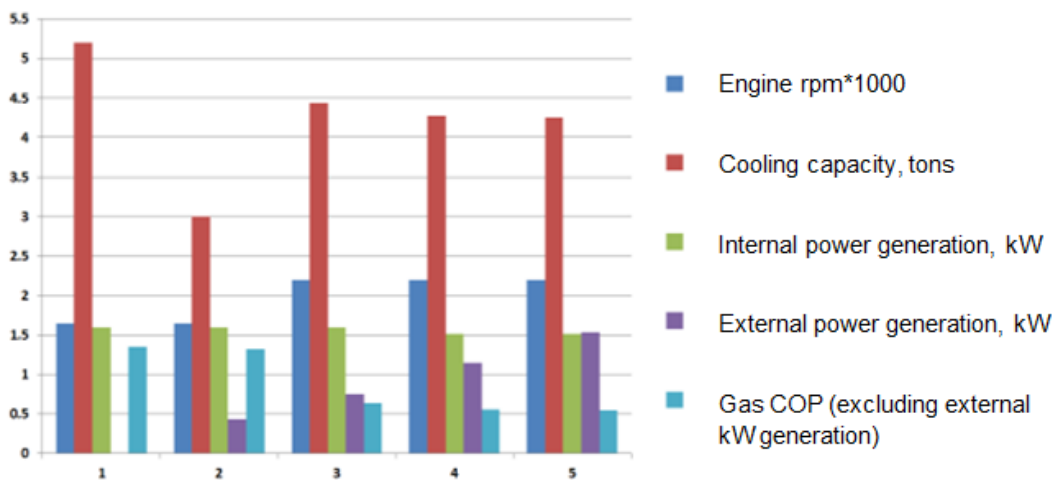


Fig. 3.27. Lab test results for prototype with low-cost generator; at 35 °C (95 °F) – x-axis indicates test number.

At 2200 rpm the system could produce much more external power but at lower efficiency. Up to 1.6 kW of external power could be produced without significant loss of cooling capacity. This is enough power to run essential household appliances during emergency grid power loss. The tests revealed that the natural gas to electricity generation efficiency of the unit is between 12-20% (not including hot water production). This suggests that, for most efficient overall operation, grid electricity should be used for the indoor and outdoor fans whenever available and only switch to the generators when grid power is lost.

Due to the low electric generation efficiency with the initial DC generators, it was decided to modify the design and use a single 5000 Watt AC generator (Figure 3.28). A control/operation strategy to use grid electricity for the unit indoor and outdoor fans whenever available was adopted. During grid outage situations, the unit controller will increase the engine speed and keep it constant and turn on the AC generator. The generator will produce approximately 1.6 kW AC power for indoor and outdoor fans and other electricity needs of the heat pump system. It will also produce approximately 1-2 kW of additional electric power for emergency external needs such as lighting, refrigerator, etc. It is expected that average electricity demand from the generator will be in the range of 2-3 kW (40 to 60% of rated output) in which the 5 kW generator efficiency is fairly high (~70%).



Fig. 3.28. Prototype with low-cost AC generator

Laboratory test performance results for the latest Beta prototype are summarized in Table 3.20. Field testing of this version began in June 2015 and a final report is expected after the 2015/2016 heating season.

Table 3.20. Beta prototype cooling mode lab test results.

OD temp (°C)	Engine rpm	SC Capacity kW	WH Capacity kW	Fuel use kW	OD Fan Watts	ID Fan Watts	Gas COP		System COP (with fan power from grid)	
							w-o/WH	w/WH	w-o/WH	w/WH
35.0	1400	5.8	2.0	3.4	442	885	1.69	2.29	1.22	1.65
35.0	1800	8.8	3.7	5.0	442	885	1.77	2.51	1.40	1.99
35.0	2200	10.9	0.0	6.8	442	885	1.61	1.61	1.34	1.34
35.0	3100	14.6	9.1	11.7	442	885	1.25	2.02	1.12	1.82
35.0	3400	16.3	10.5	13.3	442	885	1.23	2.02	1.11	1.83
40.6	3400	13.3	11.1	14.1	442	885	0.95	1.74	0.86	1.59
40.6	3000	13.7	0.0	11.5	442	885	1.19	1.19	1.07	1.07
40.6	2800	12.1	8.8	10.1	442	885	1.20	2.07	1.06	1.83
40.6	2200	11.0	7.3	6.7	442	885	1.64	2.73	1.37	2.28
46.1	2200	7.0	6.6	7.5	442	885	0.94	1.83	0.80	1.55
46.1	2800	9.8	11.2	11.5	442	885	0.85	1.82	0.76	1.64
46.1	3400	13.3	12.5	15.6	442	885	0.85	1.66	0.79	1.53
51.7	3039	10.0	10.1	14.7	442	885	0.68	1.37	0.63	1.26

4 TASK 3 – TEST FACILITY FOR NZEB TECHNOLOGIES

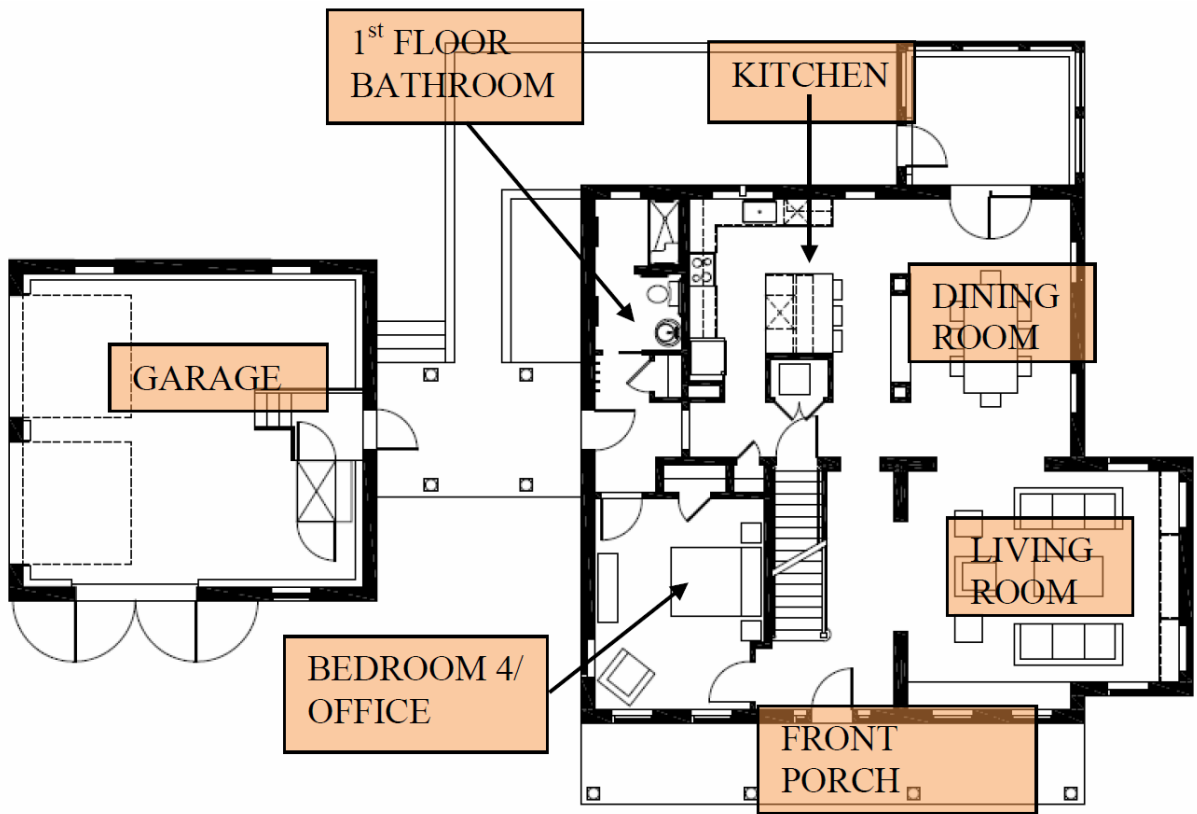
4.1 Background: Net Zero Energy Residential Test Facility, Gaithersburg, MD USA

4.1.1 Objectives for the NZERTF

In 2009, the National Institute of Standards and Technology (NIST) received American Recovery and Reinvestment Act funding for the construction of a net-zero energy residential test facility (NZERTF) on the NIST Campus in Gaithersburg, Maryland (Fanney et al. 2015). The facility was to be constructed as a typical residence for a family of four that could achieve net-zero site energy use on an annual basis. Net-zero energy use was to be accomplished through the combination of low energy loads due to a high performance enclosure, efficient mechanical systems, and low energy fixtures and appliances in combination with site-generated energy using roof-mounted solar photovoltaic panels. Following the demonstration of net-zero site energy use, the facility is to be used by NIST's Energy and Environment Division as a research laboratory to test and measure residential energy technologies, indoor environmental quality, materials, and other aspects of sustainable performance in a realistic context.

4.1.2 Building Characteristics

The NZERTF is a unique facility in that it resembles a residence yet is truly a laboratory, Figure 4.1. Among the NZERTF's unique features is access to three separate ground-source heat exchangers, a radiant basement floor heating system, a solar thermal hot water system with variable solar collector area and storage capacity, a 10.2 kW (DC) photovoltaic system, a heat recovery ventilation system, and various means of interfacing the electric grid with smart appliances. The facility also incorporates three different means of distributing conditioned air throughout the house – a sealed sheet-metal duct air distribution system; a high-velocity ducted air distribution system; and provisions to incorporate a mini-split heat pump system. The NZERTF uses a smart meter to measure the energy imported and exported to the electric grid.



First Floor and Garage

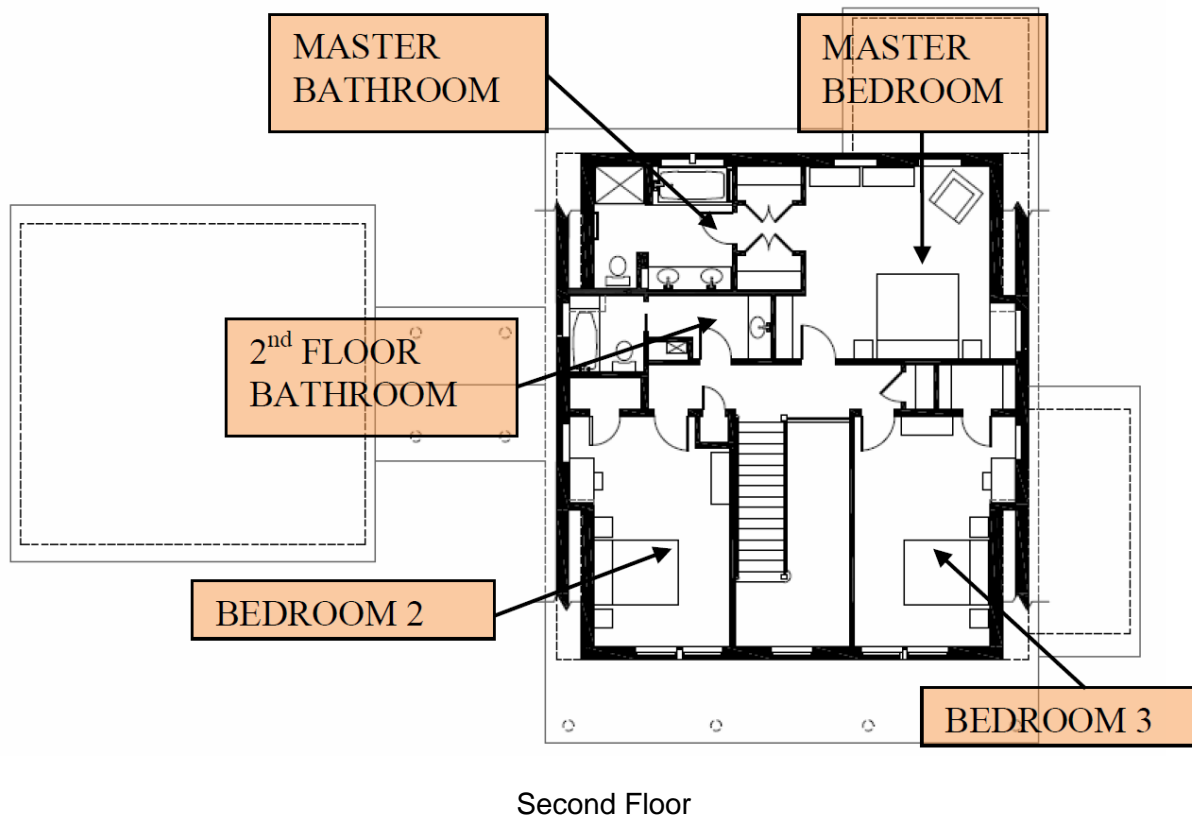


Fig. 4.1. Net zero Energy Residential Test Facility

The house faces true south and has two stories of living area (252 m²) and a full conditioned basement (135 m²). The first floor includes the kitchen and dining area, a family room, an office (optional bedroom), a full bathroom, an open foyer to the second floor, and a utility closet. The second floor consists of a master bedroom with adjoining bathroom, two additional bedrooms, a second bath, and a hallway. The finished basement contains the majority of the facility's mechanical/electrical equipment, whereas the detached garage contains the data acquisition/control equipment associated with the facility.

The heating and air-conditioning system used for the first year of operation (Year1) in the NZERTF consisted of an air-source heat pump (ASHP) system that incorporates a dedicated dehumidification cycle (Figure 4.2a). The air distribution duct system was designed for less than 125 Pa external static pressure drop at the air handler with supply and return duct airflow rates of 2039 m³ h⁻¹ with all registers fully open. The dedicated dehumidification cycle is provided by control algorithms that manage a hot gas bypass arrangement along with an additional indoor air heat exchanger that reheats the dehumidified air. The outdoor unit incorporates a two-speed scroll compressor with two modulated hot gas valves on the compressor discharge that send hot refrigerant gas through a third pipe (Figure 4.2b) to the indoor reheat heat exchanger during active dehumidification. A supply air temperature sensor provides the control signal used to proportionally modulate the flow of hot refrigerant gas to maintain a pre-set supply temperature during dedicated dehumidification. The indoor air handler unit contains a variable speed indoor fan. At the Air-Conditioning, Heating, and Refrigeration Institute (AHRI) rating conditions (AHRI 2008), the A-Test cooling capacity is 7.60 kW and the EER (COP) is 3.82 W W⁻¹. In the heating mode, the unit has a rated heating capacity of 7.80 kW. The unit has a seasonal energy efficiency ratio (SEER) of 4.63 W W⁻¹ and a heating seasonal performance factor (HSPF Region IV) of 2.65 W W⁻¹.



a)

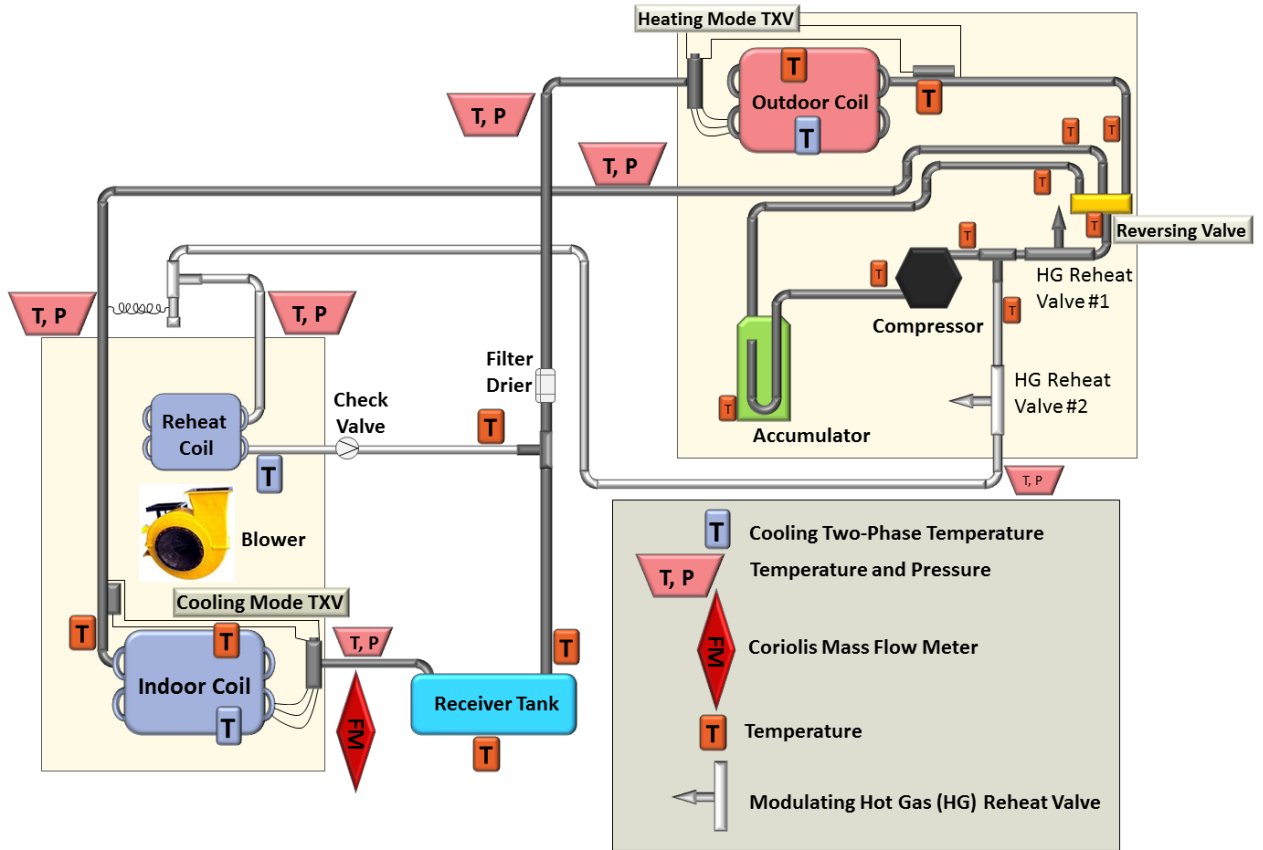




Fig. 4.2. Heat pump indoor unit, refrigerant circuiting/instrumentation (a) and outdoor unit with hot gas reheat piping (b).

4.1.3 Thermal and Electrical Load Profiles

Emulating Occupancy

A myriad of detailed choices had to be made to realistically emulate the daily activities of a family and the resulting energy impacts. These choices can have a substantial effect on energy consumption (Seryak and Kissock, 2003). Although the NZERTF was designed to have very energy efficient heating, ventilating, and air-conditioning (HVAC) systems, lighting, and appliances, it was the goal to ensure that the activities of the occupants would not be substantially different from families living in a conventional house.

Rather than just make arbitrary choices and assumptions about the lifestyle of the virtual NZERTF occupants, user profiles developed for the U.S. Department of Energy (DOE) Building America program were implemented. The Building America program is a multi-year collaboration between DOE national laboratories and U.S. home builders intended to substantially improve the energy efficiency of homes. In order to measure progress in improving the energy efficiency of homes, the Building America program has established a benchmark intended to be consistent with mid-1990s standard practices (Hendron, 2008). This benchmark includes a series of user profiles intended to represent occupant behavior. The Building America user profiles were used where applicable as the basis for determining all of the details needed to simulate occupancy in the NZERTF.

NZERTF Virtual Family

The first key decision to make is the number of people in the virtual family. According to the survey data reported in Hendron (2008), the number of occupants in a single-family house can be estimated by Equation 4.1.

$$\text{Number of occupants} = 0.59 \times N_{br} + 0.87 \quad (4.1)$$

where, N_{br} is the number of bedrooms.

Applying this equation to the four bedroom NZERTF would indicate that the average number of occupants over a large population would be 3.23 people. Since we cannot have fractions of people, it was decided that the virtual family would consist of two adults and two children. The ages of the children are arbitrarily selected to be fourteen (middle school age) and eight

years old (elementary school age). School attendance factors into the family’s daily routines. The fourteen year old is identified as ChildA and the eight year old is identified as ChildB.

NZERTF Occupancy Schedule

The occupancy schedule drives many of the energy loads in the house. To determine the schedule for appliance usage and to account for the sensible and latent load from the people, it is necessary to determine when the occupants are home including when they are in various parts of the house.

Figure 4.3 shows normalized occupancy patterns for weekdays and weekends that are used in the Building America benchmark (Hendron, 2008). Two space types are considered in this profile; bedroom and living room. The occupancy profile, in Figure 4.3, was used as a guide to develop the occupancy profile details for the NZERTF. Additional details about the virtual family must be assumed to complete the daily routine details. It is assumed that both parents work outside the home leaving the house at 8:30 a.m. and returning at 6:00 p.m. As previously noted, ChildA is a fourteen year old middle school student and ChildB is an eight year old elementary school student. It is assumed that both the middle school and the elementary school start at 8:30 a.m. and end at 3:30 p.m. Arrangements have been made for after school care for ChildB every weekday. ChildA has a variable schedule that depends on the day of the week. Both children leave the house at 8:00 a.m. ChildB returns home every day at 6:00 p.m. ChildA returns home at 6:00 p.m. on Mondays, Wednesdays and Fridays, and 4:00 p.m. on Tuesdays and Thursdays. During the summer, it is assumed that the children attend day care or camp outside of the home and follow the same schedule.

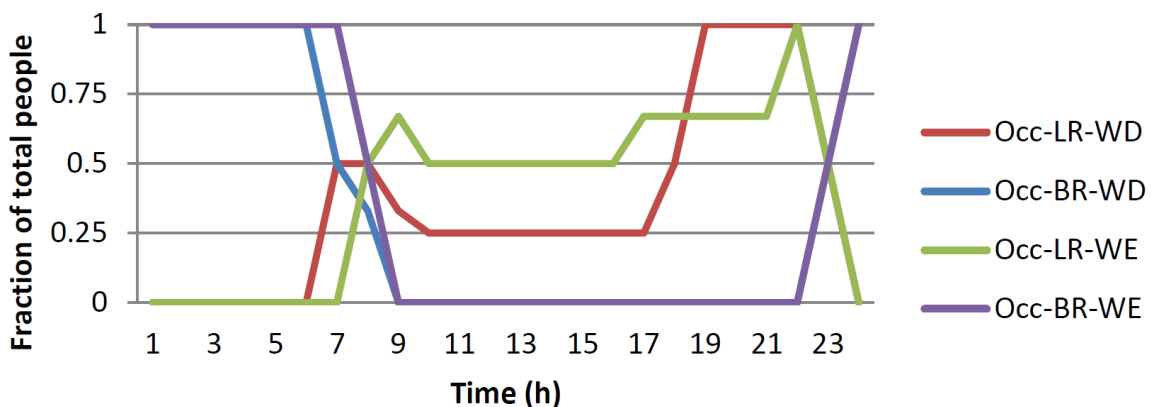


Fig. 4.3. Building America benchmark occupancy profile by day type and space type Occ-WD (occupancy weekdays) and Occ-WE (occupancy weekends), LR (living room) – BR (bedroom)

The net result is that on Mondays, Wednesdays, and Fridays the house is unoccupied from 8:30 a.m. to 6:00 p.m. On Tuesdays and Thursdays, the house is unoccupied from 8:30 a.m. to 4:00 p.m. On weekends it was assumed that at least two members of the family are at home at any given time. The family does not take vacations or host large parties or other social gatherings.

Figures 4.4 through Figure 4.8 represent the daily occupancy profiles of the NZERTF developed by applying these additional constraints to the profile shown in Figure 4.3. For the NZERTF, occupancy of the living room is taken to mean occupancy anywhere that is not in a bedroom. For simplicity and repeatability, the same weekly schedule is used for 52 weeks, irrespective of the seasons or holidays. Establishing the house occupancy pattern enables the development of detailed schedules for other energy consuming activities because occupant initiated activities must take place when the house is occupied.

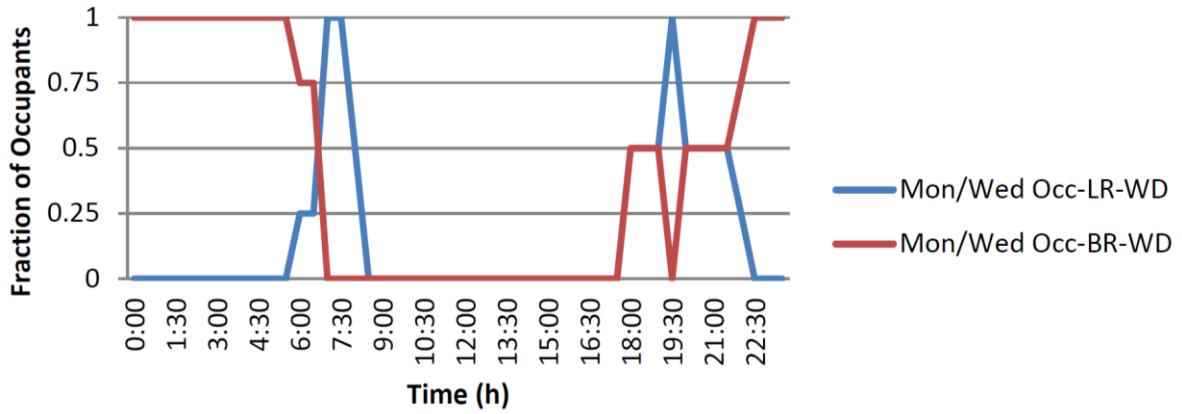


Fig. 4.4. NZERTF occupancy profile for Mondays and Wednesdays

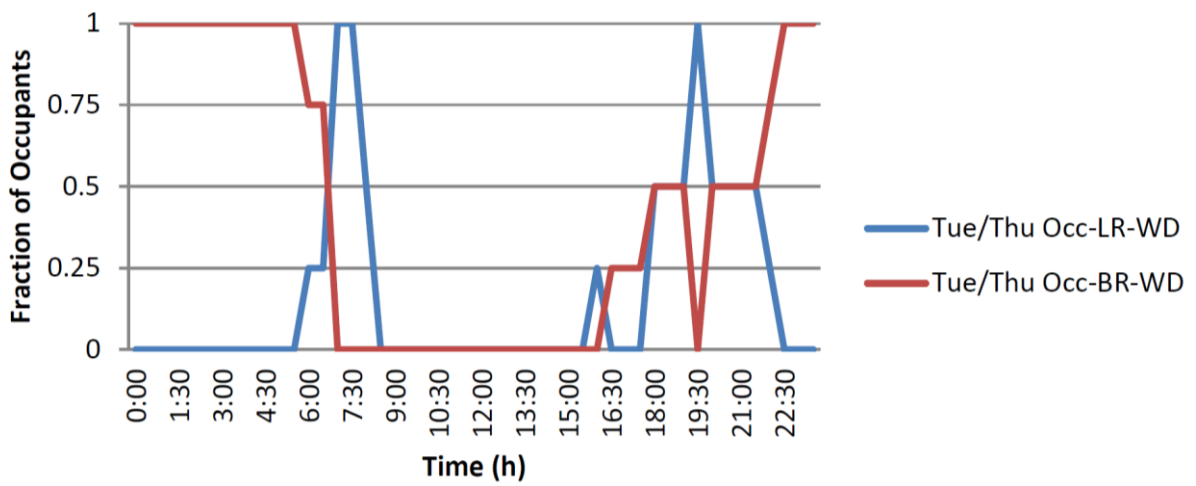


Fig. 4.5. NZERTF occupancy profile for Tuesdays and Thursdays

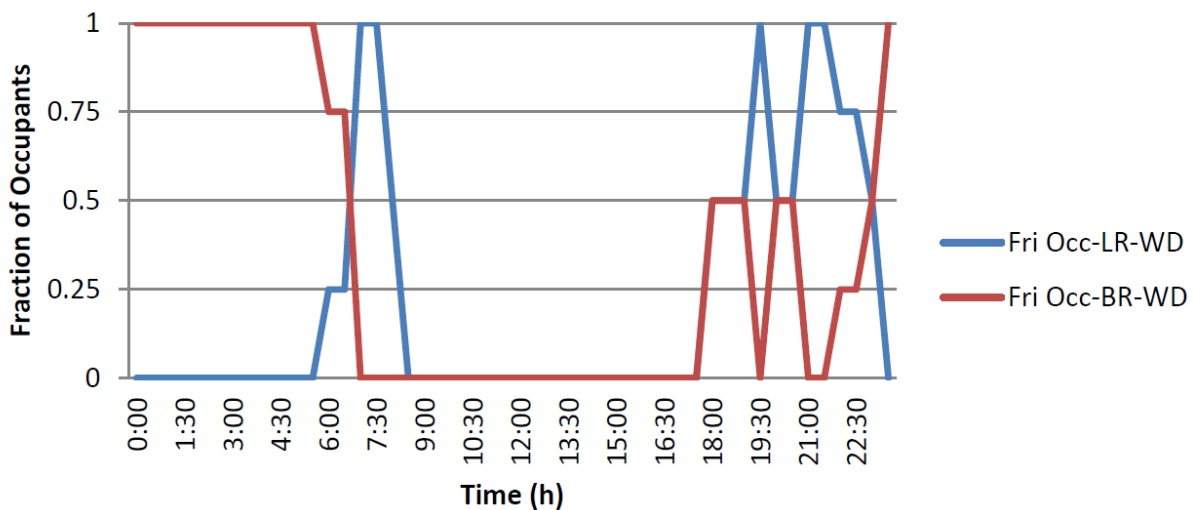


Fig. 4.6. NZERTF occupancy profile for Fridays

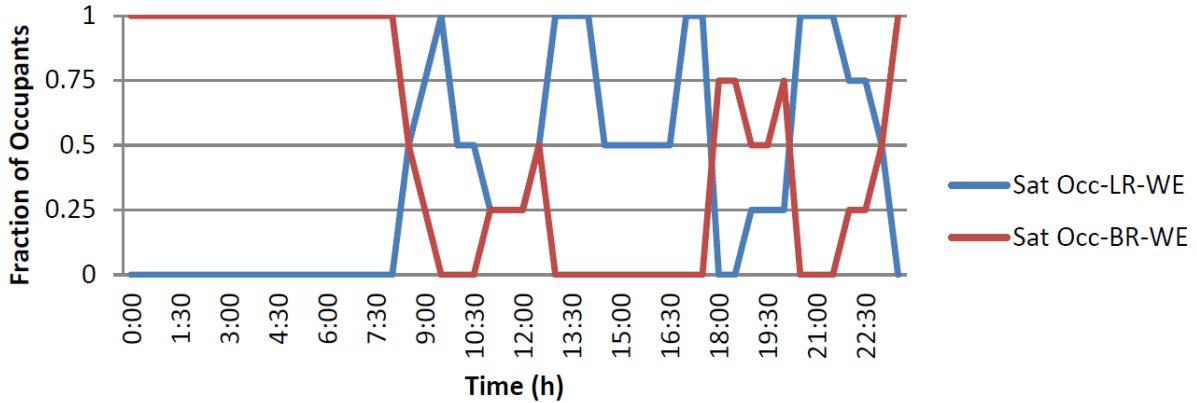


Fig. 4.7. NZERTF occupancy profile for Saturdays

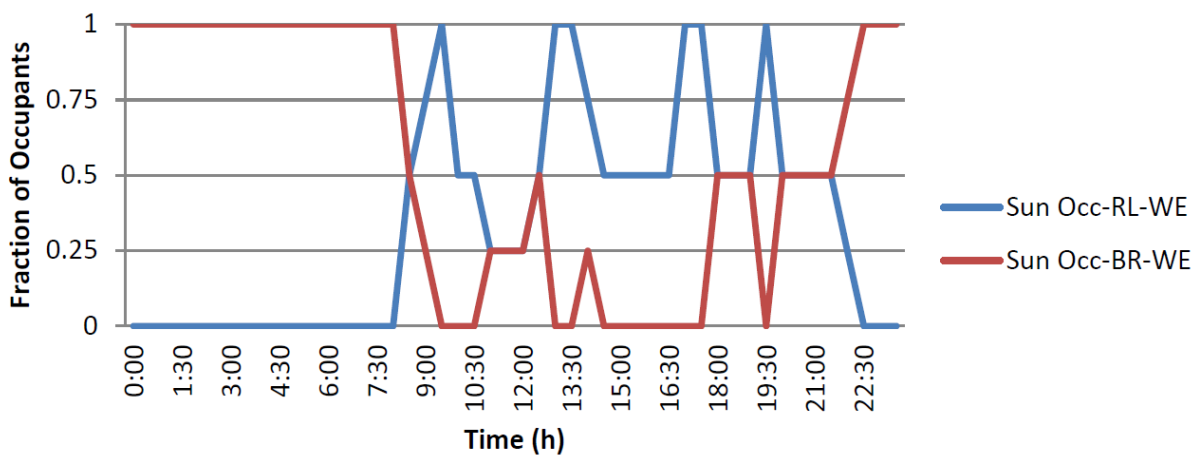


Fig. 4.8. NZERTF occupancy profile for Sundays

Occupant Generated Sensible and Latent Loads

Emulating human occupancy, in a virtual environment, such as the NZERTF, requires accounting for the sensible and latent loads generated by the presence and activities of the occupants themselves. In the NZERTF, sensible loads are simulated by resistive heaters placed in the bedrooms, kitchen, and the living room. Each sensible load emulator, representing a particular family member, is activated according to the schedule for that person. For example, when ParentA is in the master bedroom, the sensible load emulator for ParentA is activated in the master bedroom. The same procedure is applied to all family members. In contrast, the latent loads produced by the entire family and cooking activities, which are introduced as vaporized water, are combined to simplify the instrumentation. This approach can be justified because the NZERTF air-handler unit recirculates the moisture, generated locally in the kitchen, to the entire house. According to Table 1 in Nonresidential Cooling and Heating Load Calculations of ASHRAE's Handbook of Fundamentals, the adjusted sensible and latent load per person, for seated and very light work in an apartment, is 70 W and 45 W, respectively (ASHRAE, 2013a). These adjusted values are averaged for adults and children, so a single conservative value of 70 W is used for all emulators.

To emulate latent load in the NZERTF, it is essential to determine the amount of moisture dissipated by the family through respiration, perspiration, and cooking activities. According to Monteith (1972), at a skin temperature of 33 °C the heat needed to vaporize 1 gram of water is 2.398 kJ. The value of latent heat of vaporization was used to convert 45 W to its equivalent volume in liters. The estimated moisture generated per person is 0.07 liters/h. The latent load in ASHRAE (2013a) does not include the volume of moisture generated by cooking. Cooking moisture generation is obtained from the Home Moisture document published by the Minnesota Department of Commerce (Barnhart, 2012). The estimated

latent load generated for each cooking event (denoted as breakfast, lunch, and dinner) is shown in Table 4.1.

Table 4.1. Estimated volume of moisture during cooking events, adapted from (Monteith 1972), Table labeled Household moisture sources*

Cooking Event (Family of Four, Average)	Estimated Amount per Event (liters/gallons)
Breakfast	0.17 / 0.04
Lunch	0.25 / 0.07
Dinner	0.58 / 0.15

* The numbers are calculations used for target set-points and do not reflect the measurement accuracy

During the week, Monday through Friday, no one is home to prepare lunch so the moisture generated by cooking events only includes breakfast and dinner. The moisture generated on the weekends, however, includes all three meals. The daily moisture generated by the NZERTF family members accounts for the length of time that they are home. Table 4.2 shows the daily moisture generated by cooking meals and the occupants (respiration, perspiration).

Table 4.2. Total daily moisture generated by cooking events and the NZERTF occupants

Days	Daily Moisture from Cooking (liters/gallons)	Daily Moisture from People (liters/gallons)	Total Daily Moisture Cooking + People (liters/gallons)
Sunday	0.99 / 0.26	5.83 / 1.54	6.83 / 1.80
Monday	0.74 / 0.20	3.87 / 1.02	4.61 / 1.22
Tuesday	0.74 / 0.20	4.0 / 1.06	4.74 / 1.25
Wednesday	0.74 / 0.20	3.87 / 1.02	4.61 / 1.22
Thursday	0.74 / 0.20	4.0 / 1.06	4.74 / 1.25
Friday	0.74 / 0.20	3.87 / 1.02	4.61 / 1.22
Saturday	0.99 / 0.26	5.63 / 1.49	6.22 / 1.75

* The numbers are calculations used for target set-points and do not reflect the measurement accuracy

In order to introduce moisture into the NZERTF to represent the latent loads from cooking and the simulated human occupants, an ultrasonic humidifier is used. The approach used and the design of the apparatus are based on recommendations from Field Test Protocol: Standard Internal Load Generation for Unoccupied Test Homes (Fang et al., 2011). The advantage of an ultrasonic humidifier is that it creates very fine water droplets as cool fog, thereby releasing a steady rate of moisture at room temperature regardless of the ambient relative humidity.

The apparatus used in the NZERTF, shown in Figure 4.9, are commercially available humidifiers modified to enable long term operation without human intervention. The water reservoir is connected to a metered water supply line through a solenoid valve operated by a level switch. The solenoid valve is normally closed and the entire device is placed in a pan with a leak detector to enable remote detection of any water leaks.

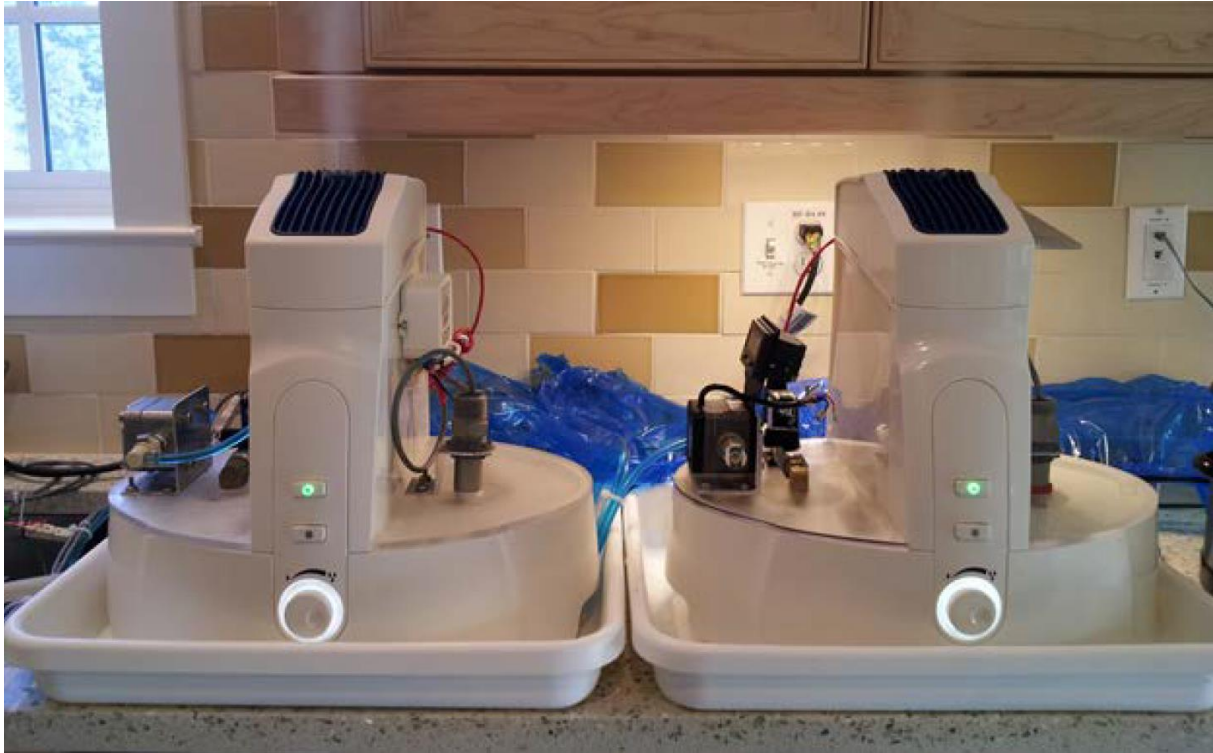


Fig. 4.9. Latent heat (moisture load) generators

Laboratory tests determined that each ultrasonic humidifier's output capacity is approximately 0.27 liters/h of moisture. Given this capacity, two ultrasonic humidifiers were installed to meet the daily required maximum latent load in Table 9. The amount of moisture introduced into the air is controlled by time. The flow meter provides a verification of correct operation.

To emulate sensible heat, eight resistance heating boxes were designed and built. Each box represents a family member so multiple boxes are placed in bedrooms, kitchen, living room, and dining room. The key components of a box are a bulb socket screw-in heater, a dimmer switch, a solid state relay, a safety fuse, and a mounting fixture for the screw-in heater (maximum power rating is 200 W). The dimmer switch controls the output power of each box, which was calibrated to 70 W, to represent the sensible heat generated by each person. The solid state relay turns the sensible heat generator on or off upon receiving a signal from the facility's acquisition/controller unit. The safety fuse is installed in-line with the hot power line to protect the circuit against current overload. Figure 4.10 shows a sensible heat generator box and the wiring diagram.

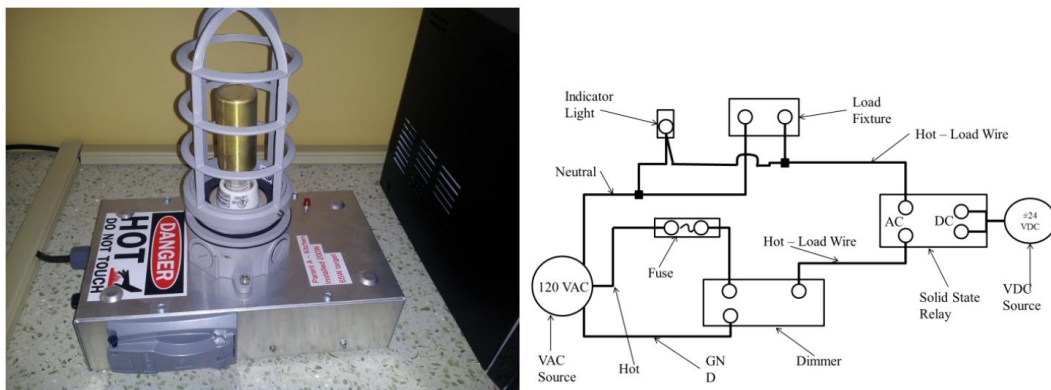


Fig. 4.10. Sensible heat generator and electrical circuit diagram

Miscellaneous Plug Loads

All plug loads are automated according to a schedule. The strategy in emulating the plug loads (including cooking appliances) in the NZERTF is to use their annual energy consumption as a target and create a schedule to satisfy that requirement. The assumed frequency of usage of plug loads, in a given day, is based on the assumed occupancy profile, which may change from one day to the next. Some plug loads involve real appliances and others, which are difficult or unsafe to automate, are emulated with resistive loads. For example, modern televisions require activation with a remote control that is not easily automated, and a coffee maker is difficult to safely turn on and off using a data acquisition/controller unit. All plug loads, including standby, that are rated less than 200 W are emulated with resistant heating boxes similar to the one shown in Figure 4.10. However, plug loads larger than 200 W are emulated with heating elements connected to a relay-box shown in Figure 4.11. A relay-box, which energizes and de-energizes these plug loads and appliances, is shown in Figure 4.12.



Fig. 4.11. The heating elements for plug loads with larger than 200 W power requirement and their relay-boxes

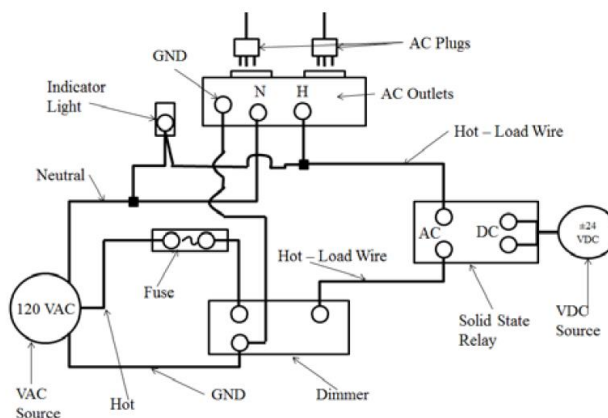


Fig. 4.12. A relay-box, wiring diagram, and a toaster plugged into it

The mechanisms to control all plug loads are separated into three main categories: time-based, criteria-based, and cycle-based. All plug loads, except the cycle-based loads, have a start-time and an end-time. In time-based control, the data acquisition/controller unit starts a load based on its start-time and turns it off when the end-time is reached. Similarly in criteria-based control, the acquisition/controller unit starts a load based on its start-time, but it

terminates the load when a certain criterion (e.g., energy consumption) has been met. For safety purposes, a timeout criterion is also applied to these loads which terminates their use if a certain elapsed time is reached. For example, when the hair dryer is energized, the data acquisition/controller unit monitors its energy consumption and terminates it when the energy consumed equals the prescribed energy. In criteria-based control, the end-time serves as a safety switch (a timeout) to prevent the loads from operating continuously in case of a malfunction beyond a predefined time window. In the cycle-based control of such operations as dishwasher and clothes washer cycles, the loads are activated based on their start-times and allowed to complete their normal cycles. The acquisition/controller unit does not terminate cycle-based loads.

4.1.4 Data Acquisition, Control Systems and Uncertainty

Whole House

Sensors were installed throughout the facility to monitor the ambient conditions as well as the performance of each particular subsystem in the house. Figure 4.13 shows a schematic that describes the sensor system in the facility. The data acquisition system is installed in the garage to separate its heat load from the house, and three poly-vinyl chloride conduits installed between the garage and the main house carry signal wire between the two locations. Two of the conduits terminate in the basement of the house, while the third terminates in the floor in the closet of Bedroom 2. The conduits going to the basement have an inner diameter of 10 cm, while the one going to the second floor has an inner diameter of 7.6 cm. Electrically-shielded flexible conduit installed within the walls during construction carry the signal extension wires to each room of the house. These extension wires carry four pairs of conductors to each location; some contain Type T thermocouple wires while others contain wire for other analog signals. Thermocouple and analog signal plug panels are installed in the walls of each room of the facility as shown in Figure 4.14, and wires are routed to devices within the room through chases to minimize tripping hazards.

Separate instrumentation systems were installed to measure the performance of the PV system, the wind speed and direction on the roof, and the electrical usage within the house. These systems used RS-232 or RS-485 serial connections to communicate their data to the main data acquisition system.

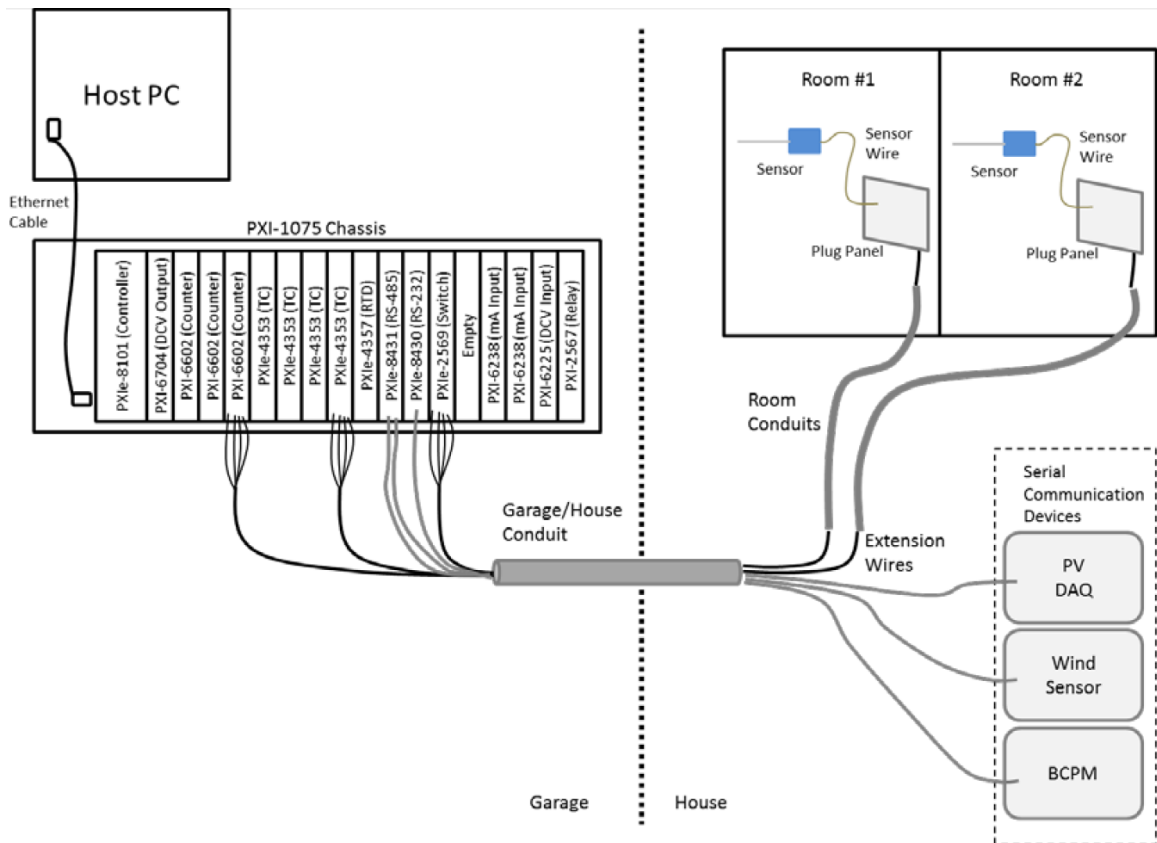


Fig. 4.13. General schematic of the whole house monitoring system



Fig. 4.14. Typical room plug panel

Heat Pump

The ASHP has its own dedicated data acquisition system that continuously monitors both refrigerant and air side conditions, Figure 4.15. Air side capacity (sensible and latent) and component power demand are continuously measured to give instantaneous values of efficiency (COP). T-type thermocouples are soldered to the outside of refrigerant piping and insulated to determine steady-state refrigerant temperatures. Pressure transducers are located at the inlet and exit of the indoor and outdoor unit refrigerant flow paths in combination with thermocouples to allow determination of refrigerant thermodynamic properties. A differential air pressure transducer monitors indoor unit air pressure drop, or external static pressure (ESP), which allows calculation of indoor airflow rates based upon previous calibration to an orifice plate. Digital output current switches monitor the status of heating, cooling, and dehumidify demand calls from the thermostat. Digital output current switches also monitor the status of the indoor blower motor, compressor, and outdoor fan. Measurements are taken and logged every 3 seconds when the indoor fan is running and every 10 seconds otherwise.



Fig. 4.15. ASHP data acquisition system

The data acquisition system is running its own operating system and stores raw sensor voltage and temperature measurement data in two files in its on-board memory. The two data files are a one-minute file and a daily file. The previous minute of data is accessed through FTP over the local network by a secondary computer located in the house garage. The secondary computer converts the raw signals to scaled engineering units and plots important parameters to present to the operator through a graphical user interface (GUI). The daily raw data file is downloaded every night to the secondary computer's hard drive and to a NIST network storage drive. This daily file is processed every day and used to generate daily and weekly summary reports. Links to these reports are posted on a NIST internal network webpage for easy distribution.

Calibrations were performed on refrigerant pressure transducers and thermocouples for refrigerant and air temperature measurement. Refrigerant circuit temperatures and air dry-bulb temperatures are measured with T-type thermocouples that were calibrated in a constant temperature bath against a pair of standard platinum resistance thermometers (SPRTs) with a total uncertainty of ± 0.02 °C at a 95 % confidence level. This calibration allowed correction of the raw temperature measurement to the SPRT's temperature by way of a linear fit. Precision error in the thermocouple temperature measurements due to the data acquisition voltage measurement and ice point correction were on the order of ± 0.4 °C. Precision error due to conversion of the measured temperature to the calibrated temperature by linear fit was on the order of ± 0.02 °C. The remainder of the uncertainty was due to measurement bias introduced by the thermocouple placement, mixing temperature stratification, and measurement noise.

Refrigerant pressure transducers were calibrated after being installed in the refrigerant circuit. A secondary pressure standard, calibrated against a deadweight tester, was attached to the refrigerant circuit while random pressures were applied to the system using dry nitrogen. The uncertainty of the secondary pressure standard was a maximum of ± 0.69 kPa at a 95 % confidence level. Precision error due to linear fit of voltage output to pressure was a maximum of ± 13.8 kPa.

The main quantities measured for the heat pump system are air/refrigerant temperature, air dewpoint temperature, refrigerant pressure, air pressure drop, airflow rate, refrigerant mass flow rate, instantaneous power, and thermostat control signals status. Table 4.3 lists the instrumentation characteristics.

Table 4.3. Instrumentation installed on ASHP

Instrument	Model ²	Range	Total Uncertainty at a 95 % Confidence Level
Transducer voltage measurement	National Instruments, cDAQ-9205	0 to 10 VDC	± 5 mVDC
T-type thermocouples	National Instruments, cDAQ-9214	-10 °C to 55 °C	± 0.6 °C
Barometric pressure	NA	67.0 to 101.5 kPa	± 1 % of reading
High pressure transducer	Omegadyne PX309-1KGI	6895 kPa	± 0.25 % of reading
Low pressure transducer	Omegadyne PX309-500GI	3447 kPa	± 0.25 % of reading
Air pressure differential (ESP ¹)	Ashcroft CX8MB	0 to 187 Pa	± 0.8 % of reading
Indoor blower and controls power meter	Ohio Semitronics W-002X5	0 to 300 VAC, 5 Amps, 1000 W	± 5 W
Indoor total power meter	Ohio Semitronics W-059E	0 to 300 VAC, 100 Amps, 20 000 W	± 100 W
Outdoor unit power meter	Ohio Semitronics W-110X5	0 to 300 VAC, 20 Amps, 4000 W	± 20 W
Supply air dry-bulb temperature sensor	General Eastern Humi-DP-XR-D	-28.8 °C to 49 °C	± 0.5 °C
Supply air dewpoint temperature sensor	General Eastern Humi-DP-XR-D	-28.8 °C to 49 °C	± 1.0 °C
Return air dry-bulb temperature sensor	Vaisala HMT330-3	-40 °C to 60 °C	± 0.2 °C
Return air dewpoint temperature sensor	Vaisala HMT330-3	-20 °C to 100 °C	± 1.5 % of reading
Outdoor air dry-bulb temperature sensor	Vaisala HMT330-3	-40 °C to 60 °C	± 0.2 °C
Outdoor air dewpoint temperature sensor	Vaisala HMT330-3	-20 °C to 100 °C	± 1.5 % of reading
Coriolis refrigerant mass flow meter	Micromotion Coriolis Elite Sensor, CMF025	0 to 2180 kg h ⁻¹	± 0.15 % of reading

1- External Static Pressure

2- Identification is not intended to imply recommendation or endorsement by the National Institute of Standards and Technology, nor is it intended to imply that the entities, materials, or equipment are necessarily the best available for the purpose.

Table 4.4 lists the total uncertainty of sensible capacity for two days in July when the heat pump operated at high and low capacity. When the unit operates in the heating mode, the total capacity is the sensible capacity; therefore, the total uncertainty of sensible capacity in

the cooling mode should be indicative of the total uncertainty of total capacity in the heating mode.

Table 4.4. Example uncertainty for sensible capacity

Date	Airflow, $\text{m}^3 \text{h}^{-1}$	$T_{in}, \text{°C}$	$T_{ex}, \text{°C}$	$C_{p,mix},$ $\text{J kg}^{-1} \text{K}^{-1}$	V_{mix} $\text{m}^3 \text{kg}_{mix}^{-1}$	Q_{sen} W	$E_{Q_{sen}}^1$ W	% $E_{Q_{sen}}$
Jul-13- 2013, 11:00 Low	1133	23.6	12.2	1021.2	0.8295	4415	184	4.2
Jul-15- 2013, 14:00 High	1466	23.7	12.6	1020.7	0.8301	5563	326	5.9

1- Total uncertainty at the 95 % confidence level

Latent capacity is also measured at the indoor air handler and is the rate of heat removal due to condensation of moisture on the indoor heat exchanger. Latent capacity is determined from the same measurements as sensible capacity, namely airflow rate, barometric pressure, inlet dry-bulb temperature, inlet dewpoint temperature, exit dry-bulb temperature, and exit dewpoint temperature. Just as with the determination of sensible capacity, latent capacity is determined from thermodynamic properties of the moist air flowing across the indoor heat exchanger. Table 4.5 lists the total uncertainty of latent capacity for two days in July 2013 when the unit operated at high and low capacity.

Table 4.5. Example uncertainty for latent capacity

Date	Airflow, $\text{m}^3 \text{h}^{-1}$	W_{in} $\text{kg}_{wv} \text{kg}_{da}^{-1}$	W_{ex} $\text{kg}_{wv} \text{kg}_{da}^{-1}$	V_{mix} $\text{m}^3 \text{kg}_{mix}^{-1}$	Q_{lat} W	$E_{Q_{lat}}^1$ W	% $E_{Q_{lat}}$
Jul-13- 2013, 11:00 Low	1133	9.547E-3	8.029E-3	0.8295	1421	445	31.3
Jul-15- 2013, 14:00 High	1466	9.120E-3	7.969E-3	0.8301	1392	565	40.6

1- Total uncertainty at the 95 % confidence level

Total capacity is the sum of sensible and latent capacity and Table 4.6 lists example uncertainty.

Table 4.6. Example uncertainty for total capacity

Date	Q_{sen} W	Q_{lat} W	Q_{tot} W	$E_{Q_{tot}}^1$ W	% $E_{Q_{tot}}$
Jul-13- 2013, 11:00 Low	4415	1421	5836	482	8.3
Jul-15- 2013, 14:00 High	5563	1392	6955	652	9.4

1- Total uncertainty at the 95 % confidence level

The coefficient of performance, COP, is a measure of cooling efficiency and is determined by dividing the total cooling capacity by the total system power demand. Table 4.7 lists the example uncertainty in the COP.

Table 4.7. Example uncertainty for COP

Date	Q_{tot} W	W_{tot} W	COP	E_{COP}^1	% E_{COP}
Jul-13- 2013, 11:00 Low	5836	1253	4.634	0.419	9.0
Jul-15- 2013, 14:00 High	6955 ^{oo}	2347	2.963	0.279	9.4

1- Total uncertainty at the 95 % confidence level

4.1.5 NZERTF Electrical Systems

The facility is equipped with two distinct electrical systems. One system consists of the circuits that would typically be in a home (“house circuits”) while the second set of circuits is used to power any instrumentation that would not typically be in a home (e.g., air sampling pumps used for short-term monitoring of indoor air quality). Each main circuit panel has a maximum current rating of 200 A, and each circuit within the panels is monitored. Receptacles using instrumentation power can be distinguished from the normal house circuits by the label “RP BB” on their faces.

The primary purpose of the electrical monitoring system is to determine whether the NZERTF ultimately produces more electricity than it consumes. It is also used to measure the electrical consumption of the various subsystems within the house and to control some occupant-driven loads, such as lights and the virtual occupants’ sensible heat.

The NZERTF’s electrical monitoring system measures electrical power and energy from two perspectives; the electricity imported into (or exported from) the house and the electricity as it is distributed throughout the house. These perspectives, of course, are interrelated. Namely, the electrical energy imported/exported depends on the relative quantities of the electricity generated by the photovoltaic system and the electricity consumed by the loads within the house. That relationship is defined in Equation 4.2 below, and a schematic of the electrical monitoring system is shown in Figure 4.15.

$$E_{NET} = E_{PV} - E_{LOAD} \quad (4.2)$$

Where E_{NET} = electrical power imported from or exported to the electrical utility,
 E_{PV} = electrical power output from the photovoltaic inverters, and
 E_{LOAD} = total electrical power consumed by all the loads within the house.

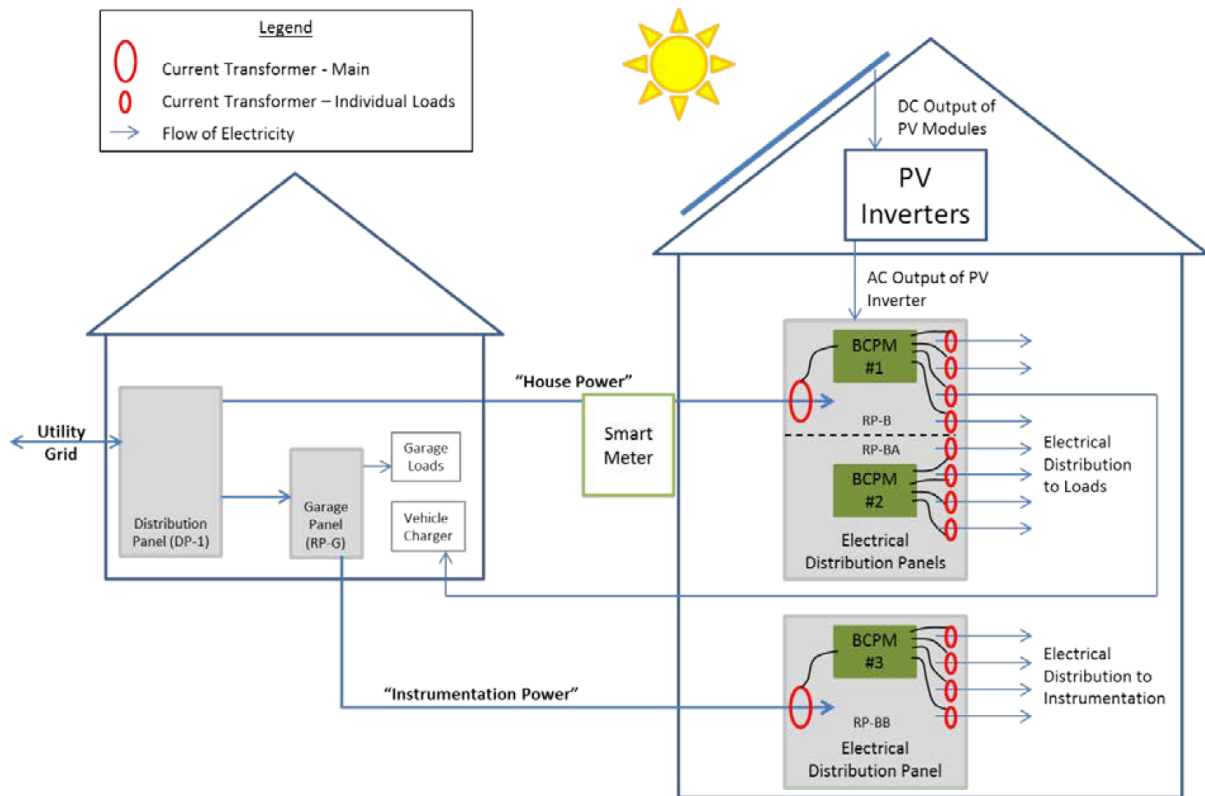


Fig. 4.15. NZERTF electrical monitoring system schematic

Physically, the electrical wiring for the site is divided into branches for House Power, Instrumentation Power, and Garage Power. Circuits on the House Power branch (electrical panels RP-B and RP-BA in the basement) are those that are typically found within a residence, such as appliances, lights, water heaters, TVs, etc. These are the circuits that will determine whether the house operates in a net-zero fashion.

The Garage Power branch (RP-G) feeds the equipment in the garage, such as the data acquisition equipment and the garage's heating and cooling system. The Instrumentation Power branch (panel RP-BB in the basement) is a subset of the Garage Power branch that is sent inside the house to power any instrumentation necessary to monitor the performance of the house or simulate activities of occupants. An electrical panel situated in the garage serves as the main distribution panel, with a single circuit from that panel feeding a separate electrical panel in the basement of the house (RP-BB). While this electricity is not counted against the net-zero energy tally for the house, the thermal load of the equipment powered on this branch must still be considered. While most of the equipment in the garage is powered by Garage Power, there are several receptacles in the garage that are fed from House Power. These are intended to provide electricity for a (future) vehicle charging station.

To measure the consumption and generation of each circuit within the NZERTF, Branch Circuit Power Meters (BCPM) were installed in each of the three electrical distribution panels in the basement (RP-B, RP-BA, and RP-BB). Each BCPM measures the electrical consumption of all 42 circuits within the panel and transmits the data to the main data acquisition system in the garage using RS-485 serial communications. Additionally, the BCPM measures the overall electrical consumption of each panel. The BCPM performs the following measurements on each circuit: power (W), current (A), power factor, and cumulative energy (Wh). The BCPM also measures the single-phase voltage at the panel.

Additionally, a separate current transducer (CT) was installed on the main line for the house power (RP-B and RP-BA) and for the instrumentation power (RP-BB). These CTs were

connected to the Auxiliary Input channels of the BCPM, and they provide a measurement of the total power, current, and energy imported or exported by the house and instrumentation power circuits as a whole.

Table 4.8 and Figure 4.16 demonstrate the expanded uncertainty of the daily energy totals for the generation, consumption, and imported electricity, and the exported electricity on a typical day, March 15, 2014. The latter value was calculated using a summation of the individual circuits as measured by the BCPM, the main line CTs on the BCPM, and the smart meter. As expected, the uncertainty for the summation of the BCPM circuits is considerably larger than the main line CTs and the smart meter. The agreement for the energy totals between the main line CTs and the smart meter is excellent, and the energy totals using the summation of circuits also matches the other two methods within the uncertainty bounds.

Table 4.8. NZERTF total energy and expanded uncertainty (k=2) of the generation (PV), consumption, imported electricity, and exported electricity as measured by the BCPM individual circuit summation, BCPM main line CTs, and the smart meter for March 15, 2014

	BCPM - Individual Circuits				BCPM - Main CT			Smart Meter		
	Gen.	Cons.	Imp.	Exp.	Cons.	Imp.	Exp.	Cons.	Imp.	Exp.
Energy (kWh)	53.3	38.9	23.9	38.3	39.6	24.6	38.3	39.7	24.6	38.1
Uncert. (kWh)	0.54	0.75	0.53	0.76	0.44	0.29	0.39	0.40	0.25	0.38
Uncert. (%)	1.0	1.9	2.2	2.0	1.1	1.2	1.0	1.0	1.0	1.0

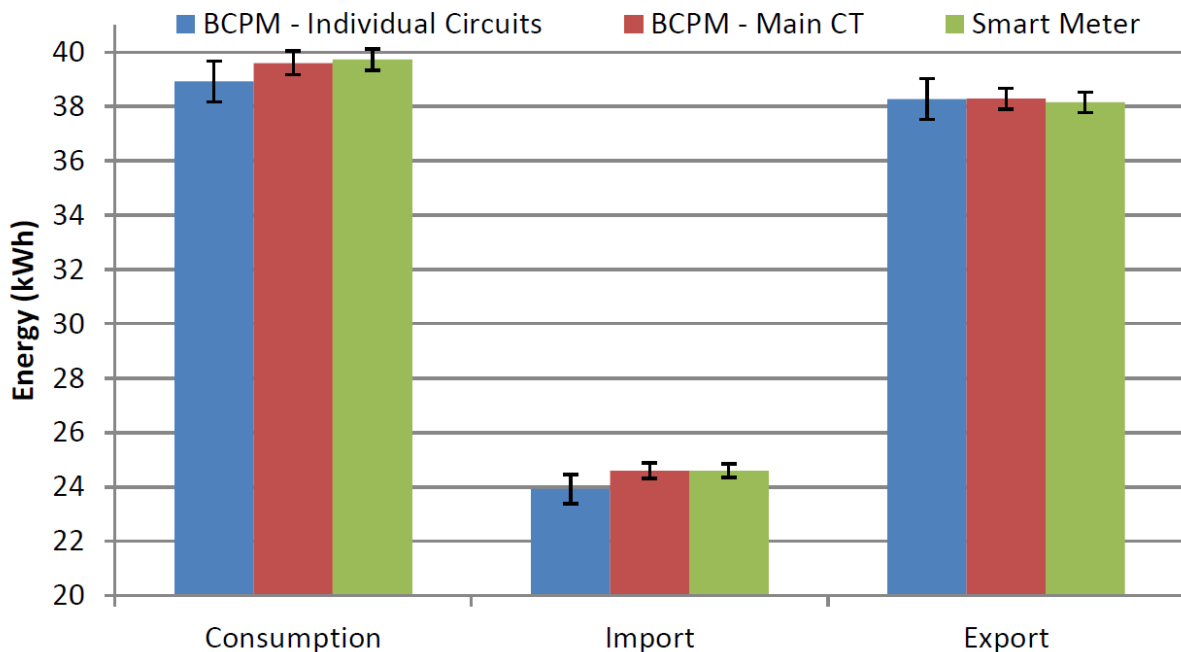


Fig. 4.16. Comparison of the NZERTF consumption, imported electricity, and exported electricity as measured by the BCPM individual circuit summation, BCPM main line CTs, and the smart meter for March 15, 2014. Error bars show the expanded uncertainty (k=2) of each measurement

4.1.6 Cost of NIST NZERTF

There will be two cost analysis approaches considered: payback period and life-cycle cost analysis. All monetary amounts are in U.S. dollars (\$). Payback period is a simplistic comparison of the initial investment costs and future cost savings while life-cycle costing is a more rigorous and complete analysis approach.

Payback period

The cost of constructing the 2012 IECC (International Energy Conservation Code) design is \$493 712, while the construction costs for the net-zero energy house design are \$656 398, which is a difference of \$162 687 (Kneifel, 2014). The annual energy cost savings is estimated to be \$4526. The simple payback approach calculates how many years it will take for the future cost savings to offset the initial investment costs (all in nominal dollars). Excluding any financial incentives available to homeowners and assuming the buyer purchases the home outright, the simple payback period is the investment costs (\$162 687) divided by the annual cost savings (\$4526), or 36 years.

A more typical home purchasing approach is to finance most of the home purchase. The most common financing option for a new home purchase is the 30-year fixed-rate mortgage. For simplicity, let's assume the purchaser makes a 20 % down payment, which eliminates mortgage insurance. The difference in down payment between the net-zero energy home design and the 2012 IECC design is \$32 537. Assuming a 4.375 % interest rate makes the additional monthly mortgage payment (principal and interest) \$650 greater for the net-zero energy design, which increases the annual mortgage payment by \$7800. The extra annual mortgage costs are 72 % higher than the energy cost savings of \$4526. Not only does the net-zero energy house cost more upfront (\$32 537), but the homeowner's monthly costs (mortgage payment plus average energy costs) are higher by \$273. The homeowner does not begin to see annual savings greater than annual costs until the 30 year mortgage is entirely paid off. It takes another 29 years (59 years in total) for the savings to offset the costs.

If currently available federal, state, and utility financial incentives are included in the analysis, the cost savings in the first year are increased by \$46 626 due to rebate and grant programs and the value of state-level Solar Renewable Energy Credits (SRECs) associated with the solar PV and solar hot water system production. The combined cost savings from the financial incentives and energy cost savings first offset the initial investment costs of an all cash purchase in Year 26, which is 10 years sooner than if the financial incentives are not included in the analysis.

In the case of a financed home purchase (a 30-year fixed-rate mortgage with a 20 % down payment), including the financial incentives makes the interpretation of the results more nuanced. The financial incentives (\$46 626) are greater than the additional down payment (\$32 537), which leads to a payback period of one year. The savings are greater than the costs until Year 5, at which point the annual costs are greater than the annual savings until the mortgage is paid off in Year 30. It takes another 19 years until the total savings offsets the total costs again in Year 49.

The simple payback approach does not take into account the time value of money. In order to do so, the future costs and savings must be discounted into present value terms. In this case we will assume the discount rate is equal to the mortgage interest rate to estimate the discounted payback period. Assuming an outright purchase, it takes 85 years for the financial incentives and present value energy cost savings to offset the initial investment costs, nearly 30 additional years relative to the simple payback period approach.

Similar to the non-discounted results for a financed home purchase, using a strict definition of the discounted payback period leads to a discounted payback of one year. However, since the annual mortgage costs are greater than the annual energy cost savings, the total costs become greater than the total savings starting in Year 6. The costs remain higher throughout the life of the mortgage plus an additional 50 years (80 years in total) for the financial incentives and present value energy cost savings to offset the initial investment costs, which is 31 years greater than the simple payback period approach.

The simple and discounted payback period approaches are limited in their usefulness, and the above example shows the limitations of using payback period to determine a project's economic feasibility. If strictly followed, selecting the net-zero energy design would have had a simple payback and discounted payback period of one year. As has been shown, this approach would miss any benefits and costs that occur after the payback period, which are important to the homeowner. In order to capture all the related benefits and costs associated with the house, it is appropriate to use a more rigorous approach.

Life-Cycle Cost Analysis

Consider the complexity of the decision for the homeowner. The net-zero energy home costs an additional \$162,687. If the homeowner finances the home with a 30-year fixed-rate mortgage with a 20% down payment at 4.375%, the additional monthly mortgage payment (principal and interest) is \$650, or \$7,800 annually. The extra annual mortgage costs are 72% higher than the energy cost savings of \$4,526. Not only does the NZERTF cost more upfront (\$32,537), but the homeowner's monthly costs (mortgage payment minus average energy cost savings) are higher by \$273. For perspective, in order to make the combination of mortgage payment and energy bill equivalent for the two homes would require a mortgage interest rate premium subsidy of almost 1.0% for the NZERTF (see Figure 4.17).

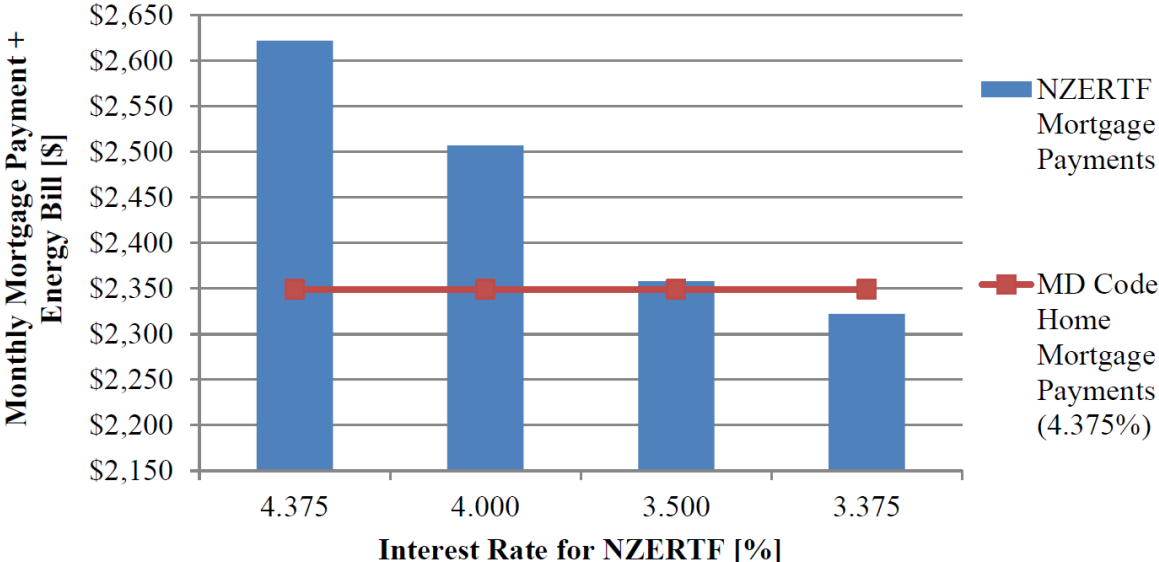


Fig. 4.17. Monthly cost to the homeowner by home design and interest rate

However, financial incentives more than offset the higher down payment (\$46,626 versus \$32,537). The homeowner walks away from closing with an additional \$14,809, but has monthly costs (mortgage payment plus energy bill) that are \$273 greater than the Maryland code-compliant home. The homeowner's investment time horizon of interest (study period) could significantly impact the owner's decision-making process. Additionally, two other important values must be considered: differences in maintenance, repair, and replacement costs of house components and the difference in resale value of the house, both of which are impacted by the homeowner's selected study period. It is important to use a well-documented, industry-accepted methodology in order to account for the variety of costs related to the house.

The life-cycle cost methodology, as defined in ASTM Standard Practice E917 (2010), considers all costs related to the house over the selected study period, whether it is construction costs, operating costs, or resale value at the end of the study period. The following analysis varies the study period from 1 year to 100 years to reflect the diverse distribution of homeowners. Figure 4.18 shows that 15 years is the approximate half-life of

homeownership, where 50.2 % of homeowners are still living in the house (i.e. survival rate). After 20 years, the rate at which homeowners move out of the house (i.e. attrition rate) is relatively constant with an average attrition rate of 2.2 % and a range of 1.5 % to 2.7 %. Assuming this rate of attrition from 31 years forward, there will be 0.1 % of homeowners in their home after 60 years, although there are sure to be outliers that remain in the same home for longer. This life-cycle analysis will focus on 30 years or fewer because approximately 65 % of all homeowners live in a home for 30 years or less.

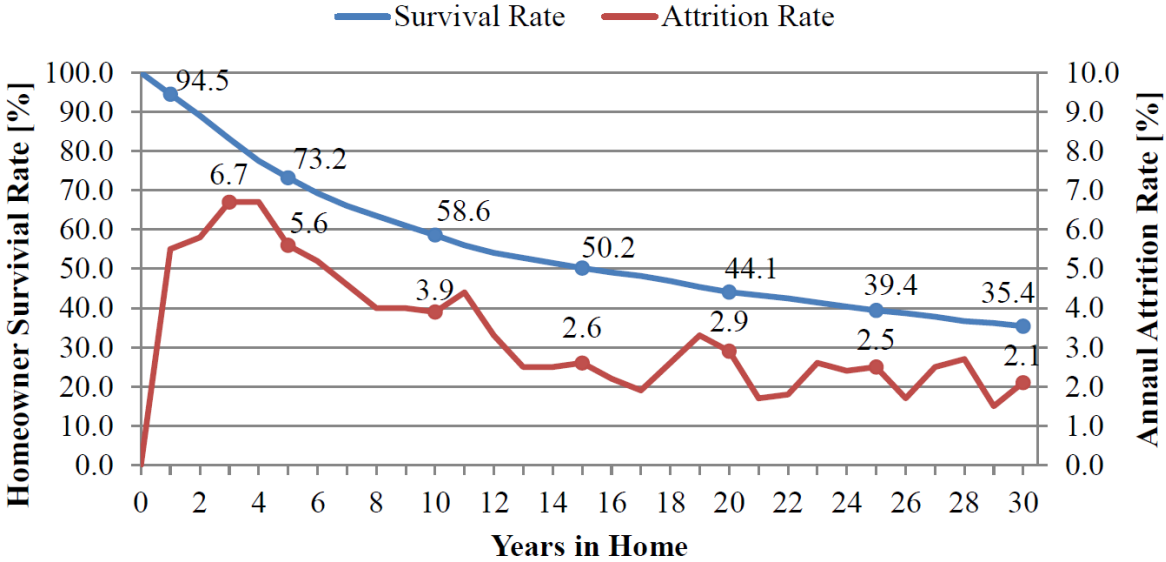


Fig. 4.18. Annual survival rate of U.S. single-family home ownership (Emrath 2009)

In order to simplify the analysis, initially assume that the homeowner remains in their home or assumes there is no home price appreciation, the higher performing building design will not fetch a higher resale price relative to the Maryland code-compliant design (no resale value), and the maintenance, repair, and replacement costs are comparable between the two building designs. Figure 4.19 shows the life-cycle cost analysis for 8 study periods from 1 year to 100 years financing with incentives. For a study period 5 years or less, the homeowner realizes net savings in present value life-cycle costs because the upfront financial incentives are enough to offset the higher down payment and future monthly costs (mortgage payments and energy bill) for the first 5 years. However, by the end of year 6 the homeowner realizes net costs, which continue to increase until the mortgage is paid in full after 30 years, at which time the energy cost savings lowers present value net costs until net cost savings is realized in about Year 85. Based on these results, it is better for the homeowner to buy the net-zero energy home if the homeowner expects to move sometime in the first 5 years, but is not cost-effective for any longer study periods. In the worst case (30 years study period), the additional present value costs is equivalent to a mark-up of 7.0 % relative to the Maryland code compliant design to get a net-zero energy, LEED platinum certified, high-performance house.

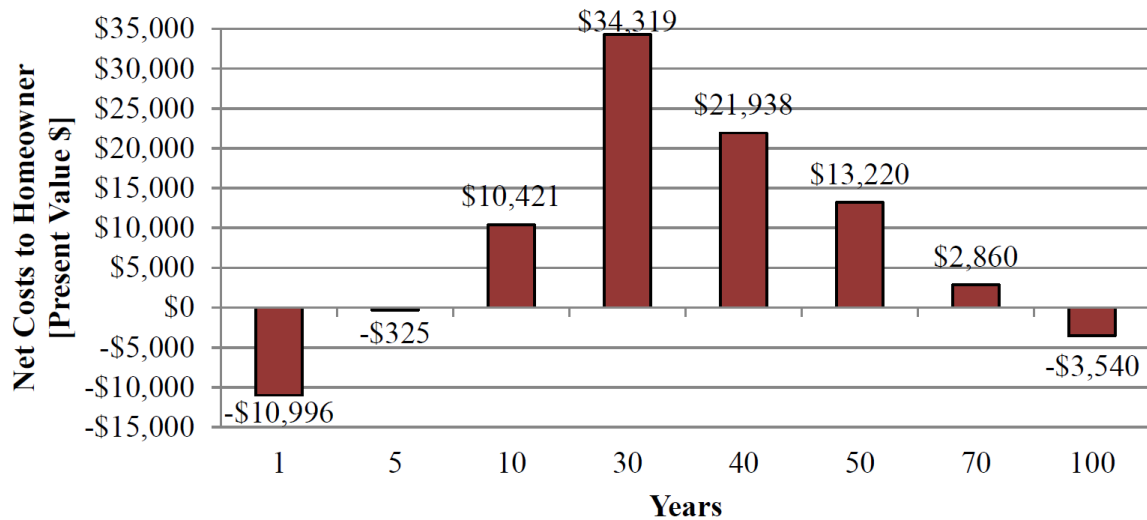


Fig. 4.19. Net costs to homeowner by study period (no resale value)

Since most homeowners will sell their home at some point, it is important to consider any potential additional resale value (residual value) of the net-zero energy house relative to the Maryland code-compliant home. There are two approaches considered in calculating residual value. The life-cycle cost (LCC) approach takes a functional life approach, assuming a linear depreciation of the residual value based on the initial additional costs, discounted to present value terms. The residual value in this case decreases over time due to fewer years of usable life for the building and discounting of the residual value back to present value terms. An alternative approach estimates the additional value of the house to be the discounted present value of the future energy cost savings. The present value of the residual in this case only decreases due to discounting.

Figure 4.20 shows the net present value costs to the homeowner across eight study periods from 1 year to 100 years for the two approaches to estimating the residual value. Once the residual value has been included in the LCC analysis, the net-zero energy home becomes more cost-effective over all of the study periods relative to the life-cycle costs without residual value shown in Figure 4.19. The homeowner realizes present value net cost savings for both residual value approaches for a 1-year, 5-year, 10-year, and 20-year study period, which includes 56 % of all home ownerships. Using the market approach, the homeowner realizes present value costs of \$775 over a 25 year study period while the LCC residual value approach leads to net cost savings of \$11 230. The homeowner realizes net present value costs for Year 30, Year 40, and Year 50 because the decrease in the discounted value of the residual value is greater than the present value of the energy cost savings. Although it is important to note that the net present value costs for either approach across those 3 study periods range from \$879 to \$9411, which is equivalent to a 0.2 % to 1.9 % mark-up of the cost of the Maryland code-compliant home (\$493 712). So in the worst case scenario, the homeowner is paying the equivalent of a 2 % mark-up for a net-zero energy, LEED platinum certified, high-performance home.

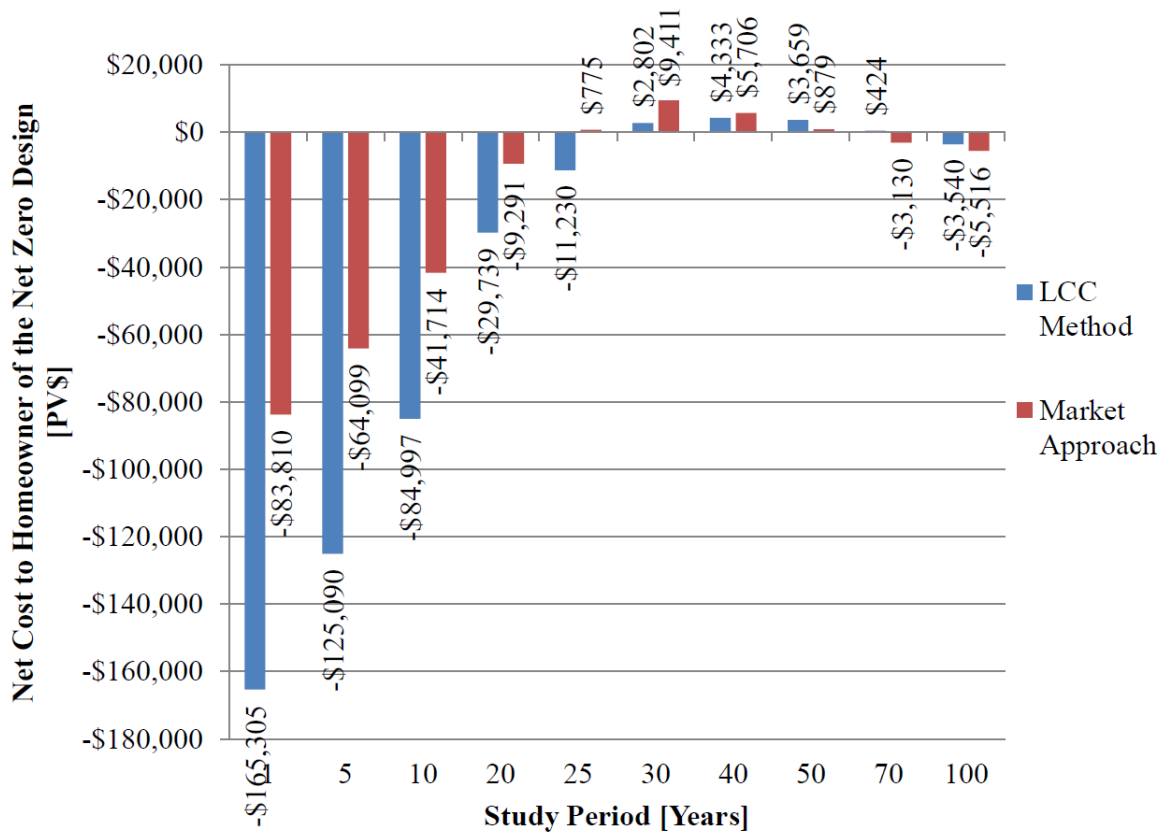


Fig. 4.20. Net costs to homeowner by study period (including resale value)

In making investment decisions, the homeowner may prefer to compare the return on investment to other investment options. Let's assume that the investment cost to the homeowner is the higher initial down payment (I). The sum of all financial incentives and future benefits and costs will be treated as net cost savings. Additional mortgage payments (M) are a negative cost savings, while energy cost savings (E), financial incentives (F), and residual value (R) are positive cost savings. The ratio of present value net future cost savings to initial investment costs, which is the savings-to-investment ratio or SIR, is calculated using the following formula:

$$SIR = \frac{E+F+R-M}{I} \quad (4.3)$$

Based on the formula, the SIR is calculated to be 1.28 to 2.61, which means the homeowner receives a total return on investment over the 10 years of 28% and 161%, respectively.

The SIR can be used to calculate an adjusted internal rate of return or AIRR, which is the estimated annualized return on investment the homeowner realizes assuming a given reinvestment rate (i) for the study period (n). In this case the reinvestment rate is assumed to be equal to the discount rate or 4.375%. The formula for calculating the AIRR is the following:

$$AIRR = (1 + i)(SIR)^{1/n} - 1 \quad (4.4)$$

Based on this formula, the AIRR is estimated to be 5.6% and 14.9%, respectively. These calculations do not account for a number of factors that will impact costs. There is assumed to be no maintenance, repair, and replacement (MRR) cost differences between the two buildings. All equipment is assumed to have at least a 10-year lifespan and, therefore, no replacement costs will occur during the study period. The relative home values

are assumed fixed, which ignores any changes in the housing market. Also excluded from the analysis are any home insurance, property tax, and income tax implications. Home insurance may be more expensive due to the higher market value of the home, but more energy efficient homes may receive a premium discount. The state of Maryland exempts many energy efficiency and renewable energy home investments, which should alleviate most, if not all, of the property tax implications. Including the itemized deduction for a home will lower the after-tax mortgage payments because the homeowner is getting some of the mortgage payment returned, and will increase the residual value estimate because a lower effective discount rate increases the value of future energy cost savings. The magnitude of the effects will depend on a variety of other factors, including income levels, tax filing status, and other tax deductions. There is also no value placed on the LEED platinum rating and related “green” features, which would vary significantly across homebuyers.

4.2 Experience with the NZERTF

4.2.1 NZERTF Energy Efficiency Results

Whole House Energy Performance Summary

The ASHP system, previously described, was used to provide the space heating/cooling during the first demonstration year. The earth-coupled heat exchangers, high-velocity air distribution system, and basement radiant floor heating system were not utilized. The house was operated as a single zone with constant thermostat set points of 23.8°C and 21.1°C during the cooling and heating seasons, respectively. Only two of the four solar thermal collectors in conjunction with the 303 L storage tank were utilized for water heating. The lights, appliances, plug loads, and sensible and latent loads associated with the virtual occupants were operated in accordance with the previously defined schedules. Selected results are presented in units of energy (kWh) and energy per unit floor area (kWh/m²) of the conditioned space, 387 m², which includes the living area (252 m²) and the basement (135 m²).

Figure 4.21 shows the daily and cumulative net electricity use for the first year of operation. A positive value indicates that the house produced more energy than it consumed and represents the quantity of energy exported to the grid. A negative value indicates that the house imported energy from the grid to meet the energy usage over the 24 hour period. For the 12 months (July 2013 through June 2014) the house produced 484 kWh more electrical energy than it consumed. The energy consumption by end use is tabulated in Table 4.9 and displayed graphically in the stacked bar chart, Figure 4.22. The top five energy end uses for the twelve month interval are: 1) space conditioning (6685 kWh; 17.3 kWh/m²), 2) plug loads (2440 kWh), 3) appliances (1868 kWh), 4) energy associated with producing hot water (sum of heat pump water heater and the solar thermal circulating pumps) (1432 kWh), and 5) lighting (435 kWh). The space conditioning energy consumption includes 514 kWh of energy consumed by the heat recovery ventilator (HRV). The energy usage by each individual appliance is shown in Figure 4.23, with the clothes dryer consuming the greatest amount in this category.

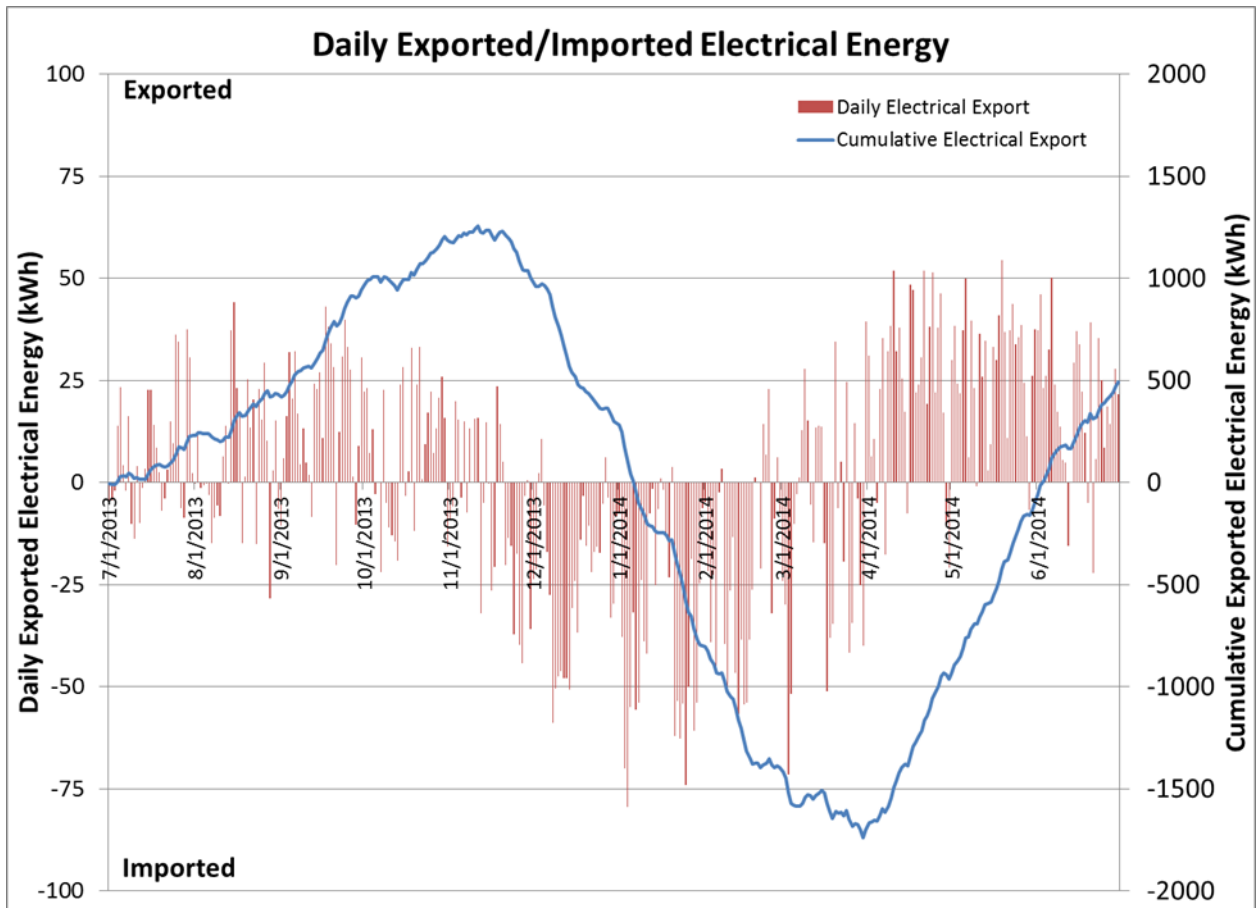


Fig. 4.21. Daily and cumulative net electrical energy usage for first test year

The solar photovoltaic system and associated inverters experienced no malfunctions over the yearlong period converting 16.8 % of the incident solar irradiance into AC electrical energy. As expected, the conversion efficiency of the photovoltaic array increases as the average cell temperature decreases, Table 4.10. The conversion efficiencies for December, January, February, and March were lower than expected as a result of the 8, 8, 12, and 10 days, respectively, when all or part of the solar array was covered with snow and/or ice for all or part of the daylight period. For all of the winter snow events, the reference cell plane of the array irradiance detector cleared well in advance of the PV array. The monthly conversion efficiencies, from direct current to alternating current, of the photovoltaic system inverters all exceeded 94.5 %.

The solar thermal hot water system provided 54 % of the energy required to meet the domestic hot water load over the twelve month interval. The solar thermal collectors were totally or partially covered with snow and/or ice during the same time intervals as the photovoltaic array. The two circulating pumps consumed 320 kWh during the year.

The solar hot water system malfunctioned for a total of 11 days in late August and early September as a result of an electrical fault in the glycol-circulating pump. The auxiliary heat pump water heater unit malfunctioned for 9 days in November and operated exclusively in the electric resistive mode as a result of a control wire becoming dislodged. Of the total energy consumed by the heat pump water heater unit, 975 kWh (88 %) was consumed by the heat pump and controls and 137 kWh (12 %) by the auxiliary resistive heating element.

Table 4.9. Monthly NZERTF thermal loads and energy consumption (kWh) by end use

Month/Year	Jul/13	Aug/13	Sept/13	Oct/13	Nov/13	Dec/13	Jan/14	Feb/14	Mar/14	Apr/14	May/14	Jun/14	Annual
Heating Load	0.0	0.0	0.0	56.4	830.4	1351.0	2156.9	1634.7	1423.5	252.7	0.0	0.0	7705.7
Cooling Load	2122.9	1392.1	937.2	306.4	1.7	0.0	0.0	0.0	0.0	66.8	603.0	1559.7	6989.7
DHW Load	252.4	217.8	238.2	268.5	283.2	325.9	343.1	330.0	340.5	300.3	276.9	250.6	3427.5
Heat Pump Heating	0.0	0.0	0.0	33.6	396.4	581.5	1254.8	753.1	650.4	113.2	0.0	0.0	3783.1
Heat Pump Cooling	700.8	481.0	345.4	142.3	15.7	0.0	0.0	0.0	0.0	13.6	177.7	511.3	2387.8
Heat Pump Water Heater	53.3	70.8	57.0	82.5	129.8	156.3	142.8	125.0	120.7	72.7	55.2	46.1	1112.2
Solar System Circulators	35.7	27.1	31.4	24.2	22.0	18.2	20.4	19.8	22.6	29.0	34.3	34.8	319.6
Lighting	37.5	31.9	36.1	37.8	36.3	36.6	36.9	32.9	36.2	38.1	39.5	35.6	435.4
Plug Loads	202.5	167.1	199.7	210.2	208.5	210.2	214.0	193.8	216.7	206.3	208.2	202.5	2439.5
Heat Recovery Ventilator	42.4	35.6	42.3	44.4	43.7	44.3	46.4	38.7	45.3	42.8	45.4	43.1	514.4
Refrigerator	36.2	30.3	36.0	35.4	32.3	34.0	34.4	31.1	34.7	34.2	35.9	35.7	410.2
Dish Washer	7.8	6.4	7.8	7.8	8.8	8.6	8.6	7.8	8.9	8.0	7.9	7.9	96.3
Cooktop	19.2	16.4	19.7	19.2	19.6	19.7	19.3	17.8	20.9	19.2	20.1	19.4	230.4
Oven	30.0	27.0	31.7	30.0	33.7	31.9	30.0	29.3	35.8	31.7	33.7	31.7	376.6
Clothes Washer	5.2	4.6	6.2	6.2	6.1	6.3	6.2	5.6	6.4	6.0	6.1	6.0	70.8
Clothes Dryer	47.6	39.8	45.9	44.8	46.8	46.9	45.7	41.2	50.8	44.1	44.2	44.0	541.8
Microwave	12.3	10.4	12.3	12.5	12.2	12.4	12.6	11.4	12.7	12.2	9.2	11.1	141.3
Total PV AC Energy	1492.7	1162.4	1399.7	994.4	839.2	481.1	800.9	729.3	965.2	1425.1	1600.0	1633.3	13523.4
Total Energy Consumed	1262.7	968.3	888.9	747.9	1025.0	1193.7	1891.4	1324.5	1269.4	689.2	733.7	1044.5	13039.2
Net Energy Export	230.1	194.2	510.8	246.5	-185.8	-712.6	-1090.6	-595.3	-304.2	735.9	866.3	588.8	484.1

Table 4.10. Monthly photovoltaic system performance

Month	Jul/13	Aug/13	Sep/13	Oct/13	Nov/13	Dec ^a /13	Jan ^a /14	Feb ^a /14	Mar ^a /14	Apr/14	May/14	Jun/14
Average Daily Incident Solar Energy on Array ^b (kWh)	292.4	270.1	283.0	190.3	160.0	108.0	149.7	183.3	207.3	271.8	309.1	325.0
Average Daily Solar Insolation on Array ^b (kWh/m ²)	5604.0	5176.0	5424.0	3648.0	3067.0	2069.0	2868.0	3513.0	3972.0	5209.0	5924.0	6228.0
Average Ambient Temperature (C)	25.7	23.6	19.7	15.0	6.8	4.3	-1.9	1.1	4.1	12.7	18.7	23.6
Average Cell Temperature During Energy Generation (C)	38.6	36.7	35.1	26.5	15.9	11.1	7.2	10.8	15.1	24.2	32.8	37.6
Average Daily Delivered DC Energy (kWh)	51.4	47.8	49.8	34.4	30.0	16.3	27.4	27.9	33.5	50.9	56.1	58.2
Array Efficiency (%)	17.6	17.7	17.6	18.1	18.8	15.0	18.3	15.2	16.2	18.7	18.1	17.9
Average Daily Delivered AC Energy (kWh)	49.3	45.7	47.7	32.8	28.6	15.4	26.0	26.7	31.9	48.6	53.7	55.7
Inverter Efficiency (%)	95.9	95.6	95.8	95.5	95.3	94.5	95.1	95.4	95.2	95.6	95.7	95.7

^aFor 8 days in December, 8 days in January, 12 days in February, and 10 days in March the PV array was fully or partially covered with snow. If these days had been excluded the array efficiencies would have been 19.2 %, 19.7 %, 19.5 %, and 19.2 %, respectively, for December, January, February, and March.

^b The Average Daily Incident Solar Energy on Array was determined using the framed area of an individual module (1.63 m²) multiplied by the number of modules (32).

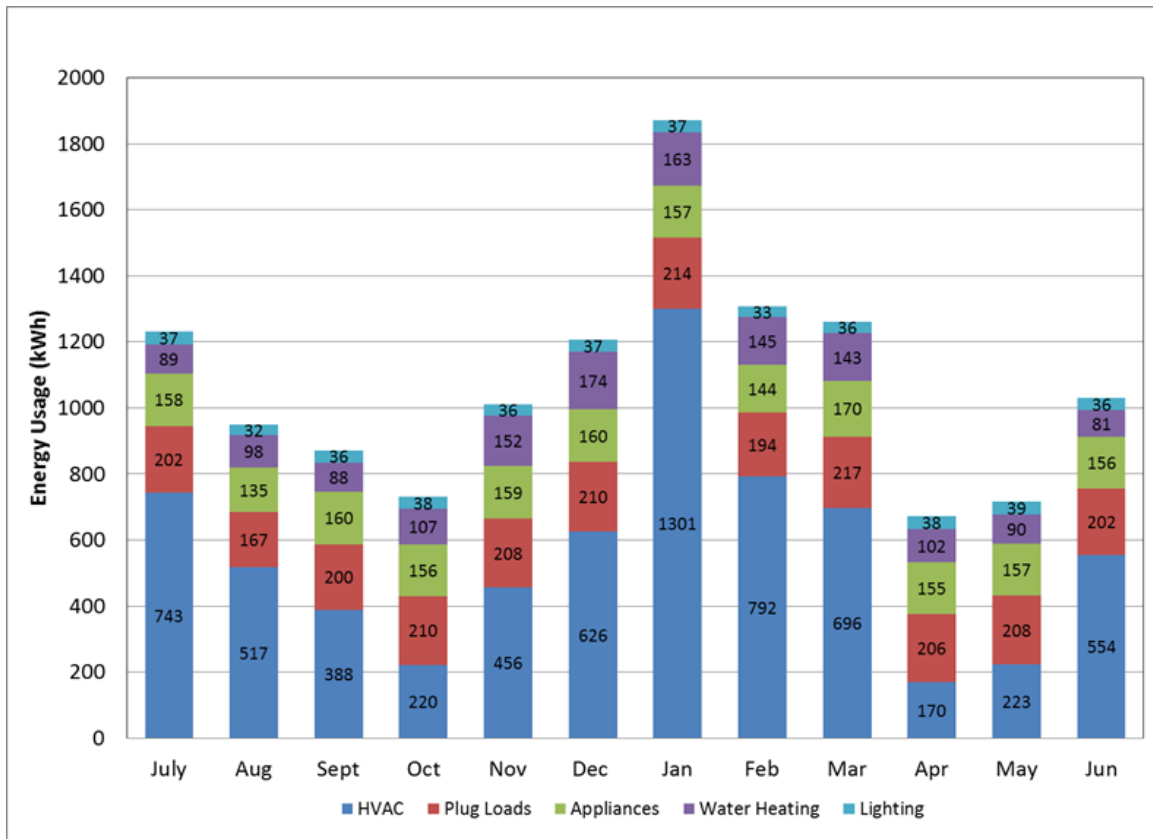


Fig. 4.22. Energy consumption by end use

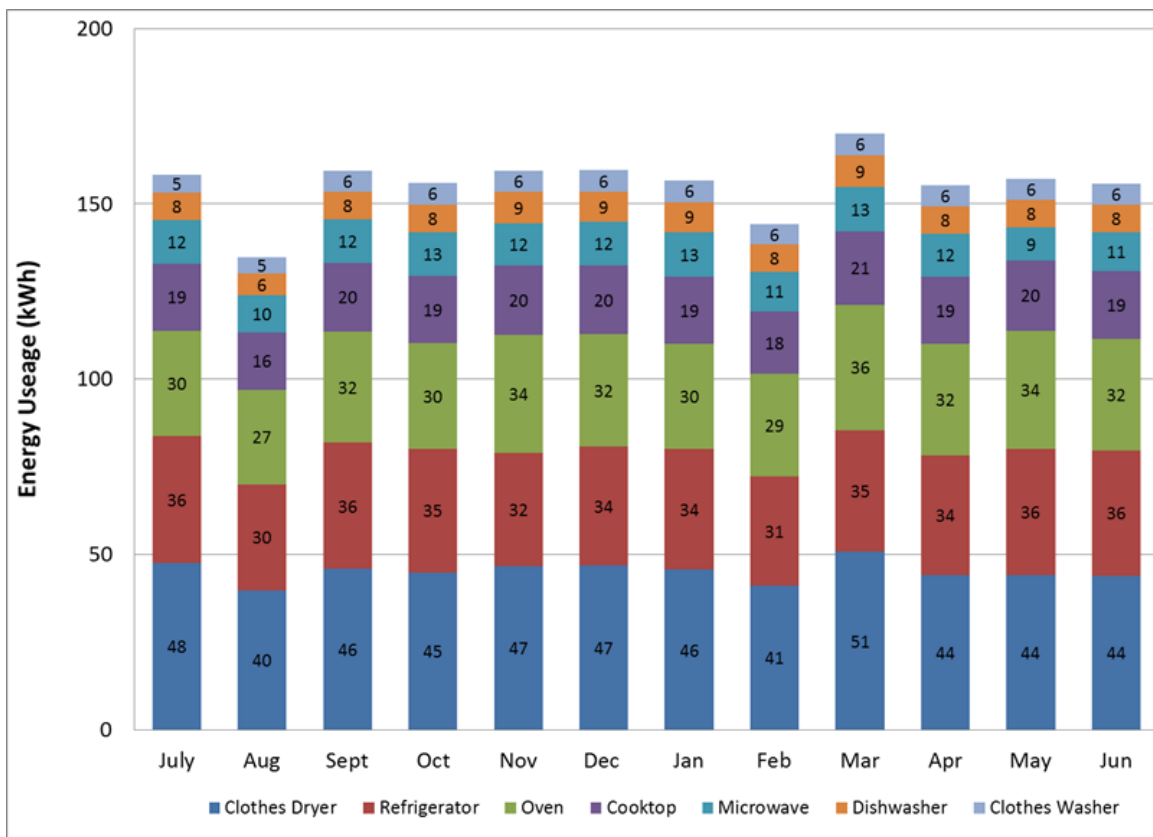


Fig. 4.23. Monthly energy consumption of the appliances (Jul-2013 to Jun-2014)

Heat Pump Energy Performance Summary

When operated in the cooling mode the unit operated with a seasonal COP (total thermal load/total electricity consumed) of 3.19 compared to the rated value of 3.82. There are two primary reasons that the measured seasonal cooling COP was less than the rated seasonal cooling COP. The seasonal cooling standby energy was 5.2 % of the total heat pump energy consumed and is not taken into account in the rating procedure used to determine rated seasonal cooling COP. The second contributor is the fact that when the heat pump operated in the dedicated dehumidification mode, the COP is significantly less than when operating in its normal mode, as seen in Table 4.11. For example, in August 2013 the heat pump operated in the dedicated dehumidification mode approximately 41 % of the time during which the measured COP was 0.89. The current rating procedure does not address the degradation in performance that may occur when a heat pump unit operates in a dedicated dehumidification mode during a portion of the cooling season.

In the heating mode, the measured seasonal COP was 2.06 compared to the rated seasonal COP value of 2.65. The seasonal heating standby energy was 3.5 % and is not considered in the rating procedure used to determine seasonal heating efficiency. The resistive heat is energized whenever the heat pump unit is in the defrost mode. The testing/rating procedure does not include the impact of resistive heat during the defrost cycle. The thermostat heating configuration allows the user to prescribe a 1st stage differential, 2nd stage differential, 2nd stage delay time, and 3rd stage differential. The differential temperature is relative to the current set point temperature and the delay time is the maximum amount of time a given stage is allowed to operate before energizing the next higher stage. The cooling and heating mode differentials and delays, shown in Table 4.12, were selected to maintain comfortable conditions throughout the year and minimize the use of resistive heat during the heating season. In the heating mode, 40 minutes was the maximum time the thermostat would permit the heat pump's compressor to operate in its high speed mode before energizing the electric resistance heat. This type of control logic appears to be effective in the cooling mode, but produced unnecessary usage of electric resistance heat in the heating mode.

During the seven months that cooling was required, the sensible to total load ratio varied from 0.58 to 0.78, Figure 4.24. Currently most high efficiency heat pump systems operate with a sensible to total load ratio of greater than 80 %. The higher latent loads associated with low energy homes will benefit from new technologies and control strategies that better address moisture removal. In the NZERTF enhanced moisture removal was made possible through the use of a heat pump that incorporated a dedicated dehumidification mode.

An analysis was performed to quantify the energy usage associated with the heat pump operation due to additional thermal loads introduced by the HRV. The HRV has two energy impacts, the fan energy and the increase or decrease in the thermal load resulting from introducing outdoor air into the house. For example, when the outdoor air temperature is lower than the indoor air temperature additional energy will be required to heat the home during the heating season compared to an identical home without an outdoor air ventilation system. During the cooling season, the introduction of outdoor air may increase or decrease the sensible and latent loads, dependent on the outdoor air temperature and moisture content relative to the indoor temperature and relative humidity. Nevertheless, the heat recovery capabilities of the HRV resulted in the provision of reliable ventilation rates with the fan energy required being largely compensated by the energy recovered. During the one-year period, the HRV consumed a total of 514 kWh in fan energy, as shown in Table 4.9. It is assumed the fan power required for the balanced ventilation system without an HRV would be equivalent to the ventilation system utilizing a HRV. Table 4.13 captures the energy impact of the HRV and ventilating to the same degree using a balanced ventilation system without a HRV.

Table 4.11. Monthly ASHP performance

Month	Jul/13	Aug ^a /13	Sep/13	Oct/13	Nov/13	Dec/13	Jan/14	Feb/14	Mar/14	Apr/14	May/14	Jun/14
<u>Thermal Load^b</u>	0.0	0.0	0.0	56.4	832.1	1351.0	2156.9	1634.7	1423.5	252.7	0.0	0.0
Heating Mode (kWh)	2122.9	1392.1	937.2	306.4	1.7	0.0	0.0	0.0	0.0	66.8	603.0	1559.7
Cooling Mode (kWh)												
<u>Heat Pump Energy Usage</u>	0.0	0.0	0.0	33.6	396.4	581.5	1254.8	753.1	650.4	113.2	0.0	0.0
Heating Mode (kWh)	700.8	481.0	345.5	142.3	15.7	0.0	0.0	0.0	0.0	13.6	177.7	511.3
Cooling Mode (kWh)												
Resistive Heat (kWh)	0.0	0.0	0.0	13.6	103.0	117.0	547.6	196.4	169.4	10.2	0.0	0.0
Avg. Outdoor Temp (°C)	26.6	24.6	20.7	15.5	7.1	4.5	-1.5	1.0	4.1	13.1	19.7	24.5
Avg. Indoor Temp (°C)	23.6	23.5	23.5	22.4	21.0	21.0	20.9	20.9	21.0	21.2	22.9	23.3
Degree Heating Days	0.0	0.0	30.7	218.8	610.0	773.5	1107.3	873.3	792.6	301.0	45.9	0
Degree Cooling Days	924.9	682.5	580.5	325.0		39.1	0.0	0.0	22.8	196.3	542.1	785.4
Heating Run Time (hr)	0.0	0.0	0.0	14.9	61.4	181.5	314.1	460.9	370.7	305.1	10.2	0.0
Cooling Run Time ^c (hr)	492.1	347.2	256.3	81.2	17.5	0.0	0.0	0.0	0.0	52.6	133.8	395.6
Dehumidification Mode (hr)	164.9	143.8	70.0	38.0	17.5	0.1	0.0	0.0	0.0	0.0	13.8	133.2
Dehumidification (l/kWh)	1.35	1.30	1.20	1.10	0.29	0.70	-	-	-	-	1.04	1.23
<u>Coefficient of Performance</u>												
Heating Mode (-)	0.00	0.00	0.00	1.68	2.10	2.32	1.72	2.17	2.19	2.23	0.00	0.00
Cooling Mode (-)	3.03	2.89	2.71	2.15	0.11	0.00	0.00	0.00	0.00	4.90	3.39	3.05
COP1 (Dehumidification) ^d	0.93	0.89	0.91	0.76	0.20	0.48	-	-	-	-	0.71	0.84

^aMissing data Aug 2 through Aug 6, 2013

^bHeat pump thermal load includes electric resistance heat.

^cCooling run time includes the time the unit operated in the dehumidification mode.

^dDehumidification COP equals the average of the daily dehumidification COP values (total latent energy divided by electrical energy during active dehumidification)

Table 4.12. ASHP thermostat settings

Mode	1 st stage differential	2 nd stage differential	2 nd stage delay time	3 rd stage differential	3 rd stage delay time
Cool	1.1 °C	2.8 °C	40 min	NA	NA
Heat	0.56 °C	1.1 °C	10 min	3.3 °C	40 min

Table 4.13. Monthly heat recovery ventilator performance

Month/Year	Jul/13	Aug/13 ^a	Sept/13	Oct/13	Nov/13	Dec/13	Jan/14	Feb/14	Mar/14	Apr/14	May/14	Jun/14
Energy Consumption (kWh)	42.4	35.6	42.3	44.4	43.7	44.3	46.4	38.7	45.3	42.8	45.4	43.1
Average Ambient Temperature (C)	26	24	20	15	7	4	-2	1	4	13	19	24
Average Outdoor Air Temp to HRV (C)	26	24	20	16	8	6	1	4	6	13	19	24
Average Indoor Temp to HRV (C)	24	24	24	22	21	21	21	21	21	21	23	24
Average HRV Exhaust Temperature (C)	26	24	22	18	13	12	9	11	12	16	21	24
HRV Effectiveness (-)	0.62	0.61	0.71	0.75	0.76	0.74	0.73	0.74	0.75	0.75	0.75	0.74
Average Flow Rate (m ³ /hr)	174	192	180	194	186	206	208	205	207	195	201	193
Sensible Load ^b Introduced by HRV(kWh)	-18.7	4.9	54.4	106.8	204.5	244.5	314.3	245.4	243.5	122.0	62.2	4.8
Latent Load ^c Introduced by HRV (kWh)	511.7	282.9	40.1	-23.5	-138.4	-106.0	-106.8	-70.7	-58.2	-76.0	-23.4	233.1
Additional Heat Pump Electrical Energy Used to Meet HRV Ventilation Load (kWh) ^d	229.6	191.6	-5.4	-30.7	32.1	154.9	417.1	201.1	189.5	-16.9	-77.0	165.0
Sensible Load Introduced by Balanced Ventilation System, No HRV (kWh)	-81.1	-10.1	122.5	236.2	491.0	591.9	763.0	593.6	591.3	293.0	133.4	-21.1
Latent Load Introduced by Balanced Ventilation System, No HRV (kWh)	513.6	290.4	62.3	12.3	-113.1	-80.4	-80.1	-52.7	-38.1	-54.3	3.7	262.1
Additional Heat Pump Electrical Energy Used to Meet Balanced Ventilation System (No HRV) Load (kWh) ^e	201.7	167.2	-15.6	1.7	58.6	198.6	538.5	229.1	232.3	29.9	-64.5	154.1
Difference in Heat Pump Energy – No HRV vs HRV Ventilation relative to HRV Ventilation (%)	-4.0	-5.0	-1.8	18.4	6.4	7.5	9.6	3.8	6.6	35.9	7.0	-2.1

^aMissing data for Aug-2 through Aug-6, 2013

^bSensible loads are the sum for the month with positive sensible indicating cooling and negative indicating heating the house.

Some days the HRV or the mechanical ventilation system helped the cooling or heating system and some days the HRV or mechanical system worked against the heating or cooling system.

^cLatent loads should be equal but differ due to using living room relative humidity and temperature for the exhaust air when doing calculations for mechanical ventilation.

HRV calculations were done with living room relative humidity and the temperature measured at the HRV for the exhaust air. A negative latent load occurred when moisture was removed from the house

^dHeat pump electrical is the reduction or increase in the energy consumed by the heat pump as the result of introducing outdoor air utilizing the HRV

^eHeat pump electrical is the reduction or increase in the energy consumed by the heat pump as the result of introducing the same quantity of outdoor air as the HRV case but with no heat recovery

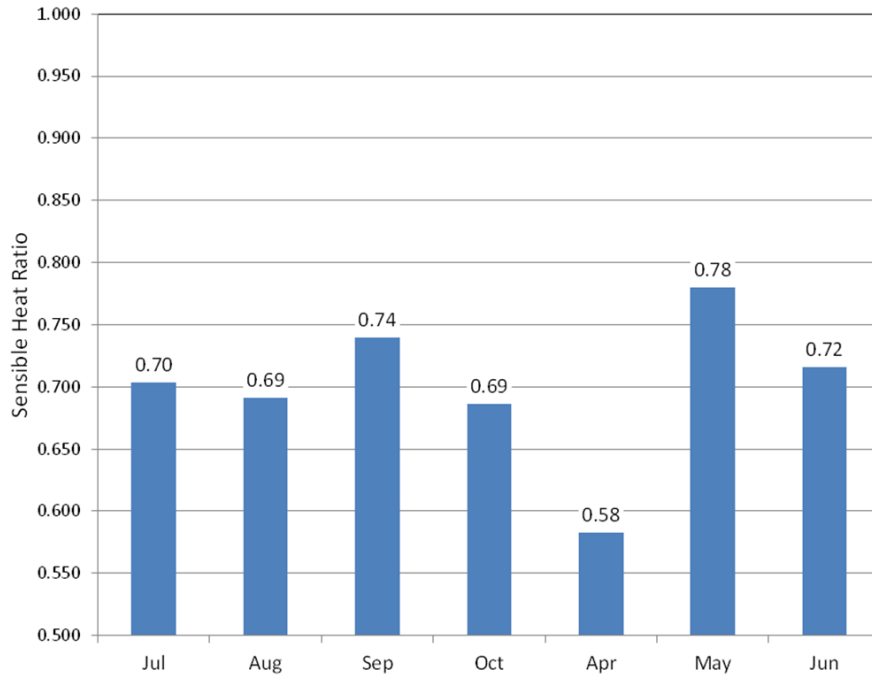


Fig. 4.24. Monthly Sensible Heat Ratio (SHR) for the cooling months

When space cooling was required, the use of the HRV resulted in an increase of 187 kWh (0.5 kWh/m²) and 1048 kWh (2.7 kWh/m²) in the sensible and latent loads, respectively, over the 12 month test interval. Using a balanced ventilation system (no HRV) that introduces the same quantity of outdoor air, the sensible and latent cooling loads would have been increased by 316 kWh (0.8 kWh/m²) and 1168 kWh (3.0 kWh/m²), respectively. When space heating was required the HRV increased the sensible load by 1402 kWh (3.6 kWh/m²) and decreased the latent load by 583 kWh (1.5 kWh/m²). Using a simple balanced ventilation system without an HRV when space heating was required would have increased the sensible load 3387 kWh (8.8 kWh/m²) and reduced the sensible load 442 kWh (1.1 kWh/m²).

Table 4.8 shows that use of an HRV increased the electrical energy consumption of the heat pump more than would have been the case if a balanced ventilation system without an HRV had been used for the months of July-2013, August-2013, September-2013 and June-2014. In those months the use of a balanced ventilation system without an HRV would have reduced the electrical energy used by the heat pump system (Table 4.3) by 4.0 %, 5.0 %, 1.8 %, and 2.1 %, respectively compared to the measured heat pump consumption using the HRV. During the months of October-2013, November-2013, December-2013, January-2014, February-2014, March-2014, April-2014 and May-2014, use of the HRV decreased the heat pump electrical energy consumption compared to the energy that would have been consumed if a balanced mechanical ventilation system without an HRV had been used with the difference ranging from 3.8 % to 35.9 %, Table 4.8. For the cooling months, when the reduction in the sensible load was greater than if a balanced ventilation system without an HRV had been used the total electrical consumption of the heat pump is greater due to the fact that the latent loads are larger and the heat pump has a significantly lower COP when operated in the dehumidification mode as compared to the normal mode. The annual energy required to ventilate the house using the HRV is the total of the additional energy to run the heat pump, 1451 kWh (3.7 kWh/m²), to meet the additional thermal load introduced by the HRV, plus 514 kWh of HRV fan energy, for a total of 1965 kWh (5.1 kWh/m²). If a balanced mechanical ventilation system without an HRV had been used the total annual energy consumed would have been 1732 kWh (4.5 kWh/m²) of additional heat pump energy to meet the load introduced by the balanced ventilation system (without an HRV) plus 514 kWh of assumed fan energy or 2246 kWh (5.8 kWh/m²). This finding is climate dependent. In this

case, the HRV would result in less energy consumption during the heating months and more energy during the cooling months compared to a mechanical ventilation system without a heat recovery ventilator.

4.2.2 Indoor Air Quality and Comfort

Charcoal test kits were deployed to measure indoor radon concentrations in the house following the EPA Protocols for Radon and Radon Decay Product Measurements in Homes (EPA, 1993). These measurements were made in the basement, first floor, and second floor. The average of all samples is below the EPA action level of 4 pCi/L (EPA, 1993). The building materials for the NZERTF were specified to have low emissions of volatile organic compounds (VOCs), including a prohibition on products with any added formaldehyde. Indoor air samples have been collected to measure the levels of approximately two dozen individual VOCs and formaldehyde in order to determine the impact of the building material specifications. These samples are collected monthly and will be used to determine if the VOC emission rates for the house change over time. Measurements (Poppendieck et al., 2015) show that the use of medium density fiberboard and particleboard with no-added formaldehyde resins for cabinetry and other finished products effectively controlled the formaldehyde emissions and kept concentrations below levels in typical new homes. Monitoring of seasonal indoor VOC concentrations (Poppendieck et al., 2015) suggests that building envelope components may be a source for some VOCs, especially aldehydes and alkanes.

Indoor dry bulb temperature, globe temperature, and relative humidity sensors are installed in the kitchen (on top of the counter), living room, master bedroom, bedroom 2, and bedroom 3 and readings are used to calculate thermal comfort parameters. Indoor dry-bulb temperature only is also measured in the attic, basement, bathrooms, office, dining room, and the entryway, but thermal comfort performance is not determined for these spaces. All measurements are recorded every 1 min.

In order to evaluate thermal comfort in selected rooms, the indoor dry-bulb temperature (T_{in}), globe temperature (T_{globe}), and relative humidity (RH) are measured. The globe temperature accounts for radiative heat transfer with interior building surfaces, as this is a primary determinant of thermal comfort. The globe temperature measurements require a correction based on the room air speed. The air speed was measured in selected rooms with a hot wire anemometer with the HRV and central air handling unit fan ON to determine this correction. It was assumed that the air speed would remain essentially constant given that the house is unoccupied and access to the house by researchers and visitors is limited. In the rooms where thermal comfort is to be evaluated, the air speed was consistently less than 0.1 m/s. The operative temperature was calculated using Equation 4.5 (Markus and Morris 1980)

$$T_{globe} = T_{in} + f_g (T_{mrt} - T_{in}) \quad (4.5)$$

where f_g is a factor based on globe size and air velocity, and T_{mrt} is the mean radiant temperature. Given that the air velocity was < 0.1 m/s and the globe size is 40 mm, f_g from Figure 3.2 in Markus and Morris (1980) is 0.48. Equation 4.5 is used to calculate T_{mrt} from the measured T_{globe} . Since these equations are valid for conditions when air movement is less than 0.1 m/s, they are valid both when the air handler fan is running and when it is off.

To evaluate the thermal comfort conditions, the operative temperature (T_{op}) is calculated as follows. From ASHRAE Fundamentals (ASHRAE 2013a), T_{op} is the average of T_{in} and T_{mrt} when the air velocity is < 0.4 m/s and $T_{op} < 50$ °C.

$$T_{op} = T_{in} + (T_{globe} - T_{in}) / (2f_g) \quad (4.6)$$

Indoor dry-bulb temperature, globe temperature, and relative humidity sensors are installed in the kitchen, living room, and the three bedrooms. These measurements are used to evaluate thermal comfort using two parameters: predicted mean vote (PMV) and predicted percentage of dissatisfied (PPD) (ASHRAE, 2010). Values of PMV between -0.5 and +0.5 and PPD < 10 are considered “comfortable.” In the summer, the occupants are assumed to be clothed between 0.36 clo (walking shorts, t-shirt) and 0.57 clo (short-sleeve shirt, trousers), where “clo” is the clothing insulation level. In the winter, the occupants are assumed to be clothed between 0.61 clo (long-sleeve shirt, trousers) and 1.14 clo (suit jacket, vest, long-sleeve shirt, trousers). It was assumed that the activity level of the occupants ranged between 0.7 met (sleeping) and 1.7 met (walking about), where “met” is the metabolic rate (ASHRAE, 2010).



Fig. 4.25. Sensors mounted in center of room to monitor thermal comfort; inset shows closeup of shielded dry bulb temperature sensor, globe temperature sensor, and relative humidity sensor

Figure 4.26 shows the PMV for the first demonstration year (Yr1) and most of the second demonstration year (Yr2). Heating months show close agreement in PMV for the first and second test years. Cooling months show a lower PMV for May and June; data for July, August and September are yet to be analyzed. The PMV values are used in the calculation of the predicted percentage dissatisfied (PPD) (ASHRAE 2010). PPD values for the first and second test years are shown in Figure 4.27. Both the PMV and the PPD are higher than the target comfort levels for the cooling months of June, July, and August.

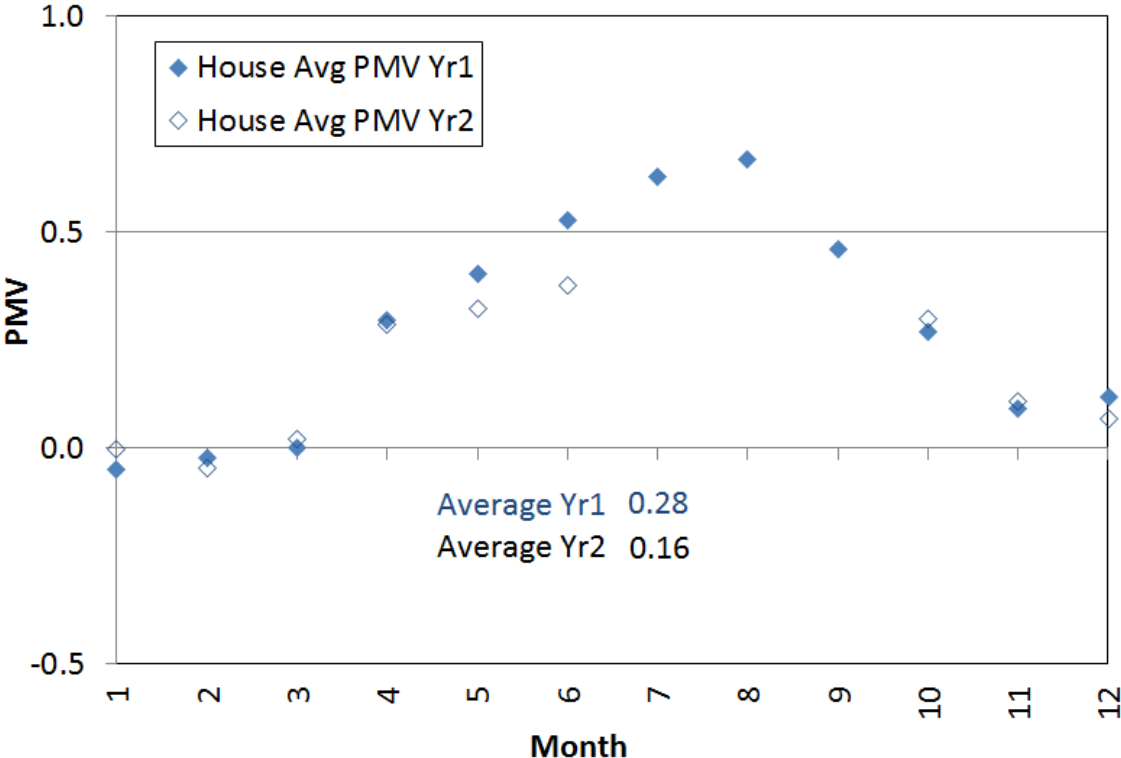


Fig. 4.26. Percent Mean Vote (PMV) for Year1(Yr1) and most of Year2 (Yr2)

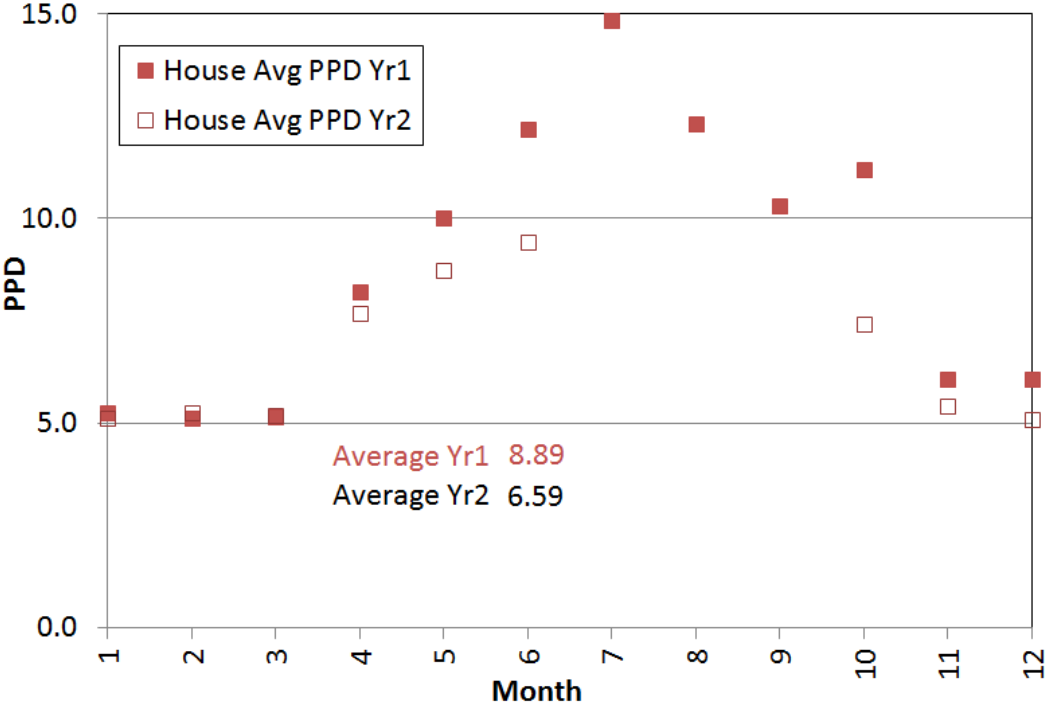


Fig. 4.27. Predicted percentage dissatisfied (PPD) for Year1 and Year2 thus far

4.3 Conclusions of field experience with the NZERTF

During the first year of operation the residence generated 13523 kWh of electricity using the 10.2 kW solar photovoltaic system. The house consumed 13039 kWh (33.7 kWh/m²) of electrical energy while meeting the electrical and comfort needs of a typical U.S. four member family, resulting in a net energy export of 484 kWh.

The solar photovoltaic system converted 16.8 % of the incident solar radiation into useful AC electrical energy. The solar thermal hot water system provided 54 % of the energy required to meet the domestic hot water load. The greatest end use of electricity within the residence was for space conditioning, followed by plug loads and appliances. Ventilating the house to exceed the ASHRAE Standard 62.2-2010 requirement using an HRV resulted in 1965 kWh (5.1 kWh/m²) of energy consumption: 514 kWh to power the HRV fan and an additional 1451 kWh (3.7 kWh/m²) of energy being used by the heat pump to meet the additional sensible and latent loads. This represents 31.8 % of the energy consumed by the heat pump, 15.0 % of the total energy consumed by the house, and 14.5 % of the energy generated by the photovoltaic system. If the HRV had provided the exact flow rate specified by ASHRAE Standard 62.2-2010 requirement, 137 m³/h versus the measured flow rate of 171 m³/h, and assuming identical fan power in both cases, it is estimated that the total energy impact of the HRV would have been 1676 kWh (4.3 kWh/m²) or 12.8 % of the house's total annual energy consumption. However, the heat recovered by the HRV comes very close to covering the fan power consumption, which serves the important purpose of providing reliable ventilation rates.

Among the lessons learned during this one year study was the significant impact that snow and/or ice can have on the output of a photovoltaic system attached to an extremely well-insulated roof. Significant periods of time were needed for the snow/ice cover to melt as a result of the well-insulated roof assembly. It was also observed that a simple control device, such as the heat pump's thermostat, can have a significant impact on the energy needed during the heating season. Despite these challenges, it was shown that net-zero can be achieved for a home slightly larger than the average size currently being constructed in the U.S. with all the amenities and features of a modern home.

As this document is being written, the NIST NZERTF is in its second test year of operations which began in October 2014. The main changes made for the second test year were the replacement of the thermostat and use of a whole house dehumidifier instead of the dedicated dehumidification mode of the heat pump. Figure 4.29 shows the latest overall electrical energy performance comparison for this new set of options. Heating mode energy use was reduced relative to the first year due to the absence of electrical resistance heating (except during defrost operations); this is very evident in the coldest heating months of January and February of 2015. The cumulative energy use between the first and second years shows the most difference for these two months. If the cumulative electrical energy trend continues, the second test year will show an electrical energy surplus well over 1000 kWh.

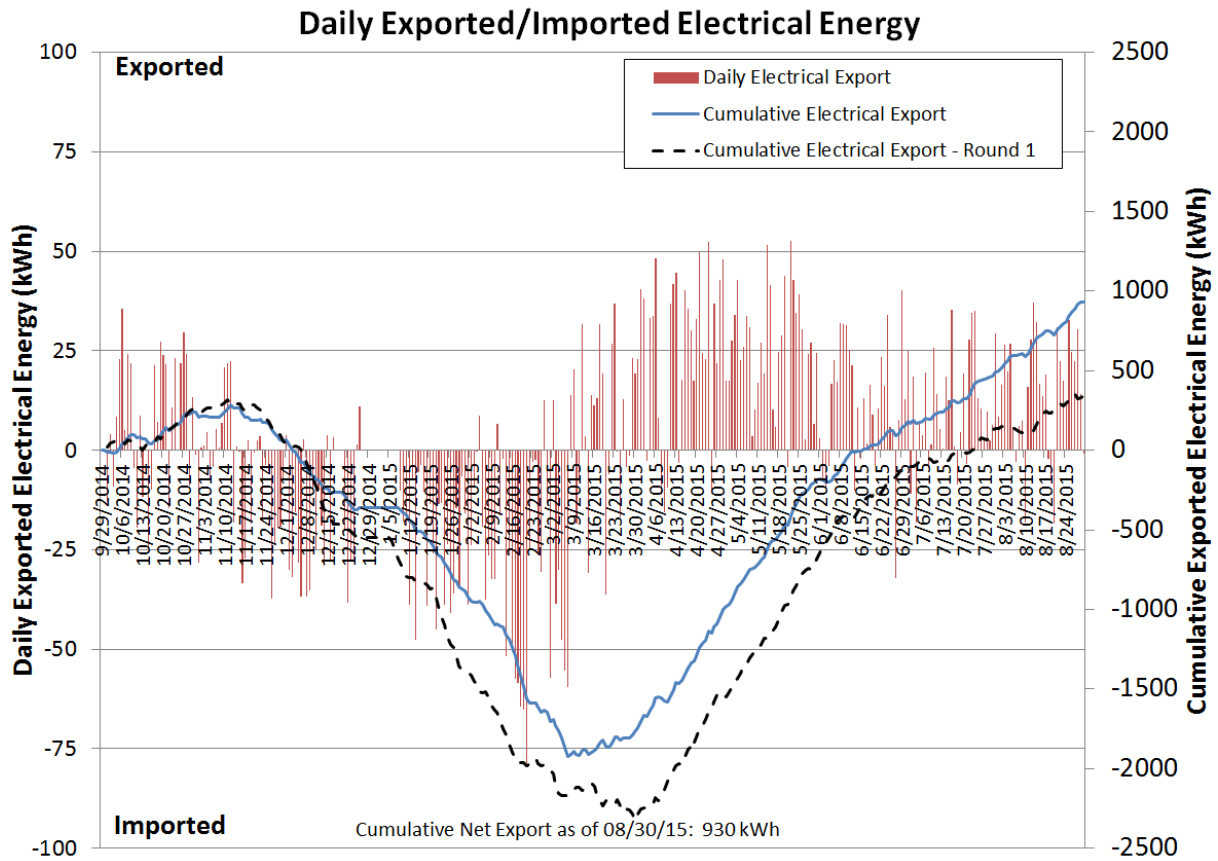


Fig. 4.29. Second year (to date) overall energy performance of the NZERTF

5 CONCLUSIONS AND OUTLOOK

5.1 ThermCom Software

Implications for thermal comfort control in nZEBs for different space heating and cooling distribution approaches.

- Radiant heat exchanger and induction-based supply unit systems (Cases I and II) result in relatively low room air velocities as compared to conventional centrally ducted or ductless forced air distribution approaches, thus minimizing any draft sensation by room occupants. The relatively larger heat exchanger surface areas (compared to ducted distribution systems) provide for better control of mean radiant temperature (MRT), and thus improving the PMV and PPD thermal comfort indices.
- Both conventional central duct systems and ductless systems (Case study III) generate significant space air temperature stratification. Generally speaking, the ducted system with large supply air velocity shows an overall best PMV distribution in heating, while for cooling, the ductless system is better. For ductless systems, adjusting the supply air vane angle according to supply air temperature can improve its PMV and PPD indices.

5.2 Integrated Heat Pump (IHP) systems

Key observations and future potential

- Electric-driven ground source integrated heat pump (GS-IHP).
 - Analytically projected annual energy savings vs. a baseline US minimum efficiency electric heat pump and water heating systems averaged ~59% (range from 57% to 61% for specific locations).
 - Annual energy savings based on field test results at a Knoxville, TN location are estimated as ~50% or more compared to the all-electric baseline.
 - ClimateMaster, Inc. introduced its Trilogy[®] Q-Mode[™] system (<http://www.climatemaster.com/residential/geothermal-heat-pumps/trilogy/>) to the US and international markets in 2012.
- Electric-driven air source IHP (AS-IHP). Two different AS-IHP system arrangements are under development by US manufacturers.
 - Single compressor or combined system
 - Features a variable-speed (VS) compressor and fans and multi-speed pump for DHW circulation.
 - Analytically projected annual energy savings vs. the all electric baseline system averaged ~52% (range from 46-47% in cold and hot climate locations to >60% in the West Coast marine climate).
 - First field test at Knoxville, TN location just completed. For the cooling season, the prototype achieved a space cooling seasonal performance factor or CSPF of 5.14 (SEER of ~17.5) and an average WH COP of 4.39. At time of this writing the heating season data is under analysis; a final report is expected by late fall 2015.
 - Two compressor system
 - The system consists of a high-efficiency (CSPF >5.3; SEER >18) ASHP for space heating and cooling coupled with a separate heat pump water heater/dehumidifier (WH-DH) unit. The two systems can be coupled via the air circulation duct system or be completely separate.
 - Analytically projected annual energy savings based on use of an ASHP with ~5.4 rated CSPF (18.4 SEER) vs. the all electric baseline

- system ranged from 33-36% for locations with relatively high DH loads. With a more efficient ASHP (rated CSPF ~7; SEER ~24) annual energy savings should exceed 40%.
- The separate WH-DH unit includes a demand DH mode for both indoor space air and ventilation air – especially useful in spring and fall months when SH and SC loads are small.
 - This IHP concept is also the most adaptable for retrofit applications.
 - A field test was just started in late summer 2015.
- Gas engine driven AS-IHP.
 - This IHP concept features a natural gas driven VS engine and scroll compressor and VS fans.
 - Simple pay back estimates for the system range from 3.5-4 years (for locations with high SH loads) to ~7.5 years for SC-dominated locations
 - Based on the 1st generation (Alpha) prototype demonstrated lab and field performance
 - Assumes a system first cost target of \$9000.
 - 2nd generation (Beta) prototype developed; lab test results showed combined SC + WH COP ranged from about 1.3-2.3 for a range of engine speeds (1400-3400 rpm) and ambient temperatures (35C to ~52C); field testing of the Beta system began in June 2015.
 - An electric-grid-independent version of the Beta prototype was developed, by adding 5 kW AC generator
 - The generator can supply power for all electric components of the system (fans, controls, etc.) and 1-2 kW extra power for external loads.
 - During electric grid outages, the prototype control approach is to ramp the engine to a high, constant speed and activate the generator to supply the unit electric needs and run essential household systems (minimal lighting, refrigerator, etc.).

5.3 NIST NZERTF future research and investigations

The NZERTF has a vast array of features and capabilities that will be utilized in the future. Over 200 future research and development opportunities suggested by 22 organizations are summarized in Domich et. al (2015). Recommended “research and development opportunities” within this document range from practical tests for assessing the airtightness of building enclosures to dynamic control of the heating, cooling, and ventilation systems taking full advantage of emerging “smart grid” capabilities.

The third year of testing will focus more on indoor environmental quality (IEQ); we will measure temperature and humidity distributions within the space hourly (or more), plus, we will add a small duct, high velocity (SDHV), variable-speed compressor, variable-speed indoor blower heat pump system. A 11 kW cooling capacity, variable-speed, SDHV air-source heat pump has been selected to operate with the existing “big duct” system in a one-day-ON, one-day-OFF alternating scheme. It is hoped that this type of side-by-side comparison under almost identical weather conditions and indoor loads will provide the best comparison. We will measure the instantaneous cooling/heating capacity and COP in addition to the added IEQ measurements mentioned above.

6 NATIONAL PUBLICATIONS IN IEA HPT ANNEX 40

Baxter, V.D., Sikes, K. 2013. State-of-the-Art Analysis of Nearly Zero Energy Buildings, Country report IEA HPP Annex 40 Task 1 United States - ORNL/TM-2013/299, Oak Ridge, September 2013, US

Davis M., Healy W., Boyd M., Ng L., Payne V., Skye H., Ullah T., 2014, Monitoring Techniques for the Net zero Energy Residential Test Facility, NIST Technical Note 1854, http://www.nist.gov/customcf/get_pdf.cfm?pub_id=917208.

Domich P.D., Pettit B., Fanney A.H., and Healy W.M., Research and Development Opportunities for the NIST Net zero Energy Residential Test Facility, NIST Technical Note 1869 (2015), Accessed Sep-8-2015, <http://dx.doi.org/10.6028/NIST.TN.1869>.

Kneifel J., 2012, Annual Whole Building Energy Simulation of the NIST Net Zero Energy Residential Test Facility Design, NIST Technical Note 1767, http://www.nist.gov/customcf/get_pdf.cfm?pub_id=912187.

Kneifel J., 2014, Life-Cycle Cost Comparison of the NIST Net Zero Energy Residential Test Facility to a Maryland Code-Compliant Design, NIST Special Publication 1172, Accessed Sep-10-2015, <http://dx.doi.org/10.6028/NIST.SP.1172>.

Munk, J. D., M. R. Ally, V. D. Baxter, and A. Gehl. 2014. Measured Space Conditioning and Water Heating Performance of a Ground-Source Integrated Heat Pump in a Residential Application. Proceedings of the 11th IEA Heat Pump Conference 2014, May 12-16 2014, Montréal (Québec) Canada.

Omar F., S. Bushby, 2013, Simulating Occupancy in the NIST Net zero Energy Residential Test Facility, NIST Technical Note 1817, http://www.nist.gov/customcf/get_pdf.cfm?pub_id=914650.

Rice, C. K., B. Shen, J. D. Munk, M. R. Ally, and V. D. Baxter. 2014a. Development of a Variable-Speed Residential Air-Source Integrated Heat Pump. Proceedings of the 11th IEA Heat Pump Conference 2014, May 12-16 2014, Montréal (Québec) Canada.

Rice, C. K., B. Shen, V. D. Baxter, S. A. Shrestha, and R. B. Uselton. 2014b. Development of an Air-Source Heat Pump Integrated with a Water Heating / Dehumidification Module. Proceedings of the 11th IEA Heat Pump Conference 2014, May 12-16 2014, Montréal (Québec) Canada.

7 LITERATURE

- AHRI. 2008. *2008 Standard for Performance Rating of Unitary Air-Conditioning & Air-Source Heat Pump Equipment*. AHRI 210/240. Arlington, VA: Air-Conditioning, Heating, and Refrigeration Institute, Arlington, VA.
- AHRI. 2013. "AHRI White Paper "Smart" Systems." Air-Conditioning, Heating, and Refrigeration Institute. (November 14, 2013).
- AHRI. 2014. "AHRI Proposed Framework for Demand Response Performance and Communication Specifications for Smart/Connected Variable Capacity Unitary HVAC Equipment." Air-Conditioning, Heating, and Refrigeration Institute. (September 2, 2014).
- ANSYS, Inc., 2006. Fluent version 6.3.26.
- ANSYS, Inc., 2011. Gambit version 2.3.16.
- Arora. C.P., 2000, Refrigeration and Air Conditioning, Second Edition, Chapter 17, pp. 571 – 615.
- ASHRAE., 2004. ANSI/ARI Standard 55-2004: Thermal Environmental Conditions for Human Occupancy. Atlanta: American Society of Heating, Refrigerating and Air-Conditioning Engineers Inc.
- ASHRAE 2007. *Ventilation and Acceptable Indoor Air Quality in Low-Rise Residential Buildings*. ASHRAE Standard 62.2-2007, Atlanta, GA: American Society of Heating, Refrigerating and Air-Conditioning Engineers.
- ASHRAE. 2010. "ASHRAE Standard 55-2010: Thermal Environmental Conditions for Human Occupancy", USA.
- ASHRAE. 2013a. ASHRAE Handbook - Fundamentals. USA
- ASHRAE. 2013b. "Standard 62.2-2013: Ventilation and Acceptable Indoor Air Quality in Low-Rise Residential Buildings". ASHRAE, USA.
- ASTM Standard E917-05(2010). Measuring Life-Cycle Costs of Buildings and Building Systems, *Annual Book of ASTM Standards*, ASTM International, West Conshohocken, PA, 2012, pp. 277-295, USA.
- Barnhart R. 2012. "Home Moisture," Minnesota Department of Commerce, http://www.homeenergyresourcemn.org/stream_document.aspx?rRID=2369&pRID=2368, accessed August-12-2015. USA
- Baxter, V. D., C. K. Rice, R. W. Murphy, J. D. Munk, M. R. Ally, B. Shen, W. G. Craddick, and S. A. Hern. 2013. *Ground-Source Integrated Heat Pump (GS-IHP) Development*. ORNL CRADA Final Report NFE-07-01000, May.
- Baxter, V. D., K. Sikes, R. Domitrovic, and K. Amrane. 2014. *IEA HPP Annex 42 Heat Pumps in Smart Grids - Task 1: Market Overview, United States*. ORNL/TM-2014/73, April.
- Berkooz, G., Holmes, P., and Lumley, J., 1993. The proper orthogonal decomposition in the analysis of turbulent flows. *Annu. Rev. Fluid Mech.*, 33, 539-575.
- Boussinesq, J., 1897, Théorie de l'écoulement tourbillonnant et tumultueux des liquides dans les lits rectilignes a grande section
- Dobos, Aron P. 2013. *PVWatts Version 1 Technical Reference*, National Renewable Energy Laboratory, Technical Report NREL/TP-6A20-60272, October. <http://rredc.nrel.gov/solar/calculators/PVWATTS/version1>

- DOE, U.S. Government. 2010. "Uniform Test Methods for Measuring the Energy Consumption of Water Heaters," Code of Federal Regulations, Title 10, Chapter II, Volume 3, Part 430, Subpart B, Appendix E.
- Dunkle, R., 1963. Configuration factors for radiant heat transfer calculations involving people. *Journal of Heat Transfer*, 71-76.
- Emrath, P., 2009. How Long Buyers Remain in Their Homes. National Association of Home Builders, Accessed Sep-10-2015, <http://www.nahb.org/en/research/housing-economics/special-studies/how-long-buyers-remain-in-their-homes-2009.aspx>, USA.
- EPA. 1993. Protocols for radon and radon decay product measurements in homes, U. S. Environmental Protection Agency, Washington D. C., http://www.epa.gov/radon/pdfs/homes_protocols.pdf, accessed Aug-14-2015. USA
- Fang X., Christensen D., Barker G. and Hancock E. 2011. "Field Test Protocol: Standard Internal Load Generation for Unoccupied Test Homes," Building Technologies Program, U.S. Department of ENERGY. USA
- Hendron, R. 2008. "Building America Research Benchmark Definition Updated December 19, 2008". National Renewable Energy Laboratory, USA
- Hendron, R. And C. Engbrecht. 2010. *Building America House Simulation Protocols*. NREL report: TP-550-49426, October. USA
- Intellichoice Energy. 2014. *Black (Dark) Start Cooling, Heating and Power Generation Demonstration Test on Military Installations Performance and Reliability Report*. Report to U. S. Department of Defense Construction Engineering Research Laboratory. October.
- ISO, 2004. ISO standard 8996:2004, Ergonomics of the thermal environment—Determination of metabolic rate, describes six methods for estimating metabolic heat production, which are divided into three levels according to accuracy. Geneva: International Organization for Standardization.
- ISO, 2005. ISO standard 7730: 2005, Ergonomics of the thermal environment – Analytical determination and interpretation of thermal comfort using calculation of the PMV and PPD indices and local thermal comfort criteria. Geneva: International Organization for Standardization.
- ISO, 2007. ISO standard 9920:2007, Ergonomics of the thermal environment—Estimation of thermal insulation and water vapor resistance of a clothing ensemble, provides an extensive database of the thermal properties of clothing and garments. Geneva: International Organization for Standardization.
- Kneifel, J. 2014. Life-Cycle Cost Comparison of the NIST Net Zero Residential Test Facility to a Maryland Code Compliant Design. NIST Special Publication 1172. http://www.nist.gov/manuscript-publication-search.cfm?pub_id=915844. USA.
- Koepke, M., 2011. Experimental investigations on the thermal comfort of an office setting conditioned by low ΔT heat exchangers, Bachelor thesis, University of Maryland, College Park and Technische Universität Berlin
- Lennox Industries Inc. 2013a. SunSource® Home Energy System Product Specifications, Publication #210664, Sept.
- Lennox Industries Inc. 2013b. SunSource® Home Energy System Application and Design Guidelines, Publication #CORP1312-L2, July 2013
- Ling, J., 2011. Energy Savings and Thermal Comfort of Separate Sensible and Latent Cooling Air-Conditioning Systems, Ph.D. dissertation. University of Maryland.
- Ly, H. V., and Hein, T. T., 2001. Modeling and control of physical processes using proper orthogonal decomposition. *Math. Comput. Modelling*, 33, 223-236.

- Markus, Thomas Andrew, and Edwin N. Morris. 1980. *Buildings, Climate, and Energy*. Pitman Pub., USA.
- Mahderekal, I., B. Shen, and E. A. Vineyard. 2012. "System Modeling of Gas Engine Heat Pump," paper # 2179 in Proceedings of 2012 International Refrigeration and Air-Conditioning Conference at Purdue, July 16-19, West Lafayette, IN.
- Mahderekal, I., 2015. Personal communication to Van Baxter, October 27, 2015.
- Monteith J. L. 1972. "Latent Heat of Vaporization in Thermal Physiology." *Nature: New biology*, vol. 236, no. 64, p. 96, 22-Mar-1972, USA
- Murphy, R.W., V. D. Baxter, C. K. Rice, and W. G. Craddick. 2007a. *Air-Source Integrated Heat Pump for Near Zero Energy Houses: Technology Status Report*. ORNL/TM-2007/112, July.
- Murphy, R.W., V. D. Baxter, C. K. Rice, and W. G. Craddick. 2007b. *Ground-Source Integrated Heat Pump for Near Zero Energy Houses: Technology Status Report*. ORNL/TM-2007/177, December.
- New Buildings Institute. (2012, March 6). Zero Energy Buildings on the Rise Across the U.S. [press release]. Retrieved from http://newbuildings.org/sites/default/files/ZEB_Report_PressRelease.pdf
- Olesen, B., *Low Temperature Radiant Heating – High Temperature Radiant Cooling*, Technical University of Denmark, ASHRAE Learning Institute, 2011
- Poppendieck D., Ng L., Schlegel M., Persily A., Hodgson A. 2014. Long term air quality monitoring in a net zero energy residential test facility designed with specifications for low emitting interior products, Indoor Air 2014, Hong Kong, China, USA
- Rambo, J. 2006. Reduced-order modeling of multiscale turbulent convection: application to data center thermal management. Georgia Institute of Technology.
- Rice, C. K. 1991. *The ORNL Modulating Heat Pump Design Tool - Mark IV User's Guide*, ORNL/CON-343.
- Rice, C. K. and Jackson, W. L. 2005. DOE/ORNL Heat Pump Design Model on the Web, Mark VII Version. <http://www.ornl.gov/~wli/hpdm/MarkVII.shtml>.
- Rice, C. K., Baxter, V. D., Hern, S. A., McDowell, T., Munk, J. D., and Shen, B. 2013. *Development of a Residential Ground-Source Integrated Heat Pump*. Conference Papers CD for 2013 ASHRAE Semi-Annual Meeting in Dallas, TX.
- Riesz, F. and Nagy, B. S. 1990. *Functional Analysis*. New York: Dover Publications.
- Risser, Roland. (2013, April). *Building Technologies Office Overview*. Presented at the 2013 DOE Building Technologies Office Program Review, Washington, D.C. http://www1.eere.energy.gov/buildings/pdfs/bto_overview_risser_040213.pdf
- Seryak J. and Kissock K. 2003. "Occupancy and Behavioral Affects on Residential Energy Use," SOLAR 2003, Proceedings of annual conference on American solar energy society, USA.
- Solar Energy Laboratory (Univ of WI), TRANSSOLAR Energietechnik, CSTB – Centre, Scientifique et Technique du Bâtiment, and TESS – Thermal Energy System Specialists. 2010. TRNSYS 16: a TRaNsient SYstem Simulation program, Version 16.01.0000
- Southwest Gas Corporation. 2014. PERC III - Residential natural gas heat pump (RGHP) Research & Development Program. Project report to the Propane Education and Research Council (PERC). December.
- U.S. Energy Star Homes Program. (2013a, June). *ENERGY STAR Certified Homes, Version 3 (Rev.0 7) National Program Requirements*.

http://www.energystar.gov/ia/partners/bldrs_lenders_raters/downloads/National_Program_Requirements.pdf?875f-d36d.

U.S. Energy Star Homes Program. (2013, June). *ENERGY STAR Qualified Homes, Version 3 Savings & Cost Estimate Summary*.

http://www.energystar.gov/ia/partners/bldrs_lenders_raters/downloads/EstimatedCostandSavings.pdf?1665-0032.

U. S. Environmental Protection Agency. (2013). ENERGY STAR. <http://www.energystar.gov>

U. S. Patent Office. 2014. United States Patent No. 8,689,574 B2. *Dedicated Dehumidifier and Water Heater*. April 8, 2014.

Vineyard, E. A. 2014. Multi-function fuel-fired heat pump CRADA. Presentation to 2014 DOE Building Technologies Office Peer Review meeting, April, Washington, DC.

http://energy.gov/sites/prod/files/2014/10/f18/emt07_vineyard_042414.pdf.

Wetter, M., "GenOpt® Generic Optimization Program User Manual Version 3.0.0". May 11, 2009, Lawrence Berkeley National Laboratory Technical Report LBNL-2077E.

ACKNOWLEDGEMENTS

The authors gratefully acknowledge the substantial contributions provided for this report from others including, but not limited to, the following individuals.

- For the IHP section: Ahmad Abu-Heiba, Moonis Ally, William Craddick (ret.), Anthony Gehl, Ayyoub Momen, Jeff Munk, Richard Murphy (ret.), Keith Rice, Bo Shen, and Ed Vineyard of ORNL; and Isaac Mahderekal of Intellichoice Energy.
- For the ThermCom section: We gratefully acknowledge the support of this effort from the sponsors of the Center for Environmental Energy Engineering (CEEE) at the University of Maryland.
- For the NZERTF section: Mark Davis, Matthew Boyd, and Harrison Skye of NIST.

Finally, the authors gratefully acknowledge Antonio Bouza of the U. S. Department of Energy's Building Technologies Office (DOE/BTO) for his support of the U. S. participation in IEA HPT Annex 40, the assembly of this report, and the ORNL technical activities summarized herein under Contract No. DE-AC05-00OR22725 with UT-Battelle, LLC.